JPC 447

TM-63-5

An Experimental Investigation of the Hypergolic Ignition of Some Polymeric Fuels with Oxygen

by

S. D. Kershner

J. R. Osborn

A. M. Mellor

Technical Memorandum

NASA Grant NsG 592

and

Thiokol Chemical Corporation

July 1968

JET PROPULSION CENTER
PURDUE UNIVERSITY

SCHOOL OF MECHANICAL ENGINEERING
LAFAYETTE, INDIANA

PURDUE UNIVERSITY

AND

PURDUE RESEARCH FOUNDATION

Lafayette, Indiana

AN EXPERIMENTAL INVESTIGATION OF THE HYPERGOLIC IGNITION OF SOME POLYMERIC FUELS WITH OXYGEN

by

S. D. Kershner

J. R. Osborn

A. M. Mellor

Technical Memorandum

NASA Grant NsG 592

and

Thiokol Chemical Corporation

Jet Propulsion Center
Purdue University

July 1968

ACKNOWLEDGMENTS

The investigation reported herein was supported by the National Aeronautics and Space Administration under Grant NsG 592 and by Thiokol Chemical Corporation. Reproduction of this report in whole or in part is permitted for any purpose of the United States Government.

Special thanks are expressed to Messrs. Melton, Scheuerlein, Ringger, Garvey and Dion for their assistance with design and operation of the experimental apparatus. The efforts of C. Merkel, W. Timmons, T. Miller, C. Fuqua, G. Hurst and T. Virgin are appreciated for their assistance during the fabrication and operation of the experimental apparatus.

Dr. R. G. Johnson, Honeywell, Inc., is acknowledged for the loan of the ultraviolet detector.

The author wishes to thank Mesdames C. Jakes, R. Kissick, J. Melton and D. Guhse for their typing skills.

The assistance of the author's wife, Jan, in typing the first draft of the manuscript is gratefully acknowledged.

TABLE OF CONTENTS

	Page
LIST OF TABLES	vi
LIST OF FIGURES	vii
ABSTRACT	ix
INTRODUCTION	1
REVIEW OF LITERATURE	5
General Discussion	5
Ignition Theories	7
General	7
Solid Phase Thermal Theory	8
Gas Phase Theory	11
The Hypergolic Theory	15
The Heterogeneous Ignition Theory	16
Experimental Investigations	18
General	18
Oxidizer Decomposition	19
Thermal Degradation of Polymers	20
Ignition of Fuels in Perchloric Acid Vapor	22
Hypergolic Ignition	23
Ignition by Radiant Heat Fluxes	25
Ignition in Shock Tubes	27
Summary and Comments	29

Page

METHOD OF INVESTIGATION 32

General 32

Ignition Experiments 32

Design Criteria 32
Ignition Test Apparatus 33
Sample Preparation 36

Mass Spectra of Polymers 36

EXPERIMENTAL RESULTS 42

Ignition Experiments 42

General 42
Ignition in Oxygen 42
Ignition Tests with Chlorine 51

Mass Spectral Results 53

General 53
CTPB Polymer 54
PBAA Polymer 55
PS Polymer 55

Summary 56

DISCUSSION OF RESULTS 59

Interpretation of Experimental Results 59

Conditions Required for Hypergolic Ignition 59
Postulated Reaction Mechanisms 65
Chlorine Experiments 74
Mass Spectral Results 75

Comparison with Other Results 76

CONCLUSIONS 85

LIST OF REFERENCES 87

APPENDIX A: NOMENCLATURE 92

Page

APPENDIX B: DESCRIPTION OF IGNITION TEST APPARATUS. 94

APPENDIX C: IGNITION TEST PROCEDURE. 107

APPENDIX D: POLYMER CONSTITUENTS. 110

APPENDIX E: CALCULATION OF IGNITION TIME BY WILLIAMS' METHOD. 111

APPENDIX F: METHOD OF ESTIMATING MASS FLUXES FROM BULK THERMAL DEGRADATION DATA. 115

APPENDIX G: TABULATED IGNITION DATA 117

APPENDIX H: MASS SPECTRAL DATA. 122

LIST OF TABLES

Table		Page
1.	Ignition Test Data.	118
2.	Mass Spectra of CTPB Polymer.	124
3.	Mass Spectra of PBAA Polymer.	128
4.	Mass Spectra of PS Polymer.	133

LIST OF FIGURES

Figure		Page
1.	Illustrative Schematic of Types of Chemical Reaction Possible During Ignition.	4
2.	Solutions of One-Dimensional Heating of Solid Phase Inert Material.	10
3.	Ignition Time vs. Oxidizer Mole Fraction at Constant Total Pressure.	13
4.	Ignition Time vs. Total Pressure at Constant Oxidizer Mole Fraction	14
5.	Ignition Time vs. Oxidizer Concentration for Room Temperature Hypergolic Ignition	24
6.	Ignition Time vs. Radiant Heat Flux Depicting Effect of Environmental Pressure	26
7.	Square Root of Ignition Time vs. Heat Flux for a PBAA-AP Propellant in a Shock Tube	28
8.	Ignition Time vs. Oxygen Concentration for End Wall Samples in Samples in Shock Tubes.	30
9.	Photograph of Ignition Test Apparatus	34
10.	Sketch of Sample Holder Assembly.	37
11.	Mass Spectrometer Sample Inlet System	39
12.	Hypergolic Ignition Data for CTPB Polymer	45
13.	Hypergolic Ignition Data for CTPB Polymer (Slow Heating Data)	46
14.	Hypergolic Ignition Data for CTPB Polymer (Averaged Slow Heating Data).	47
15.	Hypergolic Ignition Data for PBAA Polymer	49

Figure		Page
16.	Photographs of Ignited Polystyrene Sample.	52
17.	Stationary Theory of Heterogeneous Ignitions: Rate of Chemical Energy Release and Rate of Heat Loss vs. Surface Temperature.	62
18.	Comparison of the Effect of Oxidizer Concentration on Reaction Rate and Ignition Time for Different Adsorption Mechanisms	69
19.	Comparison of Hypergolic Ignition Results with Shock Tube Ignition Data	78
20.	Comparison of Temperature Corrected Hypergolic Ignition Results with Shock Tube Ignition Data	81
21.	Comparison of Shock Tube and Hypergolic Ignition Results for CTPB Propellant and Polymer	83
22.	Sketch of Ignition Test Chamber Assembly	95
23.	Schematic Diagram of Pressure Control System	98
24.	Relative Spectral Response of Photodiode Detector. . . .	102
25.	Relative Spectral Response of Ultraviolet Detector. . .	103
26.	Electrical Schematic for Ultraviolet Detector.	104
27.	Typical Oscillogram from an Ignition Test.	106
28.	Heating Curve for CTPB Sample.	123
29.	Heating Curve for PBAA Sample.	127
30.	Heating Curve for PS Sample.	132

ABSTRACT

This report presents the results of an experimental investigation of three polymeric fuels with oxygen at temperatures of about 260 to 320°C and within a pressure range of 8.8 to 20.6 atmospheres. The polymeric fuels were carboxy terminated polybutadiene (CTPB), polybutadiene acrylic acid (PBAA), and polystyrene (PS).

The investigation consisted of two parts: a determination of the ignition time of the polymers as a function of oxygen concentration and temperature and a determination of the mass spectra of the pyrolysis products of these polymers in equilibrium with one atmosphere of helium at 260°C. Ignitions were obtained for all three polymers; listed in the order of decreasing ease of ignitability they are PBAA, CTPB, and PS. The ignition times for the PBAA and CTPB polymers exhibited a low order dependence on oxidizer concentration and a strong dependence on initial temperature. The mass spectral results indicated that the maximum mole fraction of fuel vapors present under any ignition conditions was less than about two per cent.

Based on the above results, a heterogeneous reaction mechanism, assumed to be kinetically controlled by the surface reaction step, was postulated. This mechanism agrees qualitatively with the observed results.

Ignition experiments in a chlorine environment were also performed with the CTPB and PBAA polymers, but no ignitions were detected.

INTRODUCTION

Since the early 1940's solid propellant rockets have been successfully used for a myriad of scientific, commercial and military missions. The propellants utilized in these rockets may be classified into two types according to the arrangement of the fuel and oxidizer within the propellant. Homogeneous or double-base propellant is a colloid formed by gelatinizing nitrocellulose with nitroglycerin. Both nitrocellulose and nitroglycerin are monopropellants since they contain both fuel and oxidizer. Heterogeneous or composite propellants consist of particles of an inorganic oxidizer salt (usually ammonium perchlorate) which are contained within a matrix of an organic polymer. To increase the energy available from these propellants, metal particles have been added to the basic formulations, and combination propellants utilizing both composite and double-base constituents have been developed.

Of all the components required for a rocket motor (motor case, nozzle, insulation, propellant charge, etc.) the igniter has been one of the most difficult to design and develop according to a rational procedure. With the advent of the large solid propellant rocket boosters (120 in. to 260 in. dia.),

igniter development programs requiring extensive full-scale or even sub-scale testing were no longer economically feasible. Because of lack of knowledge about the ignition process, research on this problem was significantly increased beginning about 1960. Since that time several theories of solid propellant ignition have been developed and numerous ignition experiments have been conducted. The advance in the state of the art has been appreciable; computer programs are presently available for predicting the ignition transients in large solid propellant motors (1)*. As a part of their input information these computer programs require experimental data which describe the response of the particular propellant formulation to the ignition stimulus (radiant heat transfer, convective heat transfer, surface chemical reaction, etc.). These data are usually obtained in experiments designed to duplicate closely the expected stimulus in the large solid propellant motor. It would be advantageous to avoid this type of experiment. If the relative contributions of different ignition stimuli could be computed for a group of composite propellants, only a few standard tests of propellant ignitability would be needed.

---

* Numbers in parenthesis indicate publications presented in the List of References.

Admittedly this is a formidable task considering the complexity of composite propellants. Figure 1 depicts schematically the types of chemical reactions which may occur and lead to the steady combustion of the propellant. Each of the four principal theories of solid propellant ignition assume that only one of the types of reactions is rate controlling. These theories are: (a) the solid phase thermal theory, (b) the gas phase theory, (c) the hypergolic theory, and (d) the heterogeneous theory. A brief description of these theories is presented later. Each of these theories is supported by some experimental data. These supporting data were obtained for the most part under conditions highly favorable to the limiting assumptions of the theoretical models. Unfortunately, practical igniters for rocket motors seldom provide these favorable conditions (an exception is hypergolic ignition), and the description of ignition by means of a single rate controlling reaction is insufficient.

Additional information is needed about the chemical reactions which lead to ignition, in order to evaluate the relative contributions of different ignition stimulii. The objective of this report is to provide such information about the ignition reactions between two polymeric fuels and two oxidizers, oxygen and chlorine. Both chlorine and oxygen occur as oxidizer decomposition products in composite propellants which contain ammonium perchlorate oxidizer.

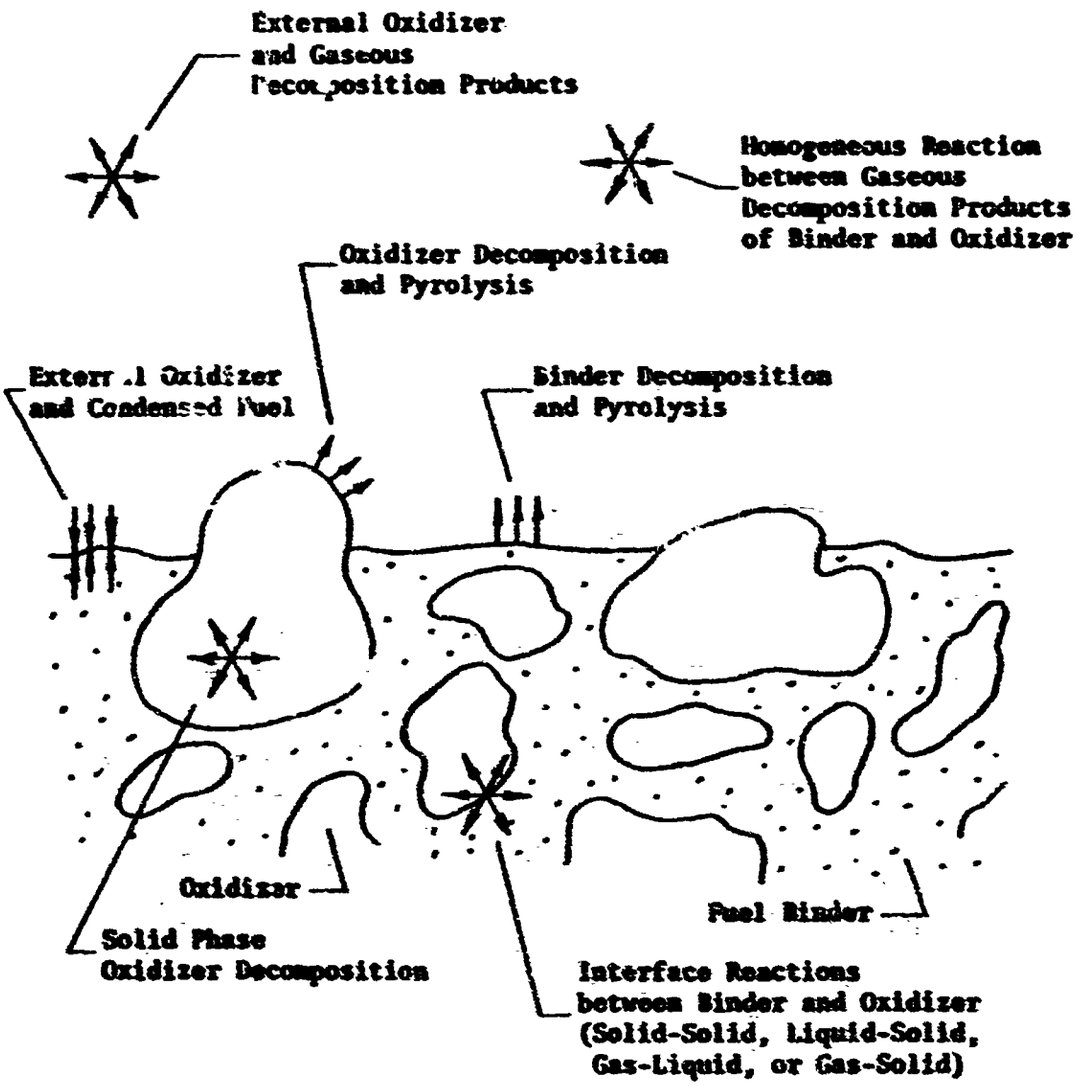

Figure 1 Illustrative Schematic of Types of Chemical Reactions Possible during Ignition

REVIEW OF LITERATURE

General Discussion

As mentioned in the introduction, the ignition and combustion of solid propellants is a complex process, involving simultaneous heat transfer, mass transfer and chemical reactions. The phenomenology of the ignition and combustion processes for both double-base and composite propellants has been well described (2,3,4). However, there is little agreement on the relative importance of the fundamental processes controlling the ignition of composite solid propellants.

One of the more fundamental difficulties in the treatment of solid propellant ignition is the definition of the ignition criterion. The state of ignition may be considered as the condition of a chemically reacting system which will proceed to self sustaining deflagration even if the ignition stimulus is removed. Mathematically this may be represented by

$$\dot{q}_{chem} > \dot{q}_{loss}$$

where $\dot{q}_{chem}$ = rate of heat generation by chemical reaction, $cal/cm^2\text{-}sec$

$\dot{q}_{loss}$ = rate of heat loss to the environment, cal/cm^2-sec.

Operationally, the state of ignition is determined by one or more of the following criteria: (a) indication of radiative emissions in the near infared, visible, or ultraviolet regions of the electromagnetic spectrum, (b) indication of a pressure rise caused by rapid generation of gases, and (c) demonstration of self sustaining deflagration upon removal of the ignition stimulus. The time interval required for ignition begins at the instant of application of the ignition stimulus and ends when one of the above operational ignition criteria has been attained. This time interval will hereafter be called the ignition time. Unfortunately, these operational ignition criteria often do not yield equal values of ignition time for the same experiment.

There are similar difficulties in defining ignition criteria for the theoretical models. The attainment of the following conditions have been utilized as ignition criteria: (a) a fixed "ignition" temperature, (b) an arbitrarily large value of the rate of temperature increase with time (say $\frac{dT}{dt} = 10^6 \frac{^oK}{sec}$), (c) some predetermined value for the rate of production of gaseous reactants at the propellant surface, (d) the point of inflection in the temperature-time curve just before $\frac{dT}{dt} \to \infty$, and (e) eventual precipitous temperature

increase after removal of the ignition stimulus. Because these different ignition criteria are utilized in the various theoretical models, comparisons between the models on a consistent basis are impossible.

Ignition Theories

General

A theoretical model of the ignition process, applied to solid rocket propellants, was first published in 1956 (5). Since that time several different ignition theories have been proposed along with improvements and modifications in each of the theories. All of the existing theories are one dimensional in the sense that the conservation equations consider only gradients in the direction normal to the solid surface.*

The following approach is taken in each of the ignition theories presented below. The controlling source of chemical heating is postulated and a one step overall reaction rate equation of the Arrhenius type is assumed to describe the chemical heating. The governing conservation equations and the necessary boundary and initial conditions are formulated. The assumptions are listed which permit the simplified form of the above equations to be utilized and which are necessary for a solution to these equations. An ignition criterion is assumed which will be compatible

---

* However, two dimensional analyses have been utilized for the problem of flame spreading on a propellant surface.

with the solution of the equations. A solution or series of solutions to the set of simplified equations is then obtained by classical techniques, dimensional analyses, numerical techniques, or a combination of these. The results of the analyses are typically presented in graphical form depicting the dependence of the ignition time upon the independent variables of interest.

The Solid Phase Thermal Theory

The solid phase thermal theory considers the ignition of semi-infinite solid phase by means of a thermal energy stimulus. It was originially developed for the ignition of double-base propellants, but it has also been applied to the ignition of composite propellants. This theory has been modeled with many different restrictive assumptions. In all models for which solutions have been obtained the following assumptions are made: (a) mass diffusion is neglected, (b) chemical reactivity of the gas phase is neglected, and (c) the rate of chemical reaction is independent of the concentration of the reactants. These assumptions are equivalent to forcing the chemical heating to occur in the solid phase and to having the temperature of the solid phase control the rate of chemical heating. Price, et al, (3) present a thorough discussion of the variations in the models of the solid phase thermal theory. The different solid phase models have utilized four of the five aforementioned ignition criteria.

The results of the simpler versions of the thermal theory predict

$$q\dot{q} = B\,(T_s - T_i)^2$$

where

q = thermal energy absorbed per unit area, (cal/cm^2)

$\dot{q}$ = thermal energy flux, (cal/cm^2-sec)

B = constant (cal^2/cm^4-sec-$^oK^2$)

T_s = temperature of solid surface, ^oK

T_i = initial temperature, ^oK

which for fixed values of "ignition" temperature and initial temperature, reduces to $q\dot{q} = B'$. Figure 2 is a graphical representation of q vs. $\dot{q}$ for one dimensional heating of a condensed phase, inert material by a constant heat flux. As may be deduced from Figure 2, the ignition time is inversely proportional to the square of the heat flux. This fact leads some investigators to depict the results of the thermal theory as graphs of log $(t^*)^{1/2}$ vs. log q with the ignition criterion appearing as a slope of -1. The more complicated variations of the thermal theory do not predict such a simple results although the experimental data are usually plotted in the above manner to indicate deviations from the simple thermal theory.

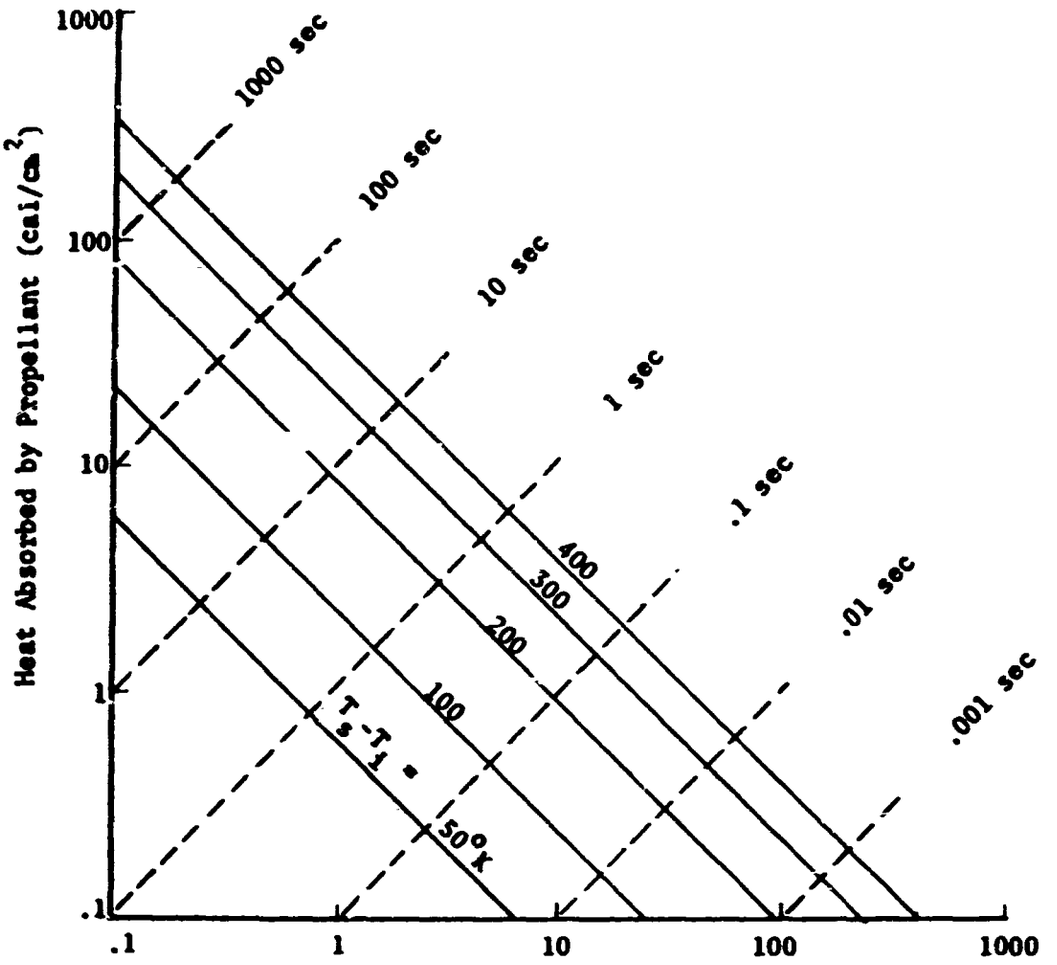

Parameter values: E/R = 25,000°K
solid density = 1.6 g/cm^3
specific heat of the solid = 0.37 cal/g-°K
thermal conductivity of the solid = 5 x 10^{-4} cal/cm-sec-°K

(from Reference 3)

Figure 2 Solutions of One-Dimensional Heating of Solid Phase, Inert Material

The Gas Phase Theory

The principal postulate of the gas phase theory (6,7,8,9) is that the rate controlling chemical reactions occur between vaporized decomposition products of the polymeric fuel and a hot oxidizing gas. This theory was originally developed in conjunction with the ignition of propellant and fuel samples in an oxygen filled shock tube. There are four variations of the gas phase theory. These variations may be classified into two categories: the convective gas phase theory (8) and (9) and the earlier non-convective gas phase theory. The most recent version (9) does not restrict the source of the oxidizing gas to the environment as do the former versions, but includes the possibility of oxidizer gas generation at the propellant-environmental gas interface. The assumptions common to all versions of the gas phase theory are: (a) the chemical heating occurs only in the gas phase, (b) the reaction rate is first order in both the concentration of the fuel vapor and in the concentration of the environmental oxygen, and (c) the mass diffusivities of all gas species are considered constant and equal to the thermal diffusivities in the gas phase (i.e. Lewis Number (Le) $\equiv \frac{D}{\alpha} = 1$). Other assumptions are made which are characteristic to a particular variation of the gas phase theory. These are described and evaluated for the two earliest gas phase theories by Price (3). The ignition criteria utilized for these theories includes both the attainment of a given value of $\frac{dT}{dt}$ and the attainment of a

fixed "ignition" temperature.

The convective gas phase ignition model as described in Reference 8 is a much more realistic model than the earlier gas phase theories. This model includes heat feedback to the fuel surface from the gas phase reaction, a temperature dependent pyrolysis rate of the fuel, and the effect of reactant consumption. While the early gas phase theory of McAlevy predicted that the ignition time is inversely proportional to the 2/3 power of oxidizer concentration, in the more recent convective theory of Reference 8 the effect of oxidizer concentration on ignition time is more complicated. Figure 3 depicts the relationship of the ignition delay as a function of the oxidizer mole fraction at constant pressure. It is observed that the slope increases with the mole fraction of oxidizer from a value approaching minus infinity to a value approaching McAlevy's limiting value of -2/3 at high mole fractions. For the same initial temperatures, activation energies, initial fuel mass fluxes, and ignition criterion ($T^* = 2700^oK$) the relationship of ignition delay as function of environmental pressure is depicted in Figure 4. The slope of the curve in this instance changes only slightly from a value of approximately -1.86. It is not surprising that the ignition time dependence is different in these two figures since changes in the total pressure alter the rate of heat transfer to the fuel surface.

The authors of the convective gas phase theory with heat feedback also note that rapid ignitions (ten to 100 milliseconds)

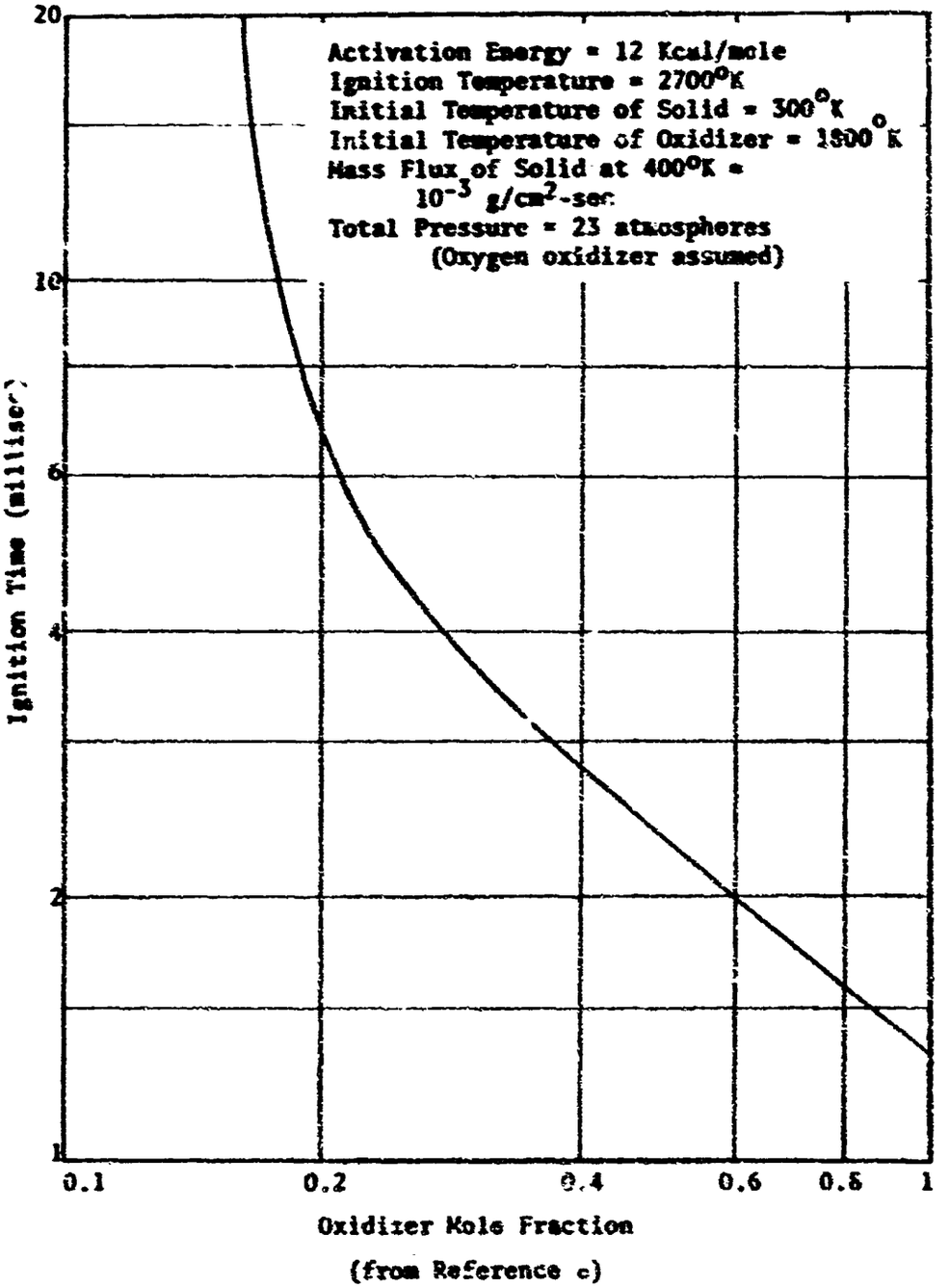

(from Reference c)

Figure 3 Ignition Time vs. Oxidizer Mole Fraction at Constant Total Pressure

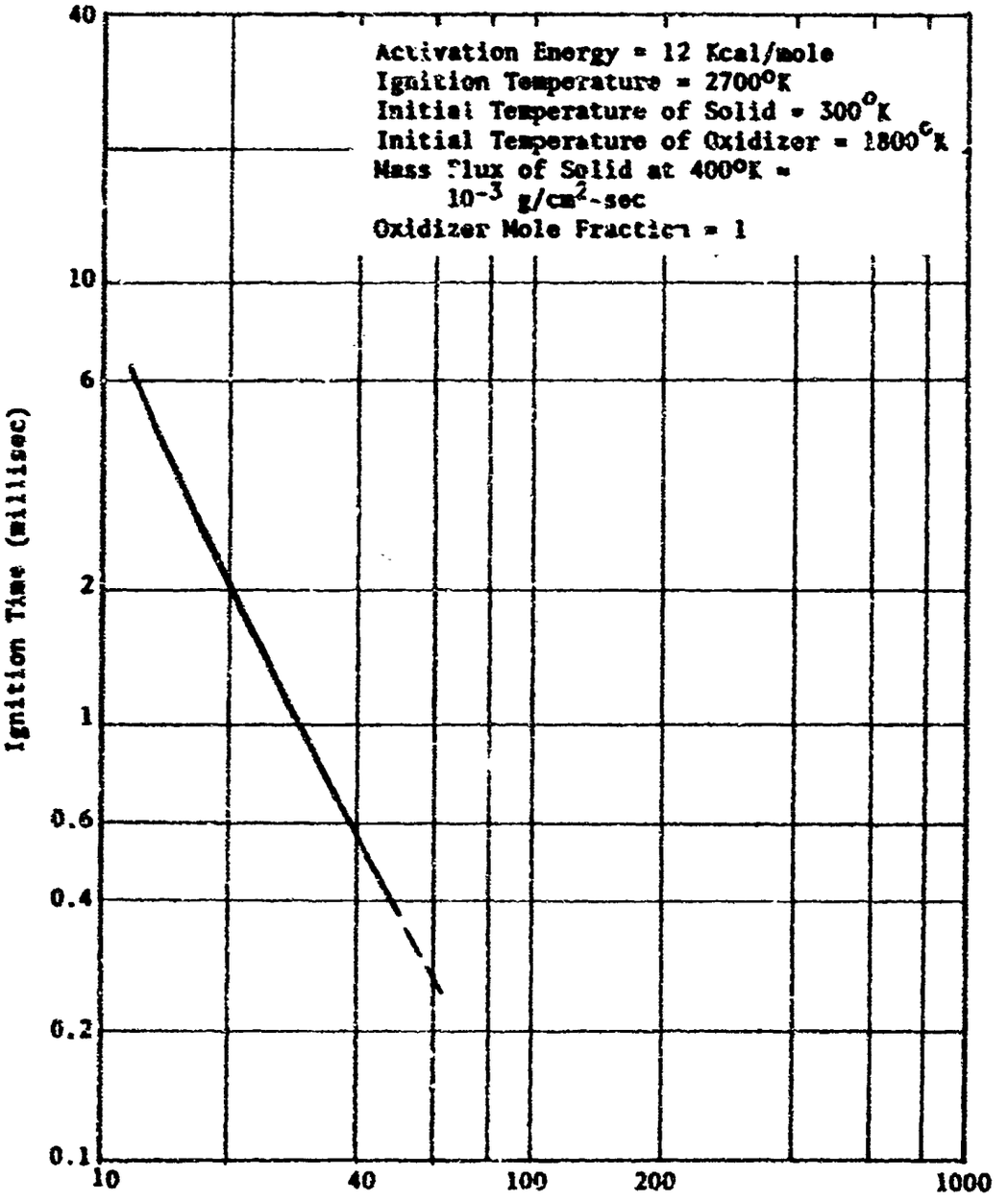

(from Reference 8)

Figure 4 Ignition Time vs. Total Pressure at Constant Oxidizer Mole Fraction

are predicted for fuel pyrolysis mass fluxes as low as 10^{-4} g/cm^2-sec. It should be noted that the activation energy, E, assumed for the fuel pyrolysis Arrhenius function is slightly less than 12 kcal/mole.

Similar to the thermal theory, the gas phase model forces the chemical heating to occur in a particular location; in this instance it is in the gas phase region.

The Hypergolic Theory

The hypergolic theory (10) was developed as a model for the hypergolic* ignition of solid propellant with powerful oxidizers (such as chlorine trifluoride and fluorine) at room temperatures. This model considers that the solid propellant (or fuel) is suddenly brought into contact with a gaseous oxidizer environment which has a fixed concentration. The chemical heating is presumed to occur in a heterogeneous reaction at the gas-solid interface, and for the simplest case the reaction rate is assumed first order with respect to oxidizer concentration.

---

* A hypergolic reaction is one which results in spontaneous ignition some time after the reactants are brought into contact at equal temperature. It is not necessary that the temperature be an arbitrarily low temperature, only that no heat transfer occurs initially between the reactants.

Other assumptions made in the model are: (a) thermodynamic and transport properties are independent of temperature, (b) chemical heating starts instantaneously upon contact of the gaseous oxidizer with the propellant, (c) the heat loss from the reaction surface is by thermal and mass diffusion (Lewis Number of unity is assumed), (d) the gaseous layer adjacent to the fuel surface and the fuel surface itself are always in thermal equilibrium, and (e) solid phase is isotropic. Since this model does not have a steady state solution, an arbitrarily high value of $\frac{dT}{dt}$ was assumed as the ignition criterion. The assumptions implict in the hypergolic model force ignition to occur at the solid gas interface.

The hypergolic ignition theory predicts that the ignition time is inversely proportional to the square of the rate of the heterogeneous reaction. For a constant initial temperature this dependence may be written $t^* = (C^o_{ox})^{-2n}$ where C^o_{ox} is the initial oxidizer concentration and n is the order of the heterogeneous reaction. The hypergolic theory does not distinguish between the methods of altering the oxidizer concentration, i. e. by changing the mole fraction at constant total pressure or by changing the total pressure at constant mole fraction.

The Heterogeneous Ignition Theory

The heterogeneous ignition theory (11) considers the ignition of a composite solid propellant which is exposed to a thermal stimulus.

This theory postulates that the controlling heat generation occurs from chemical reactions between gaseous decomposition products of the ammonium perchlorate oxidizer and the polymer surface. As in all of the aforementioned theories the analysis is one dimensional and specifies the location of the chemical heating. The chemical heating may occur either at the surface of the propellant between the gaseous oxidizer and condensed phase fuel reactants or it may occur at oxidizer-fuel interfaces in the interior of the propellant. Under conditions of low pressures or relatively weak fuel binders, the oxidizer gases which are generated within the propellant escape to the propellant surface and the predicted ignition behavior is similar to that predicted by the hypergolic theory. With high pressures or relatively strong fuel binders, the oxidizer gases which are generated within the propellant are better confined and are able to reach concentrations sufficient to assure rapid chemical heating beneath the propellant surface. For this situation the propellant is postulated to be less sensitive to the effect of external pressure because the external pressure has little effect on the concentration of the reactant gases. Although this ignition theory has been able to explain most experimental results, it should be regarded as qualitative since the values for the kinetic parameters are obtained by fitting experimental data.

The heterogeneous ignition of propellants has also been modeled by Williams (12), who presented the results of a dimensionless numerical solution in graphical form for the case of zero external

heat flux to the surface (i.e. the hypergolic case). Use of these results for predicting ignition times requires independent knowledge of the kinetic parameters of the heterogeneous reaction. Otherwise, the predicted values of ignition time may be adjusted to fit the experimental values by proper choice of activation energy and the pre-exponential factor.

Experimental Investigations

General

Many kinds of ignition experiments have been conducted on solid propellants and solid propellant motors. Some of these are (a) ignition of propellant by imbedded electrical resistance wires (13), (b) propellant ignition by hot gas generators (14), (c) ignition in shock tubes by convection and by conduction (15,16), (d) ignition by radiant energy in arc imaging furnaces or xenon lamp imaging furnaces (16,17), and (e) hypergolic ignition by flourine and chlorine trifluoride (18,19). In addition there have been extensive studies of the mechanism of decomposition of ammonium perchlorate and a few studies of a more fundamental nature such as the ignition of fuels by perchloric acid vapor.

In this section on ignition experiments only the more fundamental studies and those endeavoring to ascertain the response of the propellant to ignition stimulii will be described.

Oxidizer Decomposition

Several investigators have studied the decomposition of ammonium perchlorate (20 through 26) and the decomposition kinetics are reasonably well established for low pressures. The most recent investigators, Goshgarian and Walton (24) studied ammonium perchlorate decomposition with a Knudsen cell in a double focusing mass spectrometer. They postulate the following decomposition mechanism which occurs in three distinct rate-controlling steps.

Step I $NH_4ClO_4 \rightarrow NH_3 + HClO_4$

$HClO_4 \rightarrow HCl + 2O_2$

Step II $4NH_3 + 5O_2 \rightarrow 4NO + 6H_2O$

$2NO + O_2 \rightarrow 2NO_2$

$3NO \rightarrow N_2O + NO_2$

$2NO \rightarrow N_2 + O_2$

Step III $HClO_4 \rightarrow ClO, HClO, ClO_2, Cl_2, H_2O$

Measured activation energies of the steps one, two and three are 22.2 kcal/mole, 29.9 kcal/mole and 44.0 kcal/mole respectively. These measurements were made over the temperature range of 142°C to 252°C. The authors found that the ammonium perchlorate began decomposing at 100°C, with the nonreproducible liberation of ammonia, water, oxides of nitrogen, oxygen and hydrogen chloride. Heat treatment of the sample for 48 hours at 200°C was required before reproducible spectra could be obtained. A balanced decomposition reaction could not be written because of the fragmentation of

molecules in the ion source of the mass spectrometer and the existence of three distinct reaction rates.

An overall activation energy of 29.5 kcal/mole for the decomposition process was measured from Knudsen Cell pressures and temperatures. This value compares well with the value of 29.6 kcal/mole reported by Bircumshaw and Phillips (26).

Decomposition of ammonium perchlorate has been investigated on a very limited basis at high pressures (27). Assuming a first order overall reaction, an activation energy of 17 kcal/mole was obtained from differential thermal analyses results at pressures from 1 atmosphere to 14.5 atmospheres. These results were obtained in the temperature interval 320 to 440°C.

Thermal Degradation of Polymers

Information on the thermal degradation of polymers which are used in solid propellants is very limited at conditions of relatively low temperature (up to 280°C) and under conditions of high heating rates. Madorsky (28) presents a comprehensive summary of experimental data on the bulk thermal decomposition of polymers. McAlevy and coworkers (29,30) have investigated the thermal degradation and linear pyrolysis of polystyrene and polymethylmethacrylate. In the present report the discussion of polymer degradation will be limited to low temperature degradation of those polymers or polymer families which were utilized in the experimental programs, viz. polybutadiene and polystyrene.

Madorsky (28) reports data on the bulk pyrolysis of purified polybutadiene in the temperature range 325 to 400°C. At 325°C the

mass per cent of pyrolized product was 6.1% over a thirty minute heating period. If a linear function of pyrolysis rate versus amount pyrolized is assumed, the percentage pyrolyzed in one second is 3.39×10^{-3}%. This averaging procedure is subject to some question since at higher temperatures (380 to 395°C) the initial pyrolysis rates may be estimated to be as much as an order of magnitude higher from the data presented. On this basis a more realistic estimate of the initial pyrolysis rate of polybutadiene at 325°C would be 3.4×10^{-2}%/sec. How much lower the initial pyrolysis rates would be at 260°C is unknown.

Ryan, et al (31) have investigated the thermal decomposition of cured polybutadiene acrylic acid (PBAA) polymers under high heating rates (≈ 150°C/sec) by exposing a copper disk calorimeter coated with a thin film of polymer to the black body radiation of the interior of a tube furnace. The temperature of the copper disk was recorded as a function of time, and the first indication of endothermic reaction of the polymer was observed at a disk temperature of 290°C. The calculated surface temperature of the polymer corresponding to the endotherm was 390°C. The authors conclude that a significant fraction of the PBAA polymer does not decompose at temperatures of less than 350°C.

French and Rosborough (32) have studied the oxidation of carboxy terminated polybutadiene (CTPB) polymers. They report that although thermal breakdown occurs in uncured polybutadiene

at temperatures above 200°C, thermal breakdown of crosslinked CTPB has not been observed at temperatures up to 265°C.

Madorsky also reports data on the rate of thermal degradation of polystyrene. The lowest temperature for which degradation is reported is 290.7°C. The initial pyrolysis rate at this temperature was estimated from the initial slope of the curve of percentage of sample vaporized versus time. The value thus obtained is 1.25×10^{-6}%/sec. The activation energy given by Madorsky for polystyrene degradation is 55 kcal/mole.

The investigation of polystyrene pyrolysis by McAlevy and Hansel (29) under high heat flux conditions, indicated that the rate controlling mechanism changes at solid surface regression rates of about 3×10^{-2}cm/sec. Below this value the activation energy is about 40 to 50 kcal/mole and above this value the activation energy is about 12 to 16 kcal/mole.

Ignition of Fuels in Perchloric Acid Vapor

Pearson and Sutton (33) have investigated the ignition of fuels in perchloric acid vapor and in oxygen at one atmosphere pressure. Ignitions of typical propellant polymers were obtained at 200 to 250°C in the presence of perchloric acid vapors, while ignition of these polymers in oxygen was achieved only at temperatures above 350°C. Ignition times for these experiments were apparently measured by a stop watch or some similar technique because the values were generally reported to the nearest second

and no numerical values were reported for times less than one second. The authors also report that non-volatile fuels ignited readily with perchloric acid vapor, but that gaseous fuels ignited only in the presence of a surface at corresponding temperatures (about 200-300°C). Based on these results they concluded that a heterogeneous reaction mechanism is the most probable one for ignitions with perchloric acid vapor and for composite propellants containing ammonium perchlorate.

Hypergolic Ignition

Several investigations have been conducted on the ignition of composite solid propellants with highly reactive oxidizers such as fluorine and chlorine trifluoride (18,19,34). Data obtained with gas phase hypergolic oxidizers are usually correlated by graphs of log t^* versus log C_{ox}^o since the hypergolic ignition theory predicts that the ignition time is inversely proportional to the oxidizer concentration raised to a power equal to twice the order of the overall reaction. Figure 5 is a graph depicting this type of correlation for hypergolic ignition data.

Some investigators have reported that preconditioning of the propellant sample in an inert gas environment before exposure to the oxidizing gas (as opposed to evacuation of pre-conditioning chamber) caused an increase in the ignition time for equal values of oxidizer concentrations. The relative magnitude of the ignition time increase was greater at higher oxidizer concentrations. These results, if plotted on a log t^* versus log C_{ox}^o graph, would appear as a curve having a slope of about -2 at low

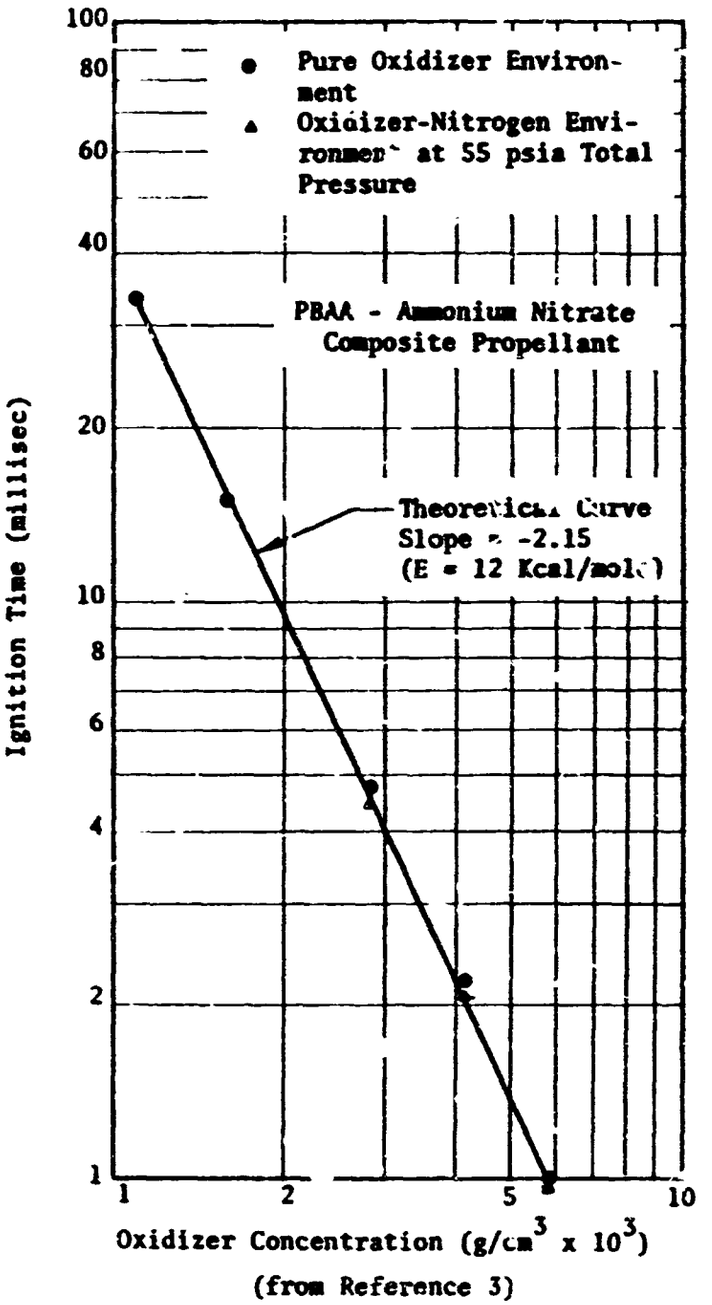

Figure 5 Ignition Time vs. Oxidizer Concentration for Room Temperature Hypergolic Ignition

oxidizer concentrations, the slope increasing toward zero at higher oxidizer concentration. The actual data are classified and cannot be presented here; however, numerical values and the conclusions drawn from these data are presented in Reference 18.

McAlevy et al (35) attempted to hypergolicly ignite polystyrene polymer in oxygen at 220°C and 14.6 atmospheres. The polystyrene was placed in a sealed glass tube which also contained an environment of nitrogen at one atmosphere. After conditioning this tube to the prescribed temperature within the hot oxygen environment, the tube was broken. No sign of ignition was observed. The authors concluded from this experiment that it was highly unlikely that hetergeneous reactions between oxygen and propellant surfaces could lead to ignition.

Ignition by Radiant Heat Fluxes

Propellant ignition by radiant energy has been investigated at several laboratories, e.g. (16,17,36). The apparatus employed for ignition testing has usually been a double ellipsoidal imaging furnace (37) employing either a carbon arc or a xenon lamp energy source. Ignition data obtained by radiant energy stimulus is usually correlated by graphs of log ignition time versus log of environmental pressure. An example of the this type of correlation is depicted in Figure 6. The ignition time dependence upon heat flux, q, and pressure, p, has been qualitatively explained by the heterogeneous ignition theory as

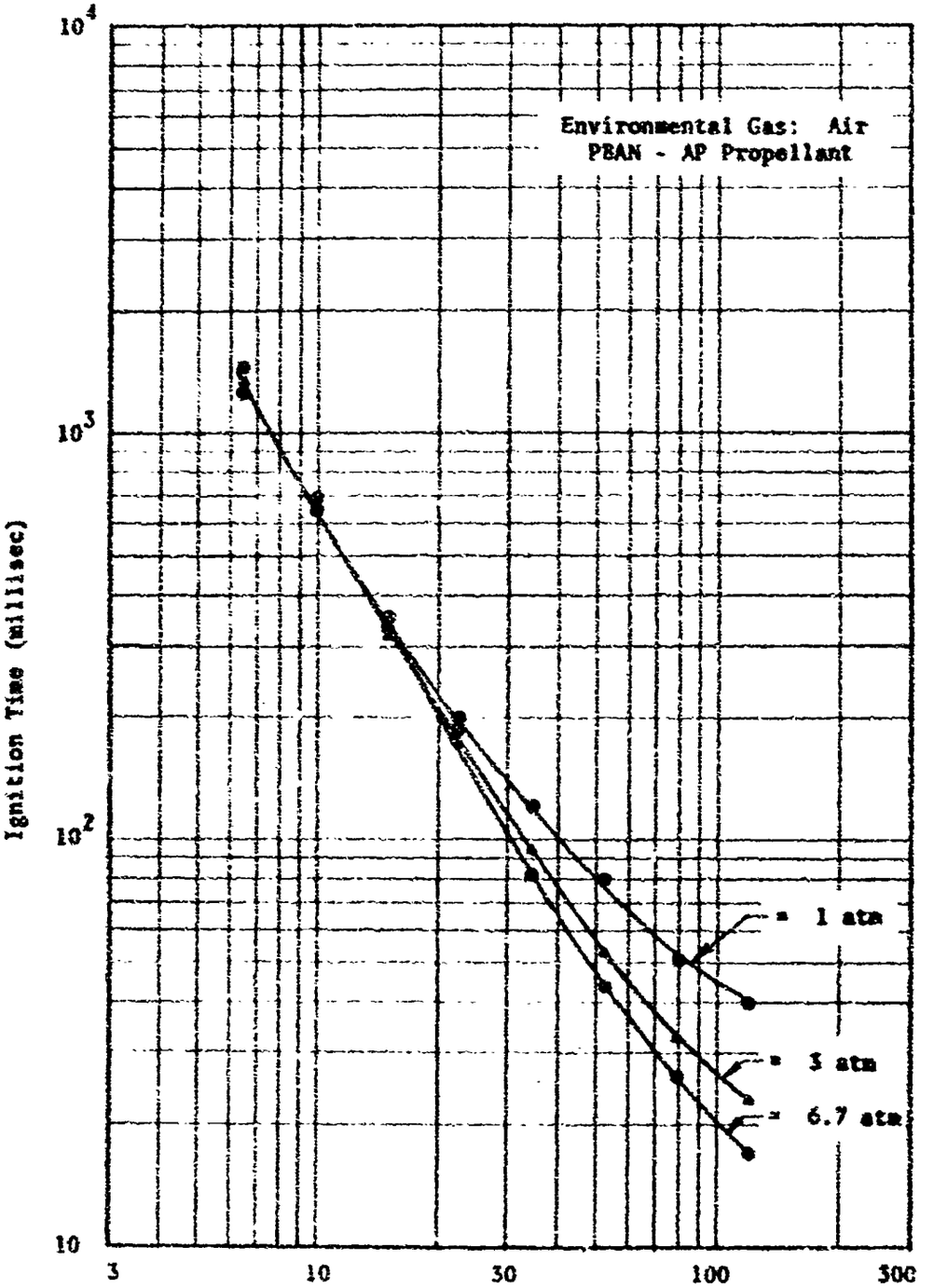

(data from Reference 16)

Figure 6 Ignition Time vs. Radiant Heat Flux Depicting Effect of Environmental Pressure

described earlier.

Testing of solid propellant ignition with arc imaging furnaces has been proposed as a standard technique throughout the propulsion industry for determination of propellant ignitability. Heat flux calibration between different laboratories is one of the many unsolved problems in this area. Summerfield and Ohlemiller recently have published a critical analysis of the arc imaging ignition testing technique (38).

Ignition in Shock Tubes

Solid propellant ignition has been studied with shock tubes in both inert and reactive environments (6,7,15,27). Propellant samples have been mounted both in an end wall configuration for conductive heating studies and on a probe in the shock tunnel mode of operation for convective heating experiments. Shock tunnel results of the convective heating mode have been correlated by Keller (15) using graphs of log ignition time to the one-half power versus log heat flux. Typical ignition results of this type are presented in Figure 7. Recall that this type of correlation is suggested by the solid phase thermal theory. For the experimental data depicted in Figure 7, nitrogen was employed as the environmental gas and therefore the chemical heating effect due to an external oxidizer was absent.

Shannon (27), however, utilized varying mixtures of nitrogen and oxygen in shock tube experiments to ignite samples of pro-

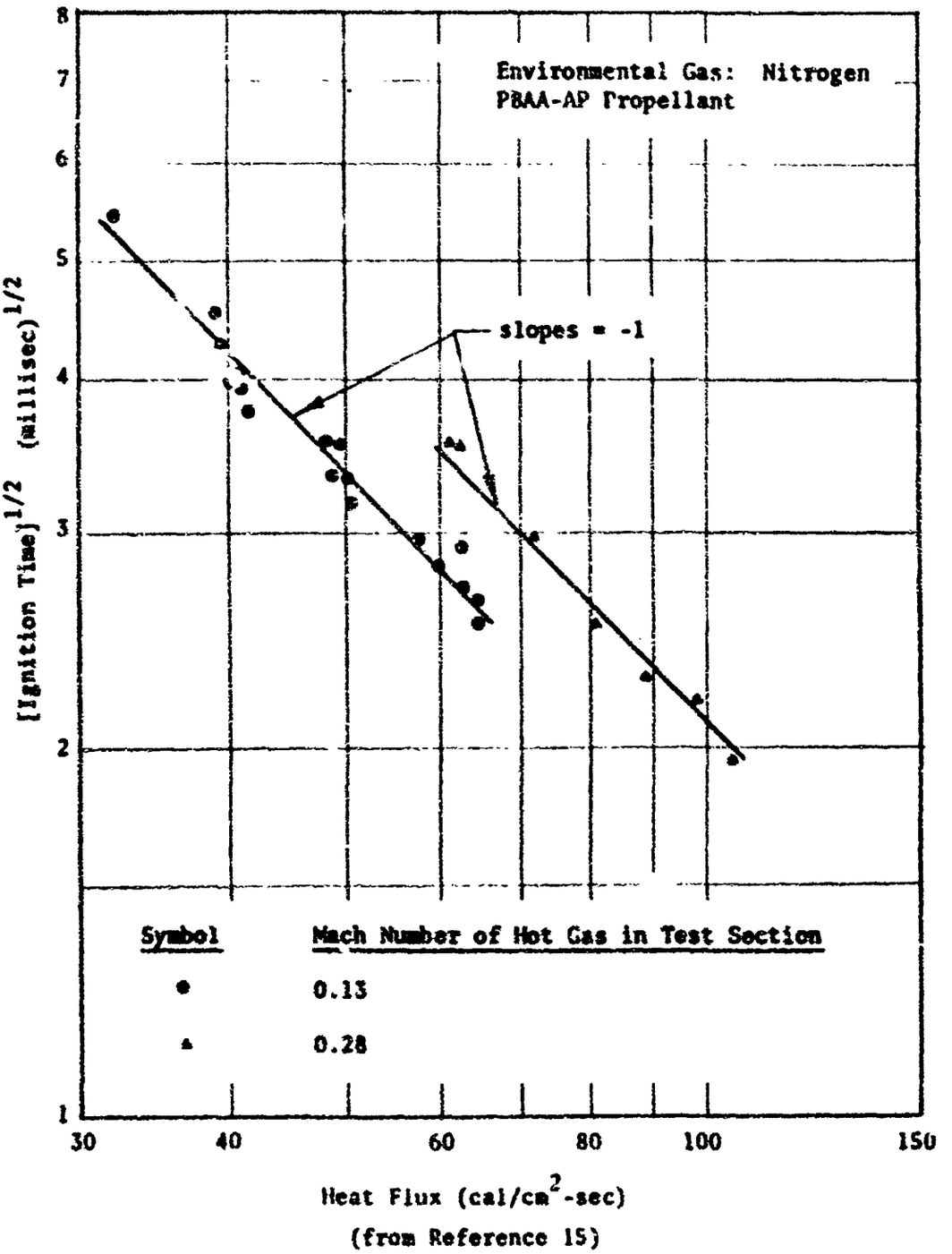

Figure 7 Square Root of Ignition Time vs. Heat Flux for a PBAA-AP Propellant in a Shock Tube

pellant and polymer which were mounted in the end wall configuration. These data are correlated by a graph of log ignition time versus log oxidizer concentration in the same manner as the hypergolic ignition theory. Results for twelve different combinations of propellant and surface preparation were reported. The straight lines fitted to these data have slopes of -1.1 to -1.6, which according to the hypergolic theory suggests an overall fractional order reaction. Shannon's data for CTPB-AP propellant are presented in Figure 8.

McAlevy utilized an oxygen filled shock tube and obtained ignition data for solid propellant fuels and polymers in an end mounted sample configuration. These data were correlated by graphs of log ignition time versus log oxygen weight fraction. Converted to absolute oxygen concentrations, data for a polystyrene fuel and a polystyrene-AP propellant are also presented in Figure 8. The slope of the lines fitting the polystyrene is approximately -2.1.

Summary and Comments

There has been much controversy between investigators over the nature of the rate controlling process in solid propellant ignition. The controlling heat generation must come from a heterogeneous reaction if one adopts the following definition due to Levenspiel (39).

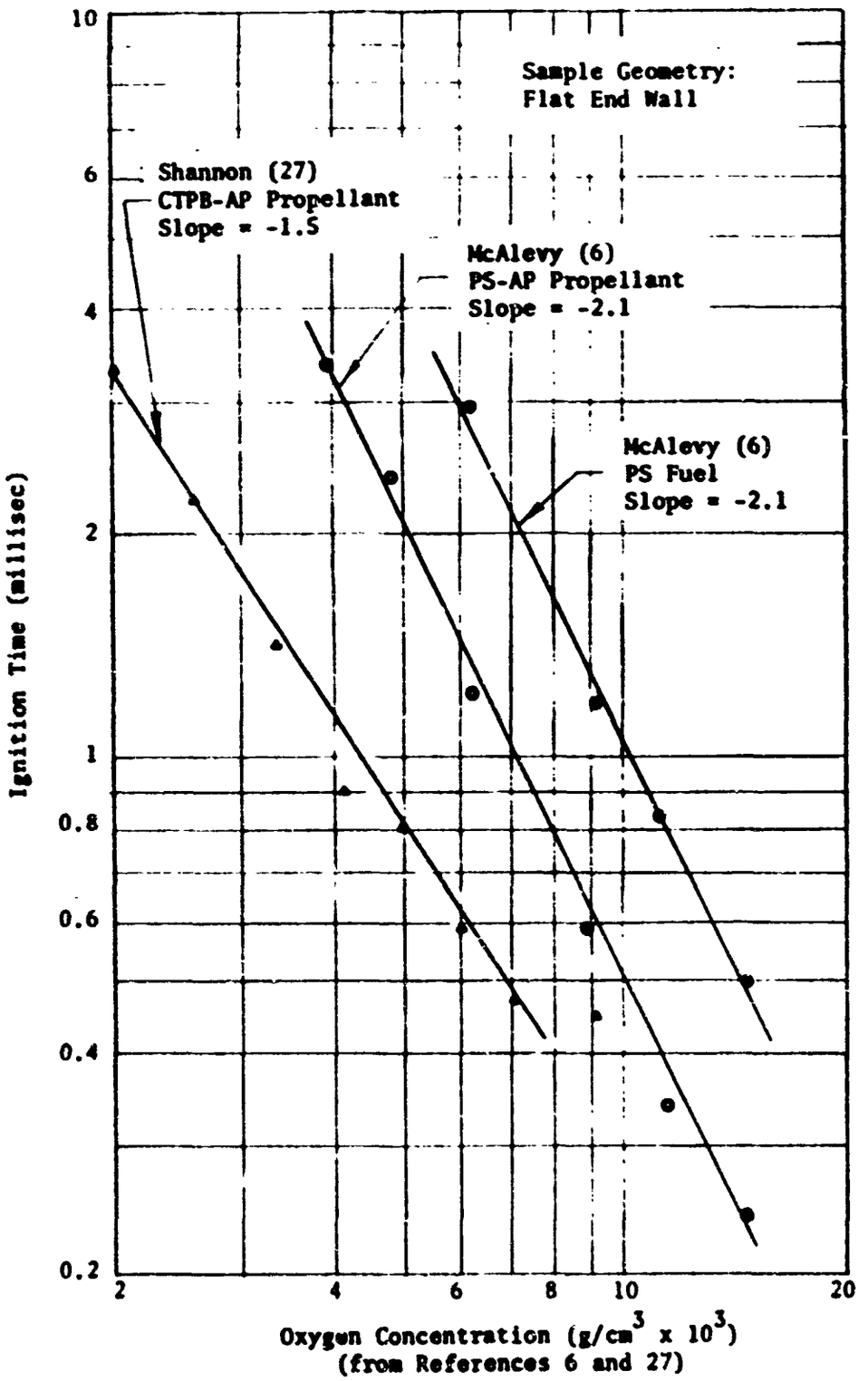

Figure 8 Ignition Time vs. Oxygen Concentration for End Wall Samples in Shock Tubes

> A reaction is heterogeneous if it requires the presence of at least two phases to proceed at the rate that it does. It is immaterial whether the reaction takes place in one, two, or more phases, or at an interface, or whether the reactants and products are distributed among the phases or all contained within a single phase.

Still, with this definition in mind, the question arises regarding the location of the principal source of exothermic reaction. It is evident from the preceding review that the location of these reactions is a strong function of the experiment, i.e. ignition stimulus, applied heat flux, external oxidizing gases, e

Although it is generally accepted that the more reactive oxidizers ignite solid propellants and solid fuels via a surface reaction, the existence of surface ignition reactions between oxygen and polymeric fuels at temperatures within the lower portion of the temperature range for ammonium perchlorate decomposition (260-320^{o}C) has not been demonstrated. The next section of this report describes the approach employed in this investigation of such reactions.

METHOD OF INVESTIGATION

General

The experimental investigations may be conveniently separated into two parts: (1) the experimental determination of ignition time as a function of the type of polymer, oxidizer species, initial temperature, initial pressure, and oxidizer concentration; and (2) the experimental determination of the pyrolysis products of three different polymers at temperatures equivalent to those at which ignition was obtained. The ignition experiments were conducted in a test apparatus especially designed for this purpose, and the pyrolysis product experiments were performed utilizing a time-of-flight mass spectrometer (TOFMS).

Ignition Experiments

Design Criteria

The ignition test apparatus (for convenience hereafter referred to as ITA) was designed to provide for "instantaneous" exposure of a polymer or propellant sample to a gaseous oxidizing environment and permit testing up to pressures of twenty atmospheres and up to temperatures of 260°C. The aforementioned value of pressure was chosen because previous experimental data have shown

that the ignition delay becomes insensitive to pressure changes above about twenty atmospheres. The design temperature was restricted to 260°C because of the physical limitations of o-ring seals.

Ignition Test Apparatus

The ignition test apparatus, ITA, described here is similar to that utilized in the hypergolic ignition investigations of Miller (18), in that a pneumatic cylinder was employed to transfer the sample of polymer or propellant into the oxidizing environment. The sample is mounted on the end of a shaft and is rapidly transferred from an inert environment into the oxidizing environment by shearing a burst diaphragm which separates two environmental chambers. Figure 9 is a photograph of the ITA illustrating all of the major components. The ITA is composed of five integrated sub-systems: (1) the pressure vessel assembly, (2) the thermal control system, (3) the pressure control system, (4) the kinematic system and, (5) the instrumentation system. Each of these sub-systems is described in Appendix B.

The sample chamber assembly consists of two chambers which are joined together with a quick detachable V-clamp: an inert chamber for sample conditioning and an oxidizer chamber containing the reactive gas species. The gases in the two chambers are separated by either one or two metal foil burst diaphragms. The pressure in the chambers may be varied over the

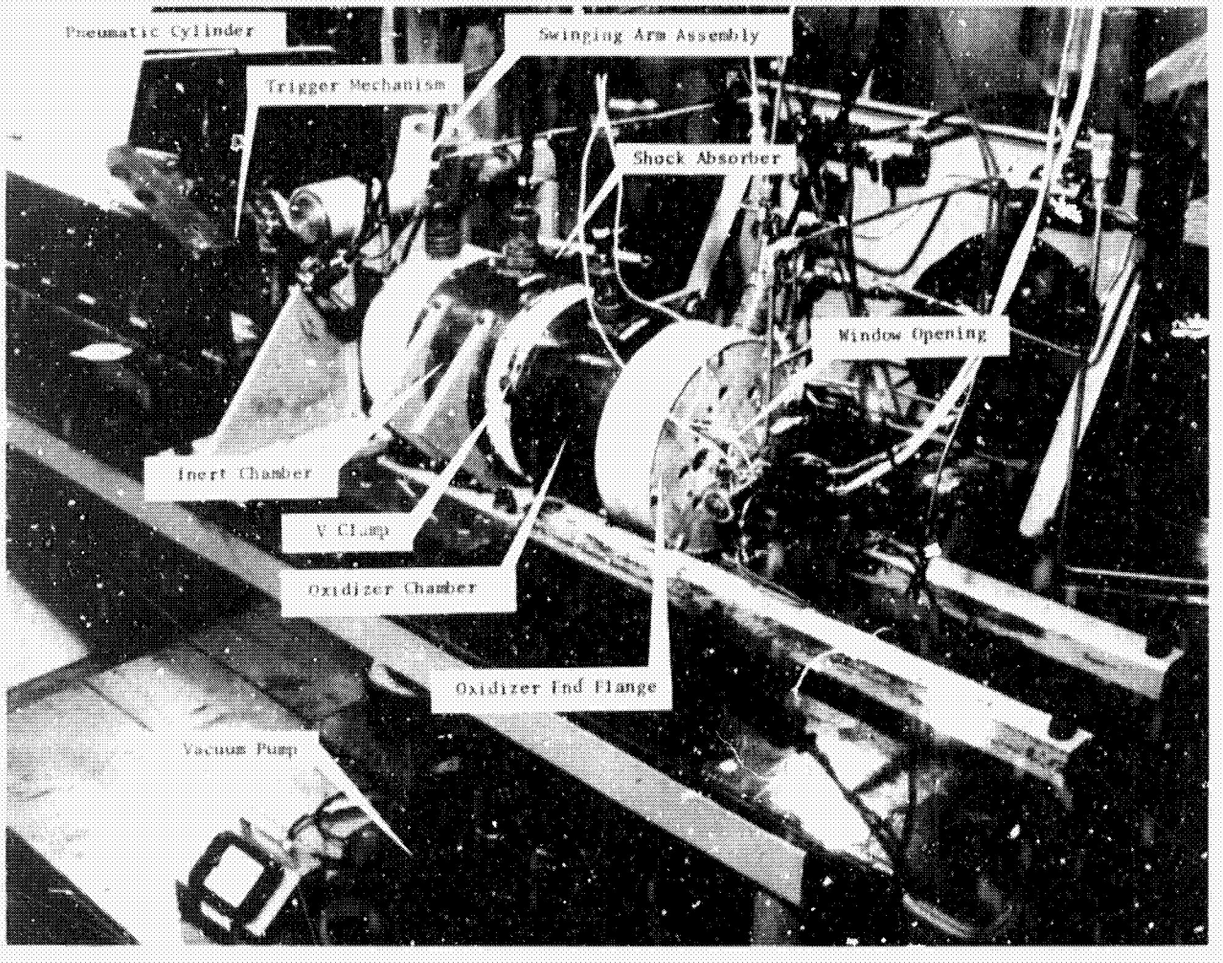

Figure 9 Photograph of Ignition Test Apparatus

range one to twenty atmospheres, and the temperatures of the inert and reactive environments may be independently varied over the range from room temperature to 260°C.

The sample of polymer or propellant is mounted in a sample holder which in turn is attached to the end of the sample shaft. The piston rod of a pneumatic cylinder is connected to the other end of this sample shaft. Release of the piston rod by a trigger mechanism accelerates the sample shaft and transfers the sample from the inert chamber through the diaphragm and into the oxidizing chamber. A shock absorber decelerates the moving parts and the sample holder comes to rest in the reactive chamber against a small annular cylinder which is mounted on the oxidizer chamber end flange. The volume of oxidizer gas enclosed by the sample holder, inner surface of the annular cylinder, and wall of the end flange is 8 cm^3. A pyrex or quartz window is mounted in the center of the end flange permitting observation of the sample from the time it enters the oxidizing chamber.

Ignition times are recorded on an oscillograph and are measured from the time the sample is exposed to oxidizing gas until an output signal is obtained by a photodetector. Two types of photodetectors were utilized, a photodiode which is sensitive in the visible and near infrared spectrum and an ioniziation detector sensitive in the ultraviolet spectrum. Ignition signals were detected at the same times with both devices.

A description of the experimental procedures employed for both the oxygen and chlorine ignition tests is presented in Appendix C.

Sample Preparation

Three types of polymers were utilized: polybutadiene acrylic acid (PBAA), carboxy terminated polybutadiene (CTPB), and polystyrene (PS). At room temperatures the PBAA and CTPB polymers are rather soft and rubbery while the PS polymer is hard and brittle. Samples of the rubbery polymers were prepared by cutting small cylinders from a 3/4 inch thick slab of the polymer gum stock using a modified cork borer. These cylinders were then trimmed to the shape of a right truncated cone of the correct size by employing a special jig. An industrial single edged razor blade (without a polymer coating) was utilized for the latter trimming process. The PS samples were machined from solid rod into the truncated cone shape.

Figure 10 is a sketch of the sample holder assembly. The retaining cap (see Figure 10) is attached to the shaft end piece with a two pin bayonet type arrangement similar to that used for the bases of miniature electric lamps. After being assembled in the sample holder, the projecting surface of the rubbery samples was trimmed with a razor blade to assure a clean surface. In the case of the PS sample a rinse with absolute ethanol and thorough drying was substituted for the surface trimming procedure.

Mass Spectra of Polymers

Mass spectra of the pyrolysis products of the three polymer samples were obtained under heating conditions similar to those

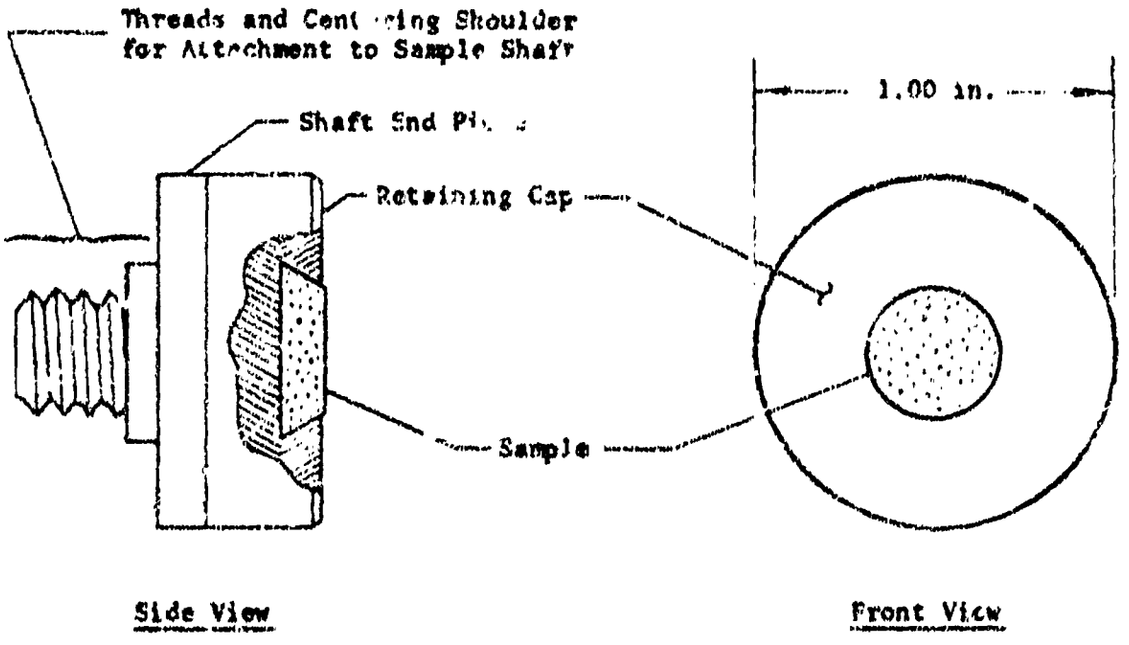

Figure 10 Sketch of Sample Holder Assembly

encountered by the polymer samples in the ITA. A Bendix Model 12-107 time-of-flight mass spectrometer was utilized to generate the mass spectra. The spectra were recorded on a Honeywell Viscorder, Model 1508.

Pyrolysis products in equilibrium with one atmosphere of helium were admitted to the ion source of the TOFMS through a Granville-Phillips variable molecular leak. The arrangement of the sample inlet system is depicted in Figure 11. A 1/8 inch diameter stainless steel rod is located inside the heated 1/4 inch tubing to permit the sample to be disturbed after a time period of 8 minutes has elapsed at 260°C. This disturbance is intended to simulate the fresh surface condition which will be described later in the experimental results.

Rectangular parallelepiped samples of polymer about 1 cm long and having a 2 mm square cross section were prepared. The CTPB and PBAA samples were freshly cut on all surfaces with a new razor blade that did not have a polymer coated edge. The PS sample was filed to final dimensions, washed in absolute ethanol, and then dried. After final cutting and cleaning the samples were handled only with clean tweezers.

Nine sets of mass spectra were recorded for each polymer. Each set of spectra consisted of two scans of the spectrum in the mass to charge (m/e) interval 4 to about 240. The first scan was made to low gain to permit measurement of the more intense peaks

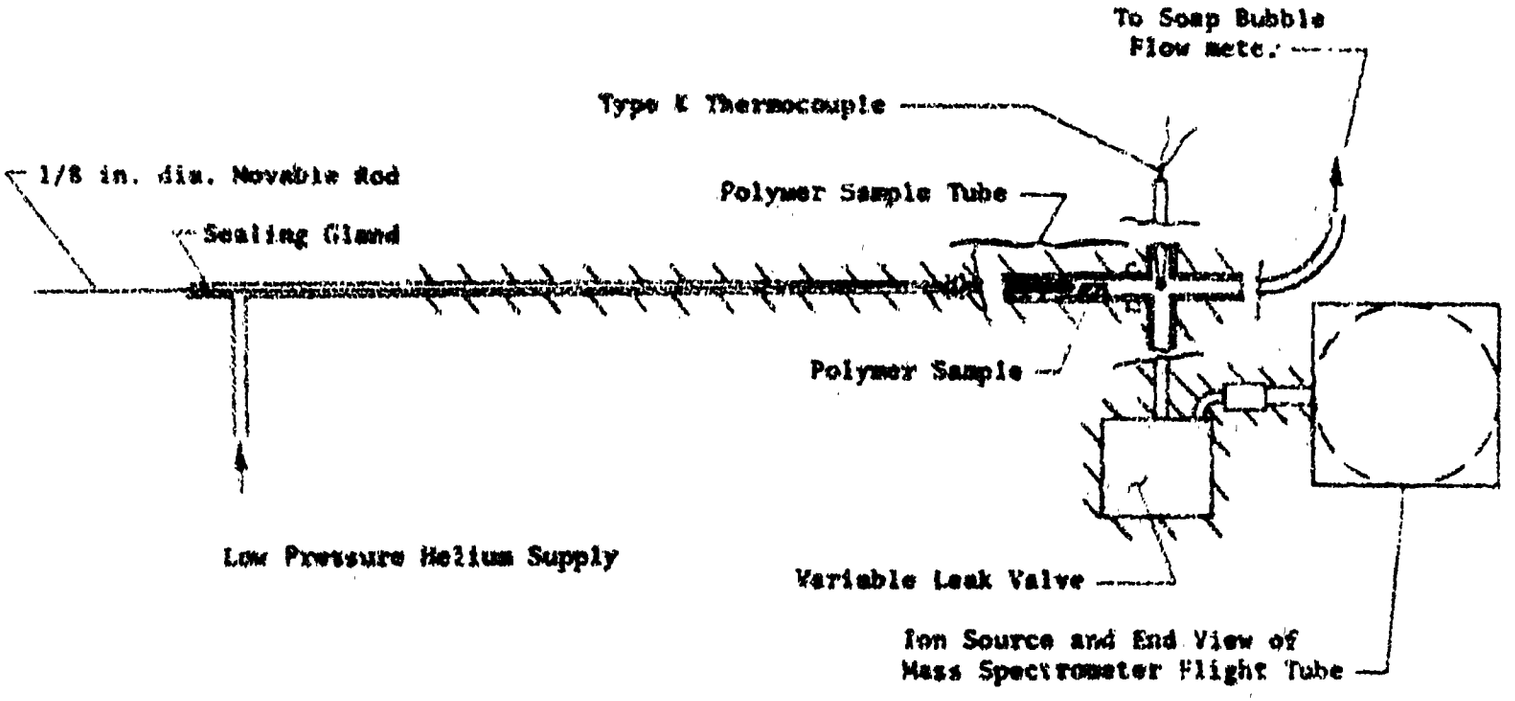

\\\\\ Denotes Heated Region

Figure 11 Mass Spectrometer Sample Inlet System

and the second scan was made at high gain to permit measurement of the low intensity peaks. For each polymer, the scans were numbered consecutively so that scans 1 and 2 represent a single set of mass spectra. In the following description of the method employed for obtaining mass spectra, each set of spectra will be identified by its pair of scan numbers.

The method of obtaining the mass spectra data follows. All components of the inlet system that were to be subjected to heating were first thoroughly cleaned, dried and if necessary baked out under vacuum to minimize the background spectrum in the TOFMS. The polymer sample tube was installed without a sample and a steady flow of helium was established past the entrance to the variable leak. The variable leak was then opened until the helium peak reached a predetermined magnitude. Background spectra were recorded at room temperature (scans 1 and 2) and with the inlet system heated to 260°C (scans 3 and 4).

Next, the inlet system was cooled to about room temperature, and a polymer sample was installed in the polymer sample tube. A new sample tube was employed for each polymer sample. Steady flow conditions were again established in the inlet system at approximately the same flow rate as that used for the background spectra.

For each polymer, spectra were recorded under the following conditions.

(1) Before starting the heating cycle (scans 5 and 6).

(2) During heating at about 150°C (scans 7 and 8).

(3) Upon first reaching 260°C (scans 9 and 10).

(4) After eight minutes at a temperature of about 260°C (scans 11 and 12).

(5) Just after recording the above spectrum, the sample of polymer was disturbed by pushing the sample with the 1/8 in diameter rod, thus exposing a fresh surface in the case of the molten CTPB and PS samples. Spectra were then recorded immediately (scans 13 and 14).

(6) Five minutes after the disturbance of the sample (scans 15 and 16).

(7) Ten minutes after the disturbance of the sample (scans 17 and 18).

The results of both the ignition experiments and the mass spectrometer experiments are presented in the next section of this report.

EXPERIMENTAL RESULTS

Ignition Experiments

General

Ignition experiments were conducted with two types of polymer samples, a carboxy terminated polybutadiene (CTPB) and a polybutadiene acrylic acid (PBAA). In addition a few experiments were conducted with polystyrene (PS) in oxygen for purposes of comparison with other ignition data. Detailed information about the polymers is presented in Appendix D.

As with other hypergolic ignition data, these data are presented as ignition time, $t^{\bullet}$, versus initial oxidizer concentration, C_{ox}^{o}. Chlorine and oxygen were used as oxidizers.

Ignition in Oxygen

CTPB Polymer. Sixty-two ignition experiments were conducted with the CTPB polymer. Fifteen of these experiments were considered invalid with respect to ignition time measurement because of various experimental difficulties. Of the remaining forty-seven experiments, ignition was obtained in twenty-five instances. Seventeen of these ignitions occurred under hypergolic conditions. These ignitions occurring under non-hypergolic conditions are not discussed here but are presented in the tabulated data, Appendix G.

No ignitions of the CTPB polymer were obtained at temperatures lower than 260 °C or at oxygen concentrations lower than 6.5 x 10^{-3} g/cm^3.

At 260°C the CTPB polymer became a thick viscous liquid and in experiments having nitrogen in the inert chamber it was noted that the molten polymer was enclosed by a thin flexible solid crust or skin after heating. This crust or skin was believed to be caused by diffusion of nitrogen into the polymer and subsequent chemical reaction. Helium was investigated as an alternate gas for heating of the propellant sample in the inert chamber. When helium was utilized, no crust or skin was apparent on the polymer surface after the heating cycle. No ignitions were obtained with nitrogen employed as the inert gas; however, the most severe initial test conditions were 260°C at five atmospheres pressure. All ignition tests subsequent to the solution of the polymer crust problem were performed with helium in the inert chamber.

It was also observed that ignition of the CTPB samples did not occur unless the molten sample was substantially deformed and a "fresh*" surface of the polymer was exposed to the oxygen.

---

* The term "fresh" surface is used here to describe a surface having no adsorbed molecules.

The significance of the surface condition will be discussed later.

The results of those experiments in which ignition occured under hypergolic conditions at a temperature of approximately 260°C are presented in Figure 12. As will be noted, the scatter in the experimental data is rather large. The major part of this scatter is believed to be due to small temperature variations the initial conditions. For the majority of the data, the inert and reactant chambers of the test apparatus were heated to 260°C from room temperature in about forty minutes. Since the rate of temperature rise in the last few minutes was less than 3°C/min, it was believed that the surface of the polymer was in substantial thermal equilibrium with the helium gas at least within the accuracy of the temperature measurment (about ± 3°C). To check this condition of thermal equilibrium, additional experiments were performed in which the temperature of the inert chamber was held constant at the prescribed test temperature for a minimum of eight minutes before exposing the sample to the oxygen. For future convenience these heating conditions will be described as slow and those for the majority of the data points will be described as normal. The data obtained with the slow heating conditions are repeated in Figure 13. It may be observed that the scatter of the data is reduced considerably under these conditions.

Figure 14 presents the averaged values of the ignition times for the slow heating data as a function of oxygen concentration.*

---

* Ignition time averaging is a common procedure employed to reduce the scatter of data and make the trend of the data more apparent (6,27).

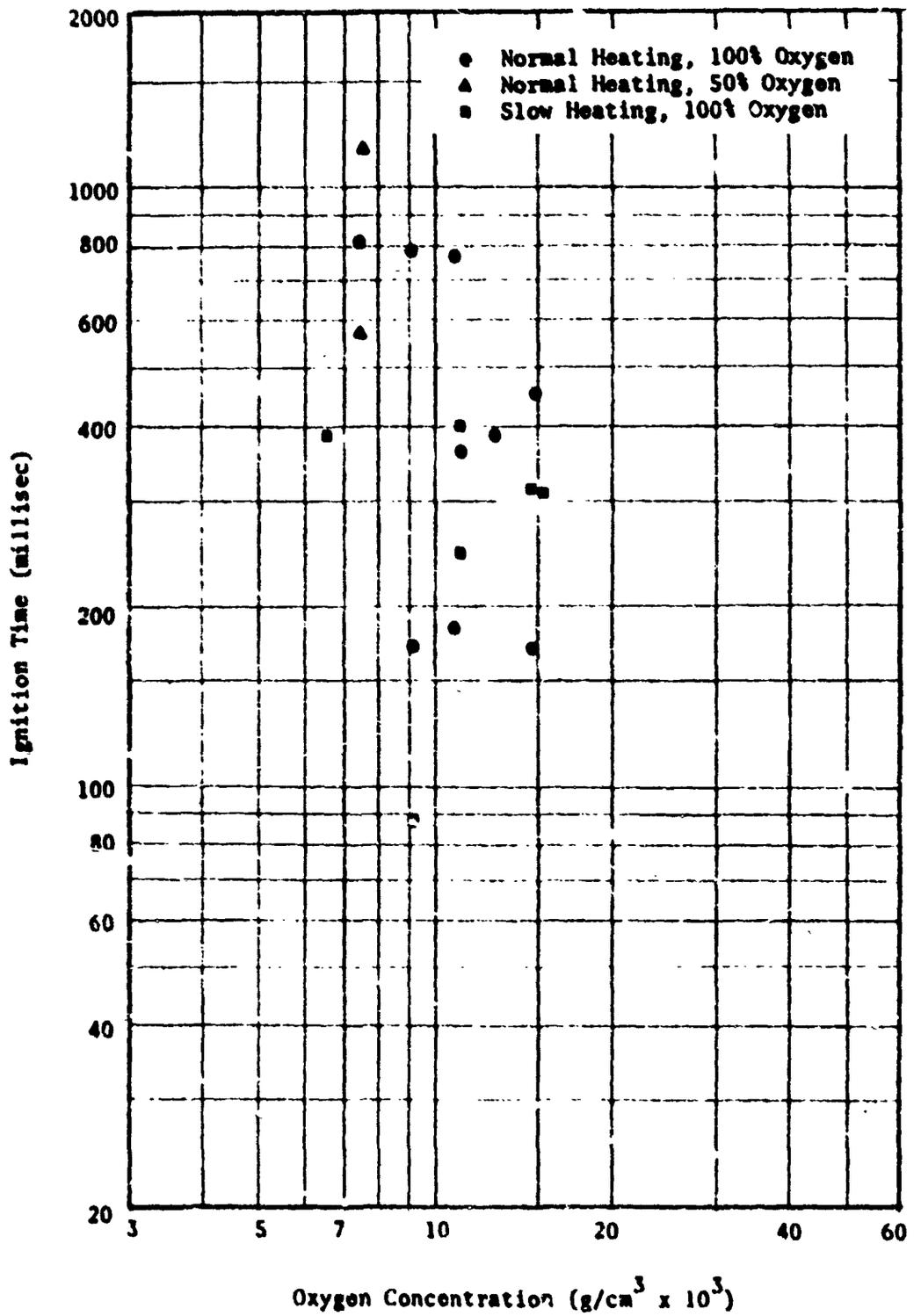

Figure 12 Hypergolic Ignition Data for CTPB Polymer

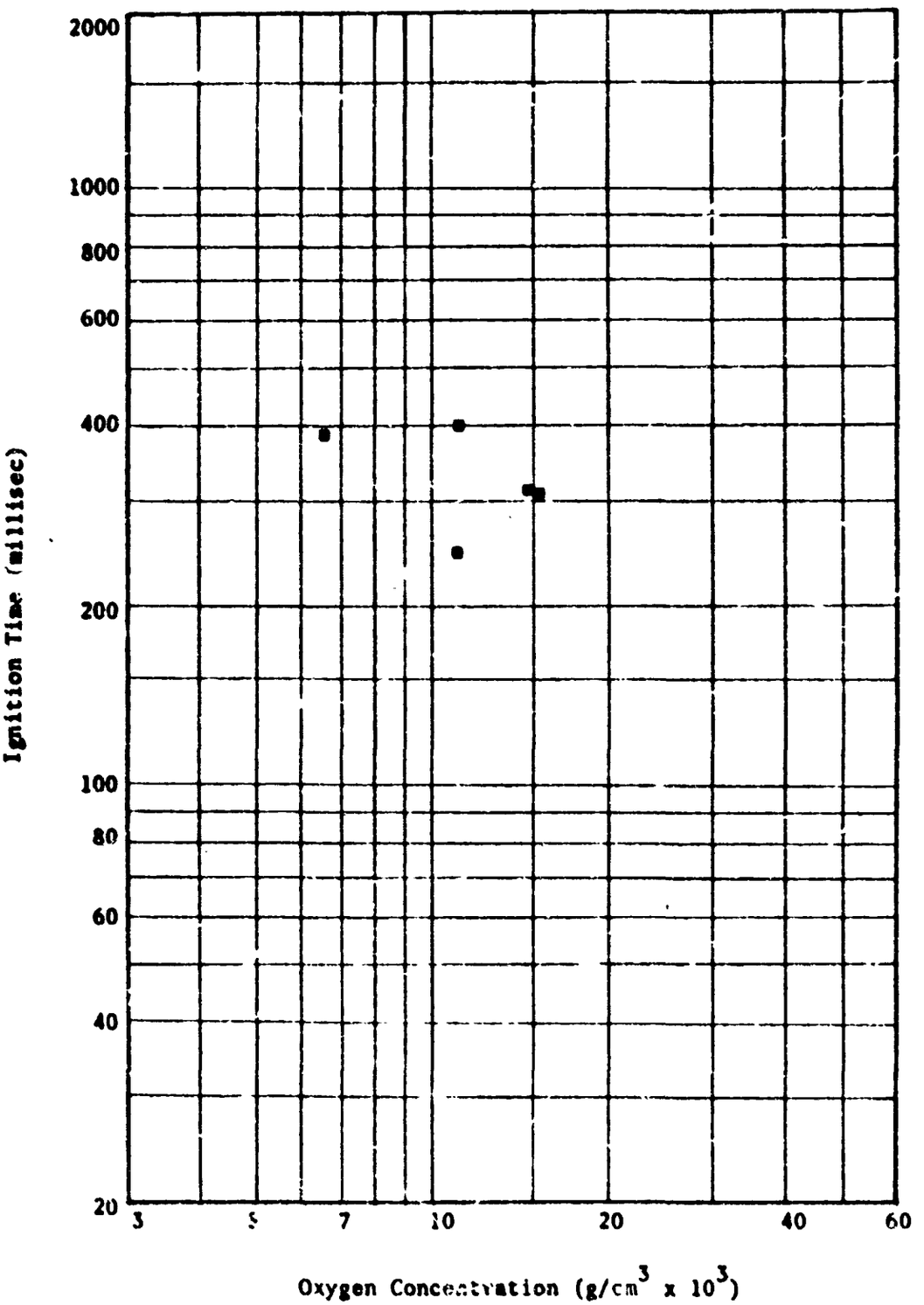

Figure 13 Hypergolic Ignition Data for CTPB Polymer (Slow Heating Data)

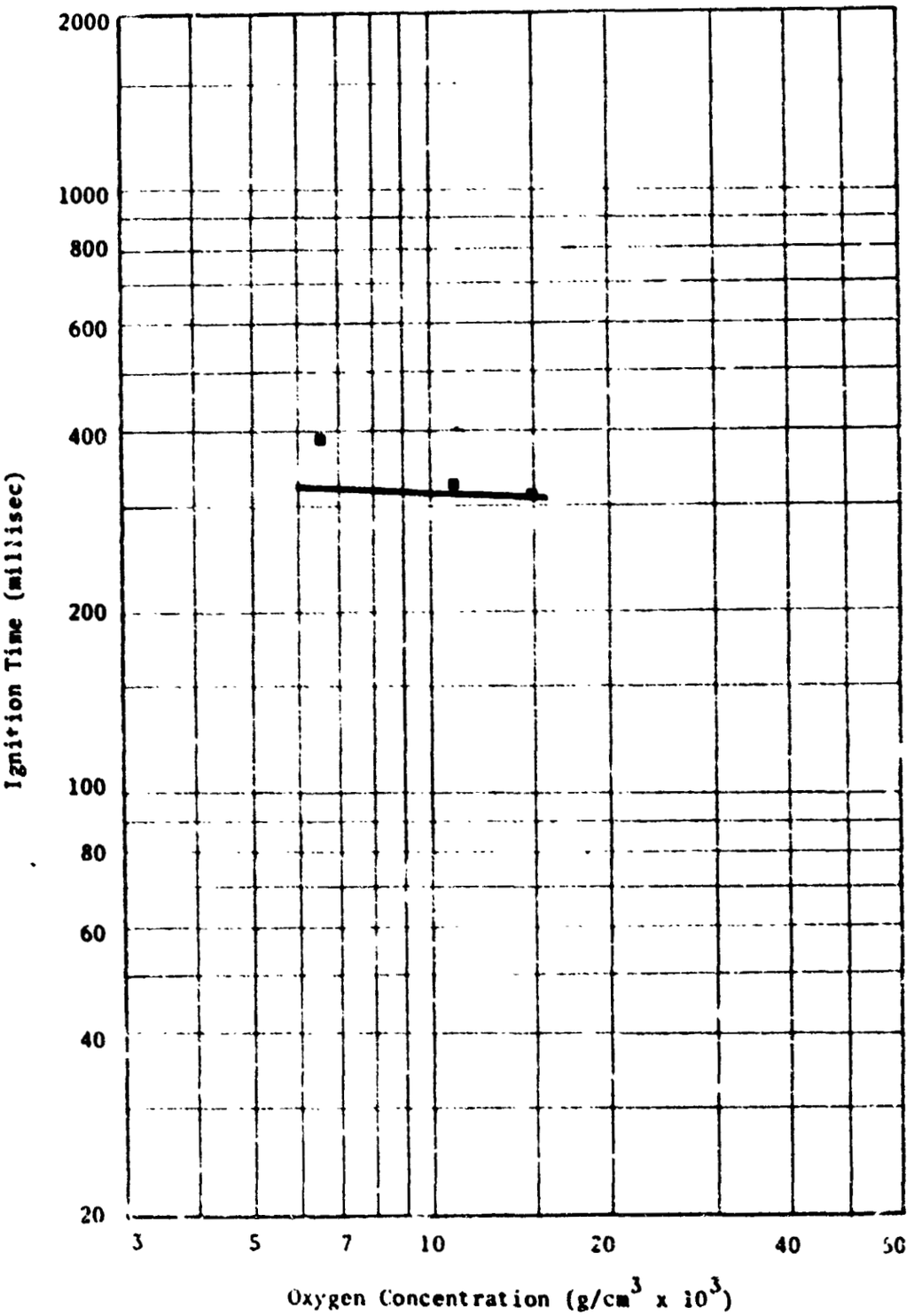

Figure 14 Hypergolic Ignition Data for CTPB Polymer (Averaged Slow Heating Data)

These averaged data now appear more consistent. The equation of the least squares fit of the original data is $t^* = 0.246(C^o_{ox})^{-0.05}$. Because of the few datum points and the large scatter of these data, not much importance should be attached to the numerical value of the slope in the least squares fit. The important feature is that the data exhibit a low fractional order dependence of oxidizer concentration on ignition time.

PBAA Polymer. Fifteen ignition tests were conducted with the PBAA polymer in oxygen environments. Four of these tests were invalid because of equipment or instrumentation difficulties. Six ignition data points were obtained under hypergolic conditions at temperatures of 260°C and in the pressure range ten to twenty atmospheres. Four experiments were conducted with oxygen-helium mixtures at 260°C and twenty atmospheres total pressure; three of these at oxygen mole fractions of 0.5 and one at 0.75. No ignitions were obtained in any of these mixed gas experiments. One experiment was conducted at twenty atmospheres and at a temperature of 321°C. The ignition time for this test was 0.014 sec. It was observed that the PBAA polymer remained a solid for all initial test conditions.

Figure 15 presents all of the ignition data obtained under slow heating conditions for the PBAA polymer in oxygen. For the 260°C data, averaging the ignition times at fixed concentrations results in three points which closely fit a straight line. However, the line drawn in Figure 15 is a least squares fit to the actual data. The equation of this

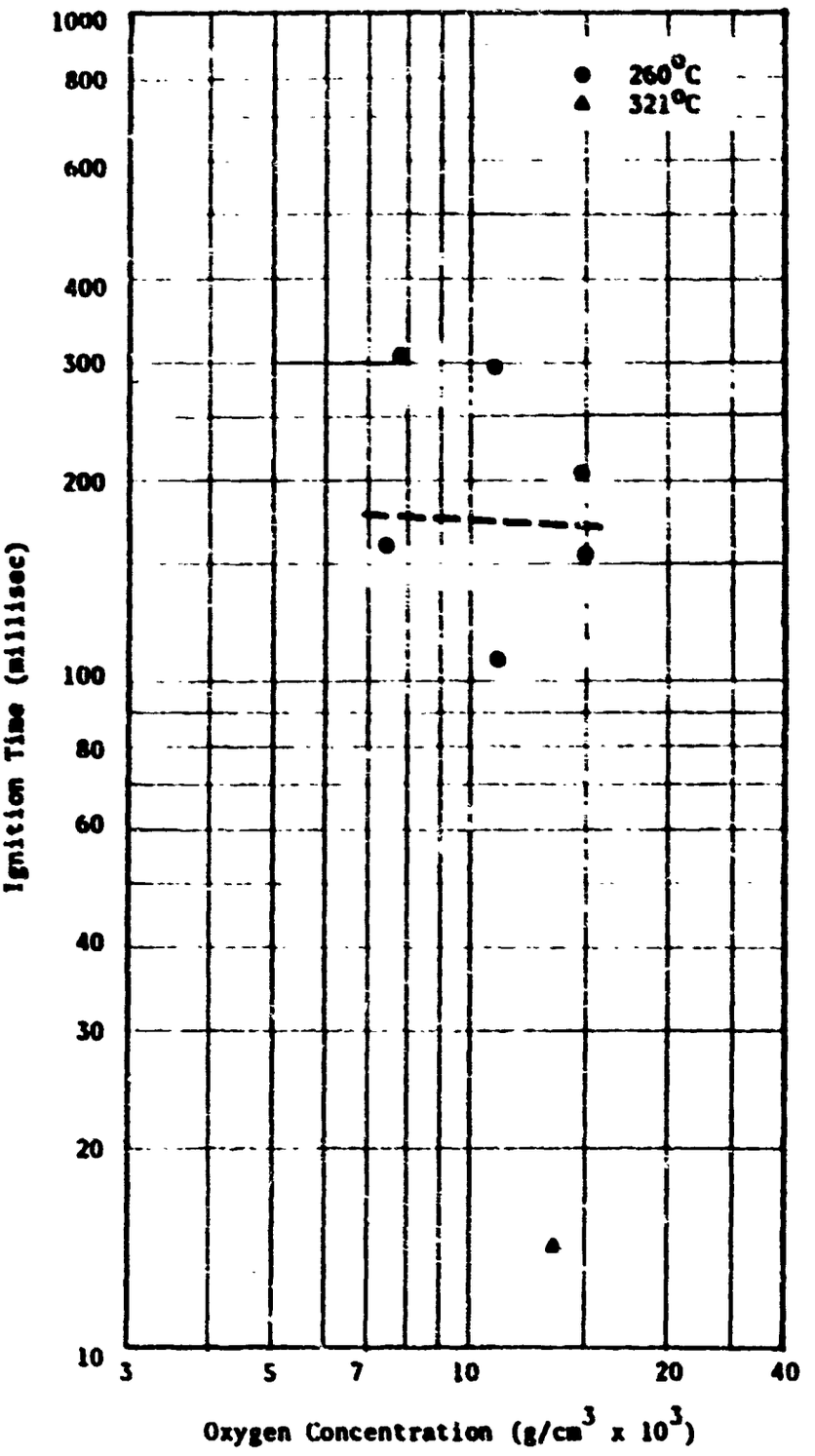

Figure 15 Hypergolic Ignition Data for PBAA Polymer

line is $t^{\bullet} = 0.139\ (C_{ox}^{o})^{-0.05}$. As in the case of the CTPB polymer, the scatter in the PBAA data reduces the confidence in the numerical value of the slope. Again the important feature is the low fractional order of the dependence of oxidizer concentration on the ignition time.

Polystyrene Polymer. Only five ignition experiments were conducted with polystyrene polymer, four under hypergolic conditions. All of these experiments were performed within the temperature range 236°C to 260°C and within the pressure interval of fifteen to twenty atmospheres. The polymer melted into a viscous liquid in all of these experiments. One experiment was performed at fifteen atmospheres and 236°C to approximate the conditions of McAlevy, et al (35). No ignition was obtained under these conditions. The four other experiments were conducted at twenty atmospheres and 260°C. Two of these tests were invalid due to the burst diaphragm sticking to the molten polymer and preventing oxygen from reaching the sample surface. However, in one of the two remaining tests ignition was obtained. The ignition time was greater than 18.1 seconds (the time at which the recording oscillograph was automatically turned off) and less than about four to five minutes (the elaspsed time before the sample was observed during the disassembly of the ignition apparatus).

The sample of polystyrene which was ignited was examined closely. The combustion at the sample surface had occured only

in a region of the surface which had been deformed during deceleration to expose a fresh surface. Adjacent areas of the sample surface that were not fresh were not burned. Figure 16 shows two views of this polymer sample.

Ignition Tests with Chlorine

CTPB Polymer. Five experiments were performed with chlorine oxidizer and CTPB polymer up to temperatures of 316°C and pressures of 10.2 atmospheres. No ignition signal was recorded from the photodiode (visible spectrum) in any experiment. However, at the most severe test conditions inspection of the sample after the test indicated that reaction had occurred. The sample had been converted to a thick carbonaceous ash to a depth of about one-half of the sample thickness.

In addition, four tests were conducted with CTPB-ammonium perchlorate propellant under less severe conditions but no ignition was detected. The detailed conditions of these tests are listed in the tabulated data, Appendix G.

PBAA Polymer. Four ignition tests were conducted with the PBAA polymer in a chlorine environment up to temperatures of 260°C and up to ten atmospheres pressure. For these experiments the ultraviolet detector previously described was utilized in addition to the photodiode detector. The reason for the use of the UV detector is presented on page 74. No ignition signals were recorded in any of these experiments. One of the four experiments was invalid for the measurement of ignition time because the polymer

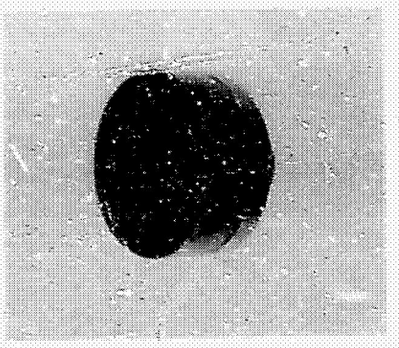

Oblique View of Sample Holder

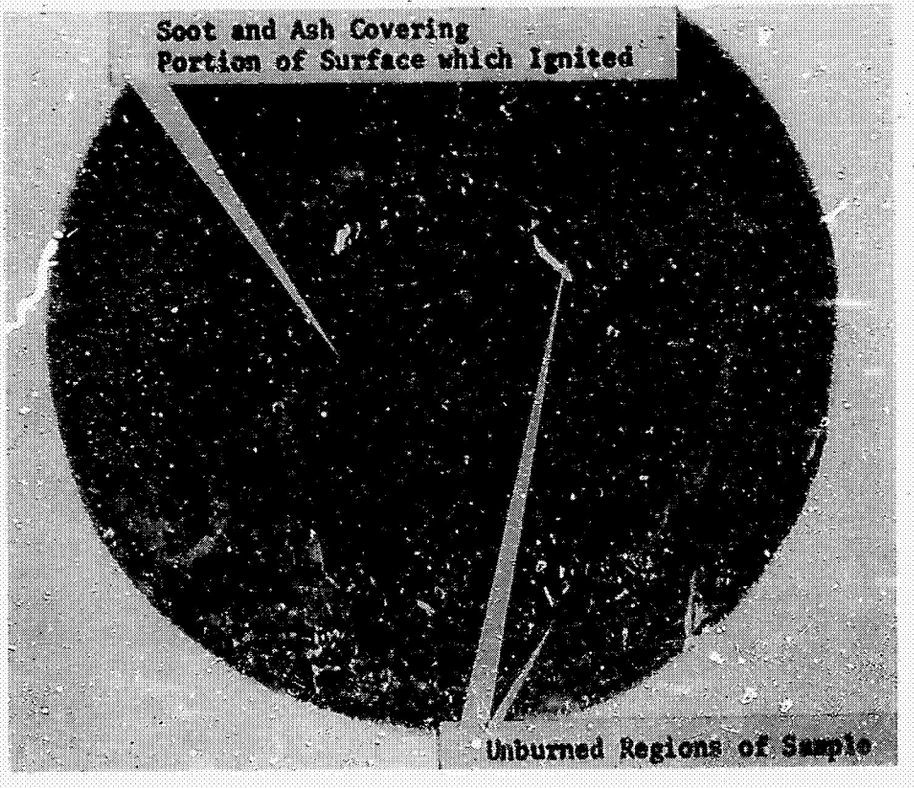

Enlarged Front View of Sample Holder

Figure 16 Photographs of Ignited Polystyrene Sample

sample was expelled from the sample holder during the deceleration process and fell to the hot bottom of the reactive chamber. Upon disassembly of the ignition apparatus the sample had been almost completely converted to carbon ash and there was fluffy carbon soot deposited on all horizontal surfaces within the oxidizer chamber.

Mass Spectral Results

General

It may be recalled that each set of spectra consists of two scans, one at low sensitivity and one at high sensitivity. The relative abundances of the ions were calculated on a uniform basis from the two scans, setting the helium peak (m/e = 4) to 100%. The net polymer spectra were obtained by subtracting the low and high temperature background spectra from the total polymer spectra at low and high temperatures respectively. In some cases the air spectrum increased under high temperature conditions due to a temperature sensitive leak in a tubing connection. In these cases subtraction of the air background spectrum was adjusted to compensate for its increase in the total spectrum.

Relative abundances were recorded to three significant figures except for those less than 1%, which were recorded to two significant figures. The value of the last significant digit is questionable, but it is believed better to report its estimated value rather than

omit it. Relative abundances less than 0.2% are not reported due to the errors associated with measuring the small deflections of these peaks.

The tabulated mass spectra are presented in Appendix H along with the heating curves for each of the polymer samples. The heating curves are marked indicating the time intervals during which the spectra were recorded.

CTPB Polymer

At room temperature the only detectable specie in the net polymer spectra is a trace of acetone. This is attributed to residue left from leak checking the vacuum system with acetone. At high temperatures small peaks were detected at m/e up to 146. The relative abundance of any of these peaks did not exceed 0.6%. Due to the complexity of the spectra, species identification was not possible. The most intense spectrum was observed just after the surface of the polymer was disturbed. A high estimate of the mole percent of polymer pyrolysis products in the most intense spectrum may be made by assuming that each peak is a parent ion peak having a relative abundance of 100%. If this is done and the mole percent of pyrolysis products is computed by the subtraction technique (Reference 40, p. 223), the result is a mole percent of less than 4%. This estimate is probably at least an order of magnitude high. Thus for the CTPB polymer there is negligible pyrolysis up to temperatures of 277^{o}C.

PBAA Polymer

At room temperature, the largest peak in the PBAA mass spectrum is m/e = 58. This peak has a relative abundance of 1.2%. All other peaks have relative abundances less than 0.3% indicating negligible vapor pressure at room temperature. The mass spectrum which was obtained during heating at about 150°C indicated the presence of about 17% of a volatile specie. This specie has been tentatively identified as benzyl chloride from uncertified mass spectra (41). This volatile specie was undetectible in all subsequent PBAA spectra recorded at 260°C.

At 260°C the PBAA spectra were too complicated for quantitative or qualitative analysis. The peaks were significantly higher for the PBAA than for the CTP" polymer. The highest pyrolysis peaks were m/e = 58 and m/e = 41 having a relative abundance of about 6.2% and 5.5% respectively. The results of a mass spectroscopic analysis by Madorsky (28) of purified polybutadiene pyrolysis products at 325°C yielded a complex mixture of sixteen types of hydrocarbons. In the case of the PBAA polymer, no increase in the spectrum was observed after disturbance of the polymer sample. This might be expected because the PBAA does not melt at 260°C.

PS Polymer

At room temperature no pyrolysis species were detected from the polymer spectra; however, styrene monomer was present for all spectra obtained at higher temperatures. Styrene was the principal pyrolysis product although there is an indication of a contribution

in the spectra due to toluene. These findings are in agreement with the results of Madorsky (28) who reports 52.7 weight percent styrene, 5.5 weight percent toluene, and 35.2 weight percent of heavier molecular weight species (m/e > 200) at a temperature at 500°C. The principal styrene peak (m/e = 104) increases from a relative abundance of 2.7% at about 160°C to a relative abundance of 15% at about 270°C. No significant increase in the styrene peak was detected after the sample was disturbed. Considering styrene as the only pyrolysis product, the mole percent of vapor may be estimated by the aforementioned subtraction technique at less than 14%. At twenty atmospheres this mole percent would be 0.7%. The maximum initial mole percent of fuel present under the conditions of PS ignition is estimated to be about 0.7%, a negligible amount. Also, the mass spectra indicate that polystyrene had the highest vapor spectra of the three polymers examined.

Summary

The experimental results may be summarized as follows.

(a) Hypergolic ignition of the three polymers was demonstrated at temperatures of 260°C and oxygen pressures of twenty atmospheres.

(b) No ignitions were obtained at temperatures less than about 260°C and at oxygen concentrations less than about 6.5×10^{-3} g/cm^3.

(c) Two polymers, CTPB and PS were molten at all initial test conditions for which ignitions were obtained. The PBAA polymer was a solid under all initial test conditions.

(d) The ignition time exhibits a low order dependence on oxygen concentration for the CTPB and PBAA polymers. The dependence of ignition time upon oxygen concentration was undetermined for the PS polymer.

(e) The initial temperature of the reactants has a strong effect of the ignition time.

(f) The data exhibited much less scatter under the slow heating conditions (eight minutes at 260°C prior to test) than under the normal heating conditions.

(g) No ignitions were obtained with the CTPB and the PS polymers unless a fresh surface was exposed.

(h) Under slow heating conditions no ignitions were obtained with helium-oxygen mixtures for either the PBAA or the CTPB polymer. Oxygen mole fractions of 0.5 and a total pressure of twenty atmospheres were utilized for the mixed gas tests of the CTPB polymer. The test temperature was 260°C in each instance. Oxygen mole fractions up to 0.75 were utilized for the mixed gas tests of the PBAA polymer at twenty atmospheres and 260°C.

(i) Under normal heating conditions (no eight minute wait at 260°C) two ignitions were obtained with the CTPB polymer at an oxygen mole fraction of 0.5, total pressure of twenty atmospheres, and temperature of 260°C.

(j) No ignitions of either the CTPB or the PBAA polymers were recorded with chlorine gas as the oxidizer. However, there was evidence of a combustion reaction in two tests. The most severe initial conditions were ten atmospheres pressure and 260°C.

(k) Mass spectra results indicated that the three polymers may be ranked in the following order of decreasing volatility; PS, PBAA, and CTPB. Furthermore the maximum possible equilibrium vapor pressure at any ignition conditions may be estimated at less than 2%.

DISCUSSION OF RESULTS

Interpretation of Experimental Results

Conditions Required for Hypergolic Ignition

The ignition data for the CTPB and PBAA polymers in oxygen indicate that there is a lower limit of oxygen concentration required for ignition at a fixed temperature. For the CTPB polymer no ignitions were obtained at oxygen concentrations less than 6.5×10^{-3} g/cm^3 and for the PBAA polymer the corresponding concentration limit is about 7.5×10^{-3} g/cm^3.

The minimum initial temperature and concentration required for ignition may be examined by the stationary state analysis of heterogeneous ignition as presented by Mellor (42). Consider a plane semi-infinite condensed phase polymer initially at uniform temperature, T_o. An oxidizing gas at uniform concentration, C_{ox}^o, and at uniform temperature, T_o, is suddenly introduced throughout the adjoining semi-infinite region. Assume that the chemical heating occurs at the interface between the condensed and gas phases. Further, consider a thin control volume at uniform temperature, T_s, enclosing only the reacting surface. The chemical heating within this thin control volume may be written as

$$\dot{q}_{chem} = \dot{m} Q$$

$$\dot{q}_{chem} = \dot{m} \left(\sum_i n_i \Delta H_{i,T_s} - \sum_j n_j \Delta H_{j,T_s} \right) \qquad (1)$$

where

$$\Delta H_{\ell,T_s} = \Delta H_{f,\ell}^{298} + (H_{T_s} - H_{298})_\ell \qquad \{\ell = i,j\}$$

where the subscript i indicates reactants and the subscript j indicates products, and

$\dot{q}_{chem}$ = chemical heating rate, cal/cm^2-sec

$\dot{m}$ = molar reaction rate, mole fuel/cm^2-sec

Q = chemical energy release, cal/mole fuel

T_s = surface temperature, ^oK

n_k = number of moles of species k per mole of fuel, mole k/mole fuel

$\Delta H_{f,k}^{298}$ = standard heat of formation of species k at 298^oK, cal/mole-k

$H_{T,k}$ = enthalpy of species k at T^oK, cal/mole-k .

If is it assumed that all portions of the surface are equally acessible with respect to diffusion and that the reaction at the surface is first order with respect to oxidizer concentration, $\dot{m}$ may be written (see Reference 43, p. 49)

$$\dot{m} = \frac{k\beta}{k+\beta} C_{ox} \qquad (2)$$

where

k = reaction rate constant with an Arrhenius temperature dependence, (cm/sec)

C_{ox} = oxidizer concentration, moles fuel/cm^3

β = diffusion velocity constant, cm/sec

$\beta = \frac{Nu\ D}{x}$

where Nu = diffusional Nusselt number, dimensionless

D = diffusivity of the oxidizer, cm^2/sec

x = characterstic dimension of system, cm.*

The chemical heating rate (Eqn 1) thus becomes:

$$\dot{q}_{chem} = \frac{k\,\beta}{k+\beta} C_{ox} \left(\sum_i n_i \Delta H_{i,T_s} - \sum_j n_j \Delta H_{j,T_s} \right) \qquad (3)$$

At low temperatures where $k<<\beta$ (kinetically controlled region) $\dot{q}_{chem}$ will exhibit an exponential temperature dependence due to k; at high temperatures where $k>>\beta$ (diffusionally controlled region) the temperature dependence of $\dot{q}_{chem}$ is given by the diffusivity. At high temperatures the diffusivity of gases increases roughly as the 1.65 power of the absolute temperature (44, p. 511). The shape of the $\dot{q}_{chem}$ curve as a function of the surface temperature is depicted in Figure 17.

Assuming that the products of the reaction do not participate in the heat transfer, Mellor (42) wrote

$$\dot{q}_{loss} = \lambda_f \frac{\partial T}{\partial x}\bigg|_{x=0^+} + \lambda_g \frac{\partial T}{\partial x}\bigg|_{x=0^-} + \varepsilon\sigma\,(T_s^4 - T_r^4) \qquad (4)$$

where

$\dot{q}_{loss}$ = rate of heat loss, $cal/cm^2\text{-}sec$

λ = thermal conductivity of the fuel (subscript f) or the oxidizer gas (g), $cal/cm\text{-}sec\text{-}^oK$

$\frac{\partial T}{\partial x}$ = temperature gradient evaluated at the interface x=0,

---

* In the semi-infinite model considered here, there is no characteristic dimension; however, one may be selected for an actual physical configuration.

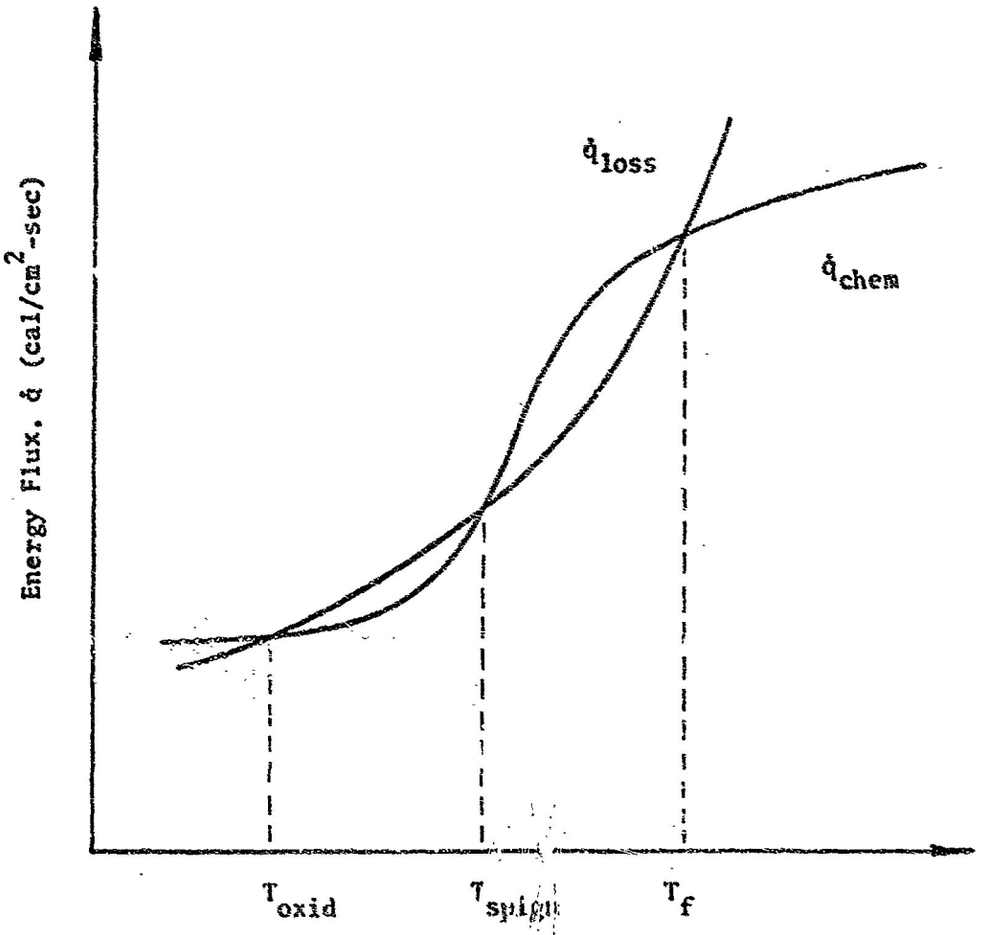

(from Reference 42)

Figure 17 Stationary Theory of Heterogeneous Ignition: Rate of Chemical Energy Release and Rate of Heat Loss vs. Surface Temperature

either into the fuel $x = 0^+$ or into the oxidizer $x = 0^-$

ϵ = surface emissivity, dimensionless

σ = Stephan-Boltzman constant, $cal/cm^2\text{-}sec\text{-}^oK^4$

T_r = effective radiation temperature of the environment, ^oK.

The shape of the $\dot{q}_{loss}$ curve is also depicted in Figure 17.

In general there will be three intersections of the $\dot{q}_{loss}$ curve with the $\dot{q}_{chem}$ curve. The temperatures corresponding to these intersections are referred to as the oxidation temperature, T_{oxid}, the spontaneous ignition temperature*, T_{spign}, and the flame temperature, T_f. The intersections which occur at T_{oxid} and T_f are stable, in the sense that a positive temperature perturbation will not result in self heating to a higher temperature. This is represented mathematically by the condition

$$\left[\frac{\partial \dot{q}_{chem}}{\partial T_s}\right]_{T=T_{oxid}=T_f} < \left[\frac{\partial \dot{q}_{loss}}{\partial T_s}\right]_{T=T_{oxid}=T_f} \tag{5}$$

However, the remaining intersection at the spontaneous ignition temperature is unstable and

$$\left[\frac{\partial \dot{q}_{chem}}{\partial T_s}\right]_{T=T_{spign}} > \left[\frac{\partial \dot{q}_{loss}}{\partial T_s}\right]_{T=T_{spign}} \tag{6}$$

*The spontaneous ignition temperature is the lowest temperature from which the interface may self-heat to combustion conditions.

Considering the effect of the products of the reaction on the heat transfer, there will be an additional heat loss term due to the mass diffusion of the products into the gas phase. However, this heat loss term will be counteracted by a reduction in the heat conduction to the gas phase, the gas phase becoming hotter due to the mass diffusion of the hot products. While the net result may either increase or decrease $\dot{q}_{loss}$, the general shape of the $\dot{q}_{loss}$ curve will not be changed.

From the above analysis it is evident that the initial temperature of the reactants must be greater than T_{spign} for hypergolic ignitions to occur. It may be observed intuitively that small changes in temperature in the range just greater than T_{spign} will result in large changes in the ignition time, since the initial net heating rate controls the induction time.* For those experiments in which ignition did not occur, the chemical heating rate was insufficient due to either of the following causes: (a) the temperature was insufficient or (b) the concentration of the reactants at the interface was insufficient. Several factors may contribute to the reduction of the reactant concentration at the interface: competitive adsorption of an inert gas, the presence of absorbed gas in the condensed phase, or poisoning of the surface by a reaction product.

---

*The induction time is the portion of the overall ignition time which elapses before the precipitous temperature rise occurs. For initial conditions near T_{spign} the induction time is a large fraction of the ignition time.

Postulated Reaction Mechanisms

Recall that the CTPB polymer and the PS polymer ignited only if a "fresh" surface was present, but the PBAA polymer ignited with a surface which initally was in equilibrium with the helium gas. The surface condition dependence of ignition and the evidence of a low order dependence of ignition time on concentration suggest that adsorption processes are important for these experimental conditions.

For a heterogeneous reaction with chemical heating at the surface the following steps must occur in series: (a) diffusion of the reactants to the surface, (b) adsorption of the reactants on the surface, (c) reaction on the surface, (d) desorption of the products from the surface, and (e) diffusion of products away from the surface. The overall reaction rate will be controlled by the slowest step of this series. In the present case of hypergolic ignition diffusion is not considered to be the rate controlling step because of the relatively low temperatures involved. Investigations of surface reactions have shown that for ordinary temperatures, gas phase diffusion rates are much more rapid than the overall rate, and therefore diffusion does not constitute the slow step (45). Because little is known about the desorption of products from a surface, the desorption step will be considered as a part of a surface reaction step which produces gas phase products.

The following analysis will consider adsorption and reaction processes (steps b and c) as the possible rate controlling steps.

Consider the following reactions to occur between an initially fresh polymer surface which is exposed to a given concentration of oxygen.

$$\text{Adsorption of } O_2: \quad O_2 + -\overset{|}{\underset{|}{S}} \xrightarrow{k_1} O_2 - \overset{|}{\underset{|}{S}} \tag{7}$$

$$\text{Reaction:} \quad O_2-\overset{|}{\underset{|}{S}} \xrightarrow{k_2} \text{Products (gas phase)} \tag{8}$$

where the notation $O_2-\overset{|}{\underset{|}{S}}$ indicates that the O_2 is adsorbed at an active site on the surface. For the ideal case of adsorption on a perfectly smooth surface with no interactions between adsorbed molecules, the Langmuir assumption of a unimolecular layer of adsorbed molecules applies. This is the simplest case of adsorption and will be assumed here because the data necessary for the application of more complicated theories are unavailable.

Assume that the reaction rate is first order with respect to the surface concentration of oxidizer. Then

$$\frac{d\, C_{ox,s}}{dt} = k_2\, C_{ox,s} \tag{9}$$

where

$\frac{d\,(C_{ox,s})}{dt}$ = rate of O_2 adsorption on the surface, mole O_2/cm^2-sec

k_2 = first order rate constant, sec^{-1}

$C_{ox,s}$ = concentration of oxygen on the surface, moles O_2/cm^2.

Let C_s be the concentration of active sites on the surface, sites/cm^2; and let θ_{ox} be the fraction of these sites which are

covered by O_2. The fraction of the surface vacant is $1-\theta_{ox}$ and $C_{ox,s} = C_s\ \theta_{ox}$. (10)

The rate of adsorption is proportional to the product of the fraction of the surface vacant and the oxygen concentration in the gas phase. The value of θ_{ox} may be obtained by applying equilibrium conditions to the rate of formation of O_2-S. Thus

$$\frac{d\ C_{ox,s}}{dt} = 0 = k_1\ (1-\theta_{ox})\ C_s\ C^o_{ox} - k_2\ C_s\ \theta_{ox} \qquad (11)$$

where C^o_{ox} is the oxygen concentration in the gas phase.

Solving Equation (11) for θ_{ox},

$$\theta_{ox} = \frac{k_1\ C_{ox}}{k_1\ C_{ox} + k_2} \qquad (12)$$

Substituting Equations (10) and (12) into the assumed reaction rate, Equation (9)

$$\frac{d\ C_{ox,s}}{dt} = \frac{C_s\ d\ \theta_{ox}}{dt} = C_s\ k_2 \left(\frac{k_1\ C^o_{ox}}{k_1\ C^o_{ox} + k_2} \right) \qquad (13)$$

or

$$r = k_2 \left(\frac{k_1\ C^o_{ox}}{k_1\ C^o_{ox} + k_2} \right) \qquad (14)$$

where

$$r \equiv \frac{1}{C_s} \frac{d C^o_{ox,s}}{d t}$$

Defining the ratio of the reaction rates, K

$$K \equiv \frac{k_1}{k_2} \tag{15}$$

and substituting K into Equation (14),

$$r = k_2 \left[\frac{K C^o_{ox}}{K C^o_{ox} + 1} \right] \tag{16}$$

The quantity in brackets may be recognized as similar to the Langmuir adsorption isotherm for a single adsorbed molecule if oxidizer pressure is substituted for C^o_{ox} (see Reference 45, p. 260). Consider now the limiting behavior of Equation (16) as a function of the oxygen concentration. At very low concentrations (i.e., $K C^o_{ox} << 1$) the reaction rate becomes

$$r \quad k_2 K C^o_{ox} \tag{17}$$

indicating a first order dependence on oxidizer concentration. At very high concentration ($K C^o_{ox} >> 1$) the reaction rate becomes

$$r \simeq k_2 \tag{18}$$

indicating a zero order reaction. The reaction rate as expressed in Equation (16) is presented in Figure 18a as a function of C^o_{ox}.

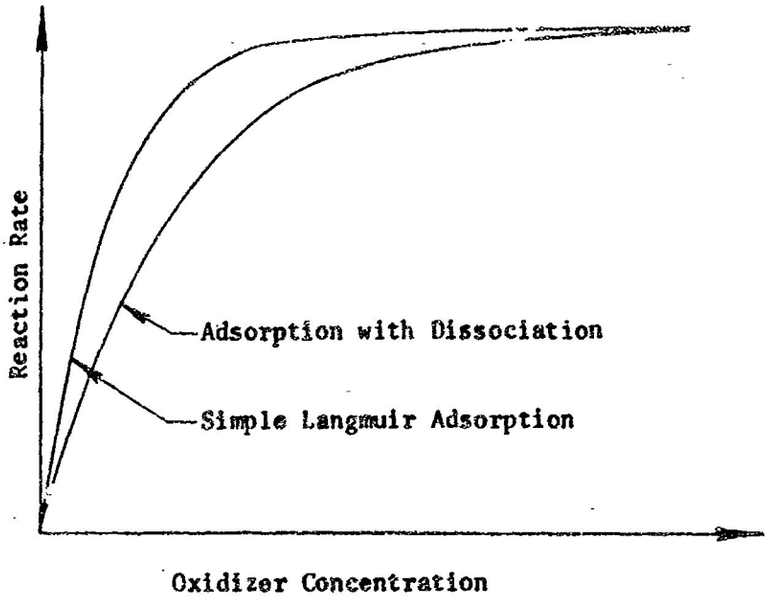

a. Reaction Rate vs. Oxidizer Concentration

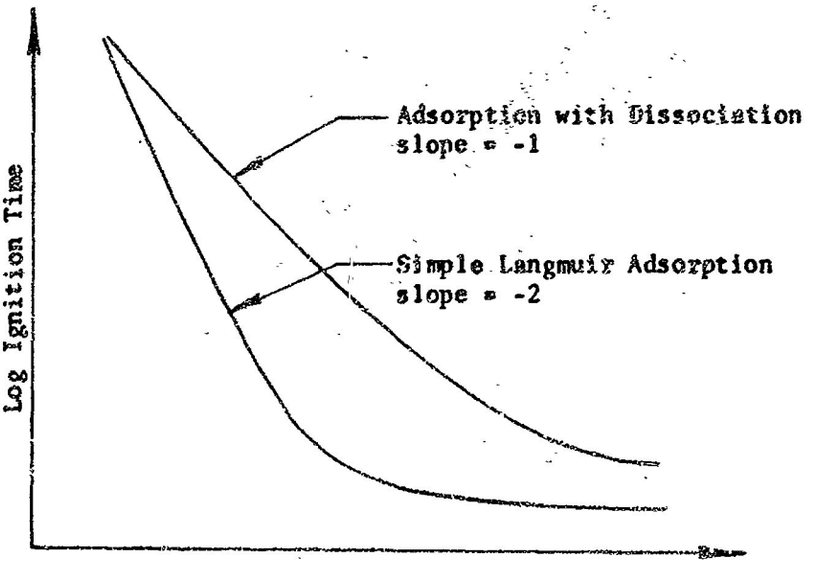

b. Log Ignition Time vs. Log Oxidizer Concentration

Figure 18 Comparison of the Effect of Oxidizer Concentration on Reaction Rate and Ignition Time for Different Adsorption Mechanisms

Recall from the discussion of the hypergolic ignition theory that the ignition time is inversely proportional to the square of the reaction rate. Utilizing this relationship, the ignition time as a function of oxygen concentration is presented in Figure 18b.

Two other adsorption isotherms will now be considered. If adsorption occurs with dissociation (as might be likely for O_2) the reaction may be illustrated as

$$O_2 + \text{-S-S-} \underset{k_{-1}}{\overset{k_1}{\rightleftharpoons}} \text{-}\overset{O}{S}\text{-}\overset{O}{S}\text{-} \tag{19}$$

and the adsorption isotherm may be written as (see Reference 45 p. 261)

$$\theta_{ox} = \frac{K^{\frac{1}{2}} (C^o_{ox})^{\frac{1}{2}}}{K^{\frac{1}{2}} (C^o_{ox})^{\frac{1}{2}} + 1} \qquad \left(K \equiv \{k_1/k_{-1}\}\right) \tag{20}$$

If this isotherm is substituted for the bracketed quantity in Equation (16), the following expression results.

$$r = \frac{k_2 K^{\frac{1}{2}} (C^o_{ox})^{\frac{1}{2}}}{K^{\frac{1}{2}} (C^o_{ox})^{\frac{1}{2}} + 1} \tag{21}$$

The low and high concentration limiting cases may be written

$$r = k_2 K^{\frac{1}{2}} (C^o_{ox})^{\frac{1}{2}} \tag{22}$$

and

$$r = k_2 \tag{23}$$

respectively.

The qualitative behavior o the reaction rate and ignition time for the case of adsorption with dissociation is also presented in Figure 18.

Another isotherm of interest is for the case of competitive adsorption of two gases; say helium and oxygen. For competitive adsorption let θ_{ox} equal the fraction of the surface covered by O_2, and let θ_h equal the fraction of the surface covered by helium. Then $1 - \theta_{ox} - \theta_h$ is the fraction of the surface bare. The rate of adsorption of O_2 is proportional to the fraction of the surface bare. Thus

$$\frac{d\,\theta_{ox}}{d\,t} = k_{ox}\, C^o_{ox}(1 - \theta_{ox} - \theta_h) \tag{24}$$

The rate of desorption* of O_2 is proportional to the fraction of the surface covered by O_2, so that

$$-\frac{d\,\theta_{ox}}{d\,t} = k_{-ox}\,\theta_{ox} \tag{25}$$

At equilibrium these rates are equal, whence

$$K_{ox}\, C^o_{ox} = \frac{k_{ox}}{k_{-ox}}\, C^o_{ox} = \frac{\theta_{ox}}{1-\theta_{ox}-\theta_h} \tag{26}$$

Similarly it may be shown for helium,

---

* The desorption under consideration here is not the desorption of products. It is rather the reverse step of the assumed equilibrium reaction for the net adsorption of reactants.

$$K_h C_h^o = \frac{k_h}{k_{-h}} C_h^o = \frac{\theta_h}{1-\theta_{ox}-\theta_h} \qquad (27)$$

Solving Equations (26) and (27) simultaneously for θ_{ox} and θ_h,

$$\theta_{ox} = \frac{K_{ox} C_{ox}^o}{1 + K_{ox} C_{ox}^o + K_h C_h^o} \qquad \theta_h = \frac{K_h C_h^o}{1 + K_{ox} C_{ox}^o + K_h C_h^o} \qquad (28,29)$$

As before, the reaction rate expression may be obtained by substitution of Equation (28) for the bracketed quantity in Equation (16). Thus

$$r = k_2 \frac{K_{ox} C_{ox}^o}{1 + K_{ox} C_{ox}^o + K_h C_h^o} \qquad (30)$$

This reaction rate for competitive adsorption is useful for the analysis of the ignition results with helium-oxygen mixtures. Recall that ignitions were not obtained with mixtures of helium and oxygen under the conditions of slow heating. The reaction rate for competitive adsorption, Equation (30), in the limiting case of high concentrations (i.e. $K_{ox} C_{ox}^o + K_h C_h^o >> 1$)

becomes

$$r \approx \frac{k_2 K_{ox} C_{ox}^o}{K_{ox} C_{ox}^o + K_h C_h^o} \qquad (31)$$

This predicts that the reaction rate will be reduced with mixed gases,

agreeing qualitatively with the observed experimental data. For the low concentration limits (i.e. $K_{ox} C^{o}_{ox} + K_h C^{o}_h << 1$) Equation (30) becomes

$$r = k_2 K_{ox} C^{o}_{ox} \tag{32}$$

indicating that the reaction rate is independent of the helium concentration. This limiting case agrees qualitatively with the results of the shock tube ignition experiments.

Recall that two ignitions were obtained at oxygen mole fractions of one-half under the normal heating conditions. The averaged ignition times for the mixed gases is slightly greater than the averaged times for pure O_2. These data agree qualitatively with the proposed mechanism, although one might expect that the increase in ignition time should be greater.

The fact that a fresh surface was required for ignition of the molten polymers in the present experiments suggests that the adsorbed helium may have diffused into the molten polymer. Thus, after the polymer surface was moved into the oxygen environment, the adsorbed helium molecules desorbed very rapidly (since the helium concentration in the oxidizer chamber is nearly zero) only to be replaced on the surface by more helium molecules which are diffusing from an interior region near the surface of the molten polymer. This inhibition of chemical heating rate need not be very great to prevent ignition if the initial conditions are near the spontaneous ignition temperature.

If a fresh surface was exposed, the layer of polymer containing the adsorbed helium was physically removed and the rate of chemical heating would not be inhibited. In the case of the solid polymer, no fresh surface was necessary, and it is postulated that diffusion of the helium into the solid was insufficient to significantly retard the reaction rate.

Chlorine Experiments

Although chlorine is a very reactive element, the temperature of flames with chlorine is much lower than the temperatures of fluorine or oxygen flames (46). Hydrocarbons burn readily with chlorine in diffusion flames and very nearly all of the carbon containing combustion products appear as soot, i.e. solid carbon. Hydrogen chloride gas is the principal gas phase product. The above description of chlorine flames was summarized from Reference (46) and agrees with observations of the present investigation for the two instances in which there was evidence of combustion.

After the photodiode detector had failed to indicate any sign of ignition for the experiments with the CTPB polymer, a more sensitive ultraviolet detector was obtained from Honeywell, Inc. and utilized to check for possible HCl emissions in the ultraviolet region. A system of bands of emission spectra occuring in a hollow cathode discharge has been reported for HCl in the wavelength interval 1980-2375A (47). As reported earlier, no ignitions were

detected with either sensor. It is unknown whether the detectors were sensitive enough to obtain a signal from the flame, or whether the combustion occured between the time the oscillograph was stopped and the time that the sample was observed. The use of a spectrometer was considered for determining the visible and ultraviolet spectra of the chlorine-polymer flame. However, this was not done because of the time and cost involved in modification of the experimental apparatus.

Mass Spectral Results

The mole fraction of the pyrolysis products from the three polymers differed considerably, the PS polymer having the greatest mole fraction of gaseous products, and the CTPB polymer having the least. There is no direct relationship evident between the mole fraction of pyrolyized fuel and the ignition time. The ignition time was greatest for the PS polymer but was the least for the PBAA polymer which had the intermediate mole fraction of fuel vapor.

The previously presented bulk pyrolysis value for polystyrene was converted into an estimated mass flux utilizing the conservative procedure presented in Appendix F. The mass flux corresponding to the bulk pyrolysis of rate of 1.25×10^{-6} %/sec is 2.69×10^{-8} g/cm^2-sec. These rates are for a temperature of 290.7°C.

Employing the same technique for estimating mass flux in the case of purified polybutadiene, the value of bulk pyrolysis presented in the review of polymer degradation is equivalent to a mass flux

of about 7.3×10^{-5} g/cm^2-sec. Recall that these bulk pyrolysis data were obtained at 325°C. The initial mass flux at this temperature may be as much as an order of magnitude higher, as discussed previously. However, information in the literature review indicates there is a considerable difference between the thermal degradation of purified polybutadiene and that of the crosslinked polymers such as CTPB and PBAA which are utilized for propellant binders. The results of French and Rosborough (32) and those of Ryan, et al (31) indicate that thermal breakdown of CTPB and PBAA polymers does not occur at 265°C and at 350°C respectively. It is therefore reasonable to believe that the pyrolysis mass fluxes for CTPB and PBAA are much lower than those of the PS polymer for the temperature interval 260° to 300°C. The mass spectra of the pyrolysis products also indicate the same relative relationship for the mole fraction of fuel vapors.

Because of the low fuel mass fluxes and the low equilibrium concentrations of fuel molecules in the gas phase (< 2.0% at ten atmospheres) it is considered highly unlikely that exothermic gas phase reactions supply more than a very small fraction of the chemical heating until the preciptious temperature rise occurs.

Comparison With Other Results

The present ignition results in oxygen may be compared to the ignition of similar polymers and propellants in oxygen filled shock tubes. The results of McAlevy (6) and Shannon (27) as previously

presented in the literature review are depicted in Figure 19 along with the present results. As to be expected, the ignition times are much different due to the difference in experimental conditions. Hermance in a dimensional analysis of hypergolic ignition has presented the following relationship for the dimensionless time variable, (see Reference 7, p. a25).

$$\tau = \alpha_s \left[\frac{Q\,(C_{ox}^{o})^{n}\, Z\, E \exp(-E/RT_o)}{\lambda_s\, RT_o^{2}} \right]^{2} t \qquad (33)$$

where

α_s = the thermal diffusivity of the solid, cm^2/sec

Q = heat release of chemical reaction, cal/g

$(C_{ox}^{o})^{n} Z$ = reaction rate coefficient for the assumed Arrhenius type reaction, g/cm^2-sec

Z = pre-exponential factor

C_{ox}^{o} = initial oxidizer concentration

n = overall order of the reaction with respect to oxidizer concentration, dimensionless

E = activation energy, cal/mole

λ_s = thermal conductivity of the condensed phase, cal/cm-sec-^{o}K

R = universal gas constant, cal/mole -^{o}K

T_o = bulk temperature of the oxidizer gas, ^{o}K

t = time, sec.

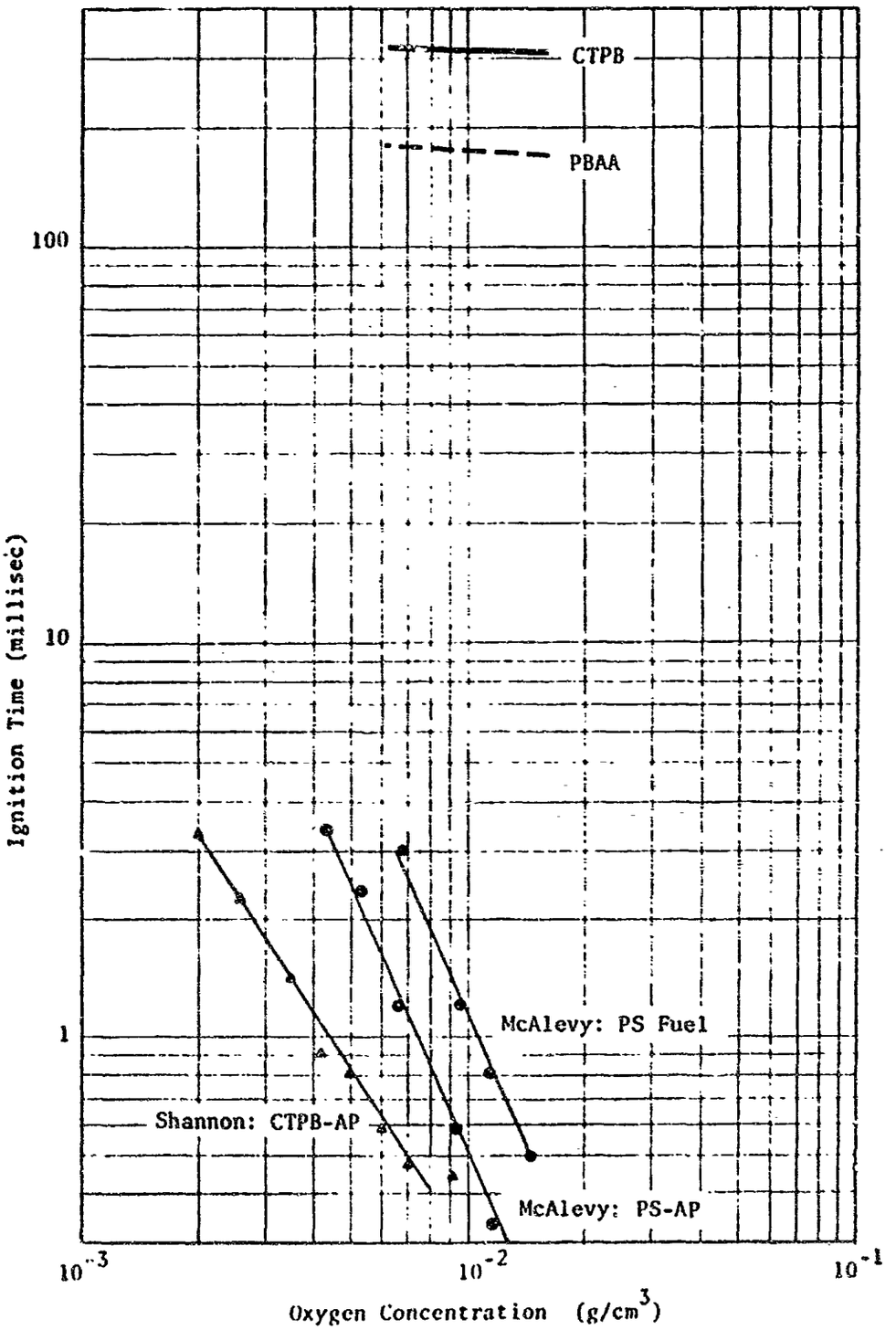

Figure 19 Comparison of Hypergolic Ignition Results with Shock Shock Tube Ignition Data

For a specific experiment, the following factors in Equation (33) may be considered approximately invariant with respect to temperature and oxidizer concentration: α_s, Q, Z, λ_s; and R is a constant. Let the dimensionless time, τ assume the value τ^*, at the real ignition time, t^*. It is reasonable to assume that the dimensionless ignition time, τ^*, has a fixed numerical value for all hypergolic ignition conditions of a specific oxidizer gas and condensed phase fuel in a manner similar to the dimensionless results of the non-stationary ignition theory of Semenov (42,43).

Solving Equation (33) for t^*,

$$t^* = \frac{\tau^* \lambda_s^2 R^2}{\alpha_s Q^2 Z^2} \left[\frac{T_o^2 \exp (E/RT_o)}{E (C_{ox}^o)^n} \right] \tag{34}$$

In order to select a value for the activation energy, E, the ratio of the ignition times for two data points was equated to the ratio of right hand side of Equation (34) assuming that τ^* is constant. Thus

$$\frac{t_a^*}{t_b^*} = \left[\frac{T_o^2 \exp (E/RT_o)}{E (C_{ox}^o)^n} \right]_a^2 \left[\frac{E (C_{ox}^o)^n}{T_o^2 \exp (E/RT_o)} \right]_b^2 \tag{35}$$

where the subscripts a and b indicate that times, temperatures and concentrations are evaluated from the experimental data of test a and b. The two data points selected for this calculation were obtained

for the ignition of the PBAA polymer at temperatures of 260°C and 321°C and at $C_{ox}^{o} \simeq 1.3 \times 10^{-2}$ g/cm^3. The value of the activation energy required for τ^* to be constant was computed by Equation (35) and was found to be ≃ 16 kcal/mole. This value of activation energy appears reasonable when compared to the value of ≃ 12 kcal/mole selected by Anderson and Brown for correlation of hypergolic ignition of propellants in fluorine and chlorine trifluoride (34,3).

In order to check the hypothesis that τ^* is a constant, τ' was computed for the data of McAlevy and Shannon which was presented earlier in Figure 8. These calculations were made using the bulk gas temperature behind the reflected shock wave as T_o. Even though Equation (33) was not derived for the case of external heat transfer, i.e. shock tube ignitions, τ^* deviated less than 20% from its mean value when compared for a specified experimental apparatus, oxidizer gas and condensed phase fuel or propellant. For the data examined, the ratio of concentration variations was about three to one and the temperature variation was about 140°C.

Equation (35) may also be employed to estimate the initial test temperature which would be required in the hypergolic experiments in order to reduce the ignition times to the order of magnitude of the shock tube ignition times. If a test temperature of 360°C is assumed, the ignition times are reduced by a factor of one-sixtieth. The results of this calculation are presented in Figure 20. As observed in Figure 20, shock tube ignitions still occur more quickly even though the temperature of the gas at the surface of the shock tube sample is only about 125°C. Such a disparity between the ignition

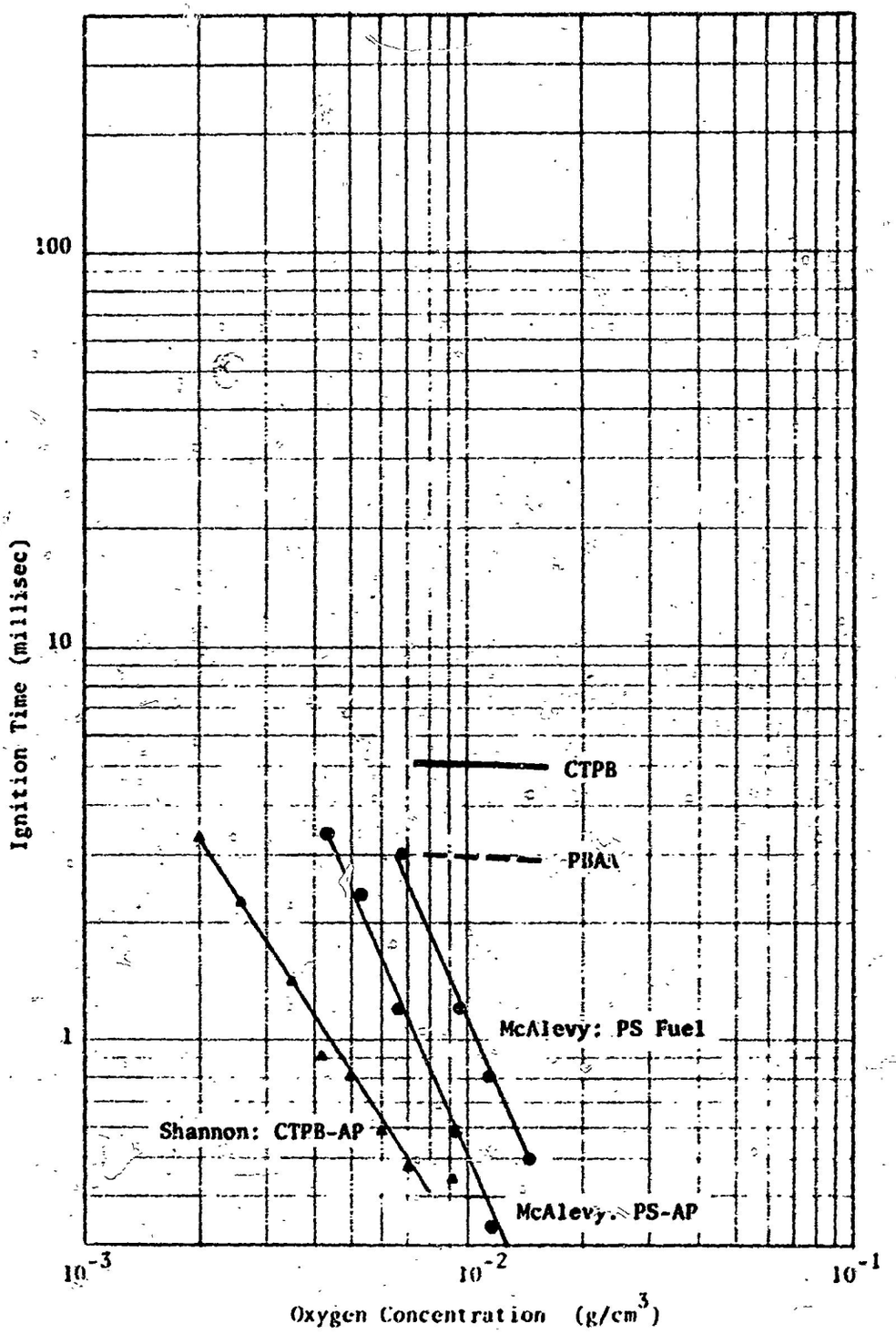

Figure 20 Comparison of Temperature Corrected Hypergolic Ignition Results with Shock Tube Ignition Data

times and the gas temperature at the surface of the sample is to be expected because of the effect of heat flux to the sample surface in the shock tube experiments.

If the straight line data correlation is removed from the data of Shannon and a smooth curve is fitted by eye, a change in the slope of the curve is apparent (see Figure 21). Furthermore, the shape of this curve is the same qualitatively as that presented in Figure 18. The experimentally determined slope of this curve is about - 1.5 at low concentrations. This value is midway between the value of the slope for the case of simple Langmuir adsorption and the case of adsorption with dissociation. The slope of - 1.5 suggests a fractional order of the overall reaction, and implies that such a simple reaction mechanism is only qualitatively correct.

The more significant feature of Figure 21 is the agreement between the present hypergolic data and the CTAB shock tube data regarding the dependence of ignition time on oxidizer concentration at higher concentrations. This agreement suggests that the controlling reactions are of the same type for both experiments. Of the twelve sets of ignition data presented in Reference 27, ten sets exhibit an increase in slope as the oxygen concentration approaches its higher limit. It is also stated by Shannon that some indication of an increase in slope was noted for oxygen concentrations greater than 10^{-2} g/cm^3, but the data were erratic and were not reported.

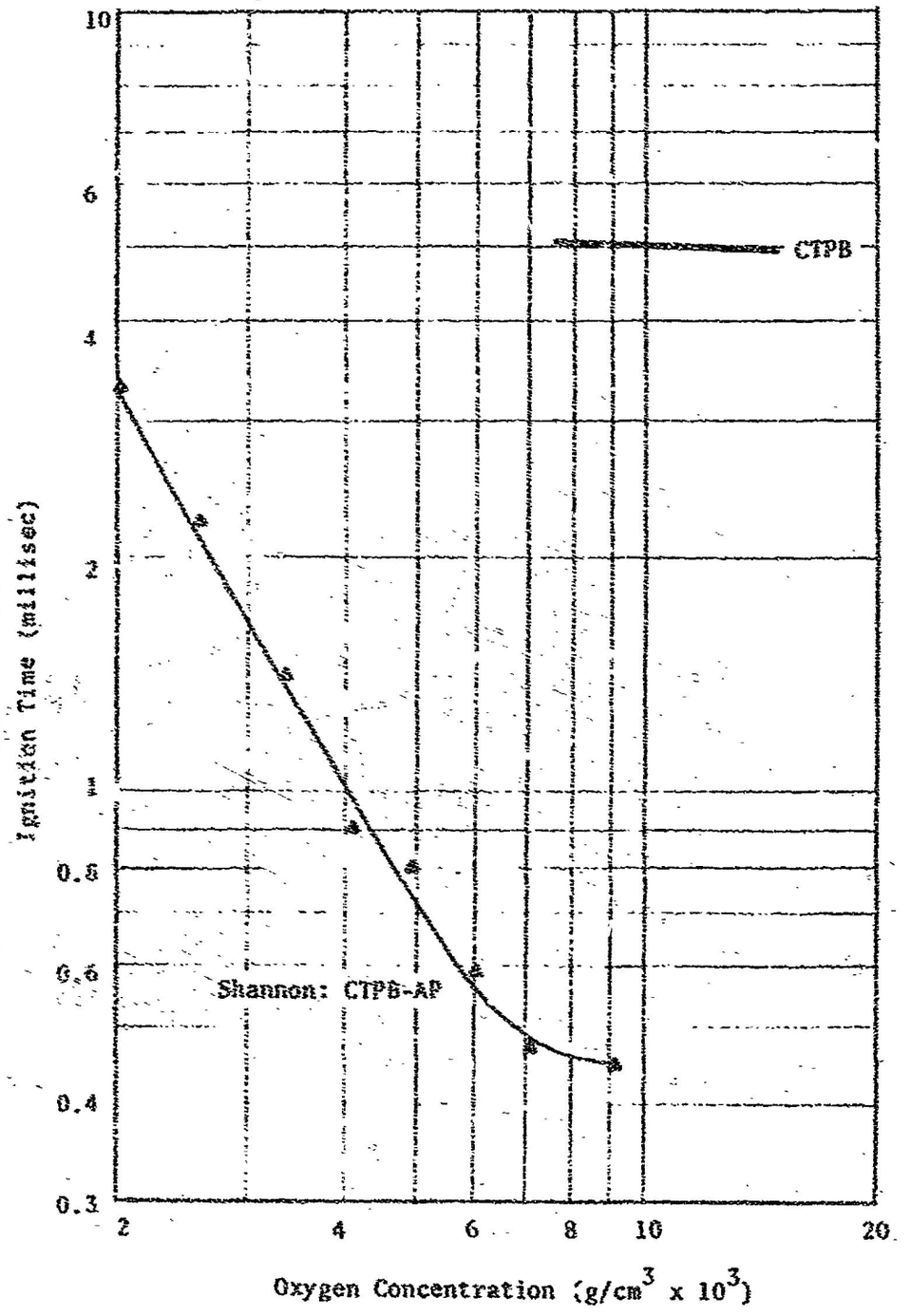

Figure 21 Comparison of Shock Tube and Hypergolic Ignition Results for CTPB Propellant and Polymer

It should be recalled from the discussion of reaction mechanisms that the increase in slope may be due to two complementary effects, the effect of an inert diluent in the gas phase which is competitively adsorbed on the fuel surface and that of the limiting case of high concentrations.

The present experimental results were also compared with the nondimensional solution of the hypergolic ignition problem presented by Williams (12). Details of the computations and the source of kinetic parameters and thermophysical properties are presented in Appendix E. The predicted ignition time (for an activation energy = 16 kcal/mole) was about seven orders of magnitude too low. However, since the ignition time is inversely proportional to the square of pre-exponential factor a decrease in this factor by three and one-half orders of magnitude results in close agreement between the predicted and experimental values of ignition time. The results of this comparison exercise are neither very good or very bad considering that pre-exponential factors are often uncertain by as much as six orders of magnitude.

CONCLUSIONS

The principal conclusion of this investigation is that heterogeneous ignition reactions between gaseous oxygen and polymeric fuels occur hypergolically under temperatures low enough to warrant their consideration as sources of chemical heating in the overall ignition process. A review of data on the pyrolysis rates of polymers and the experimental examination of equilibrium mass spectra of these polymeric fuels leads to the conclusion that gas phase exothermic reactions are unlikely to control ignition under the present experimental conditions. It is concluded that these ignition reactions are kinetically controlled rather than diffusionally controlled from the strong dependence of ignition time upon the initial temperature. A heterogeneous reaction mechanism which assumes that the rate of surface reaction is controlling has been postulated and agrees qualitatively with the experimental results.

From the ignition experiments with chlorine gas, it is concluded that chlorine-polymer reactions alone do not contribute significantly to the ignition process.

With regard to the overall ignition process for composite propellants, the results of this investigation support the concepts of the heterogeneous ignition theory. It is further concluded that there are significant differences in the ignition behavior of

polymers and that the chemical structure of the polymer and the nature of the pyrolysis products must be considered in the description of the ignition process.

LIST OF REFERENCES

1. Fullman, C.H., and Nielsen, F.B., "Theoretical and Experimental Investigations of Ignition Systems for Very Large Solid Propellant Motors," United Technology Center, UTC-2012-FR2, Sunnyvale, Calif., May 1963, (AD336177), CONFIDENTIAL.

2. Huggett, C., Bartley, C.E., and Mills, M.M., Solid Propellant Rockets, Princeton University Press, Princeton, N.J., 1960.

3. Price, E.W., Bradley, H.H. Jr., Dehority, G.L., and Imbiricu, M.M., "Theory of Ignition of Solid Propellants," AIAA Paper 66-64, Jan. 1966.

4. Derr, R.L., and Osborn, J.R., "An Experimental Investigation of the Gaseous Phase Reaction Zone in a Composite Solid Propellant," TM 67-6, Jet Propulsion Center, Purdue University, Sept. 1967.

5. Frazer, J.H., and Hicks, B.L., "Thermal Theory of Ignition of Solid Propellants," J. Phys. Colloid Chem. 54, 872-876 (1950).

6. McAlevy, R.F. III, "The Ignition Mechanism of Composite Solid Propellants," Aeronautical Engineering Laboratory Report No. 557, Princeton University, 1961. (AD263440).

7. Hermance, C.E., "Solid Propellant Ignition Studies: Ignition of the Reaction Field Adjacent to the Surface of a Solid Propellant," Aeronautical Engineering Laboratory Report No. 674, Princeton University, 1963. (AD428602).

8. Hermance, C.E., Shinnar, R., and Summerfield, M., "Ignition of an Evaporating Fuel in a Hot Oxidizing Gas Including the Effect of Heat Feedback," Aeronautical and Mechanical Sciences Report No. 752, Princeton University, 1966. (AD628931).

9. Hermance, C.E., and Kumar, R.K., "Gas Phase Ignition of a Solid Fuel Containing an Oxidizer," AIAA Paper No. 68-496, June 1968.

10. Anderson, R., Brown, R.S., Thompson, G.T., and Ebeling, R.W., "Theory of Hypergolic Ignition of Solid Propellants," Presented at the American Institute of Aeronautics and Astronautics, Heterogeneous Combustion Conference, Palm Beach, Florida, 11-13 December 1963. (AIAA Paper 63-514).

11. Anderson, R., Brown, R.S., and Shannon, L.J., "Ignition Theory of Solid Propellants," Presented at American Institute of Aeronautics and Astronautics, Solid Propellant Rocket Conference, Palo Alto, Calif., 29-31 January 1964. (AIAA Preprint 64-156).

12. Williams, F.A., "Theory of Propellant Ignition by Heterogeneous Reaction." AIAA Journal, Vol. 4, No. 8, August 1966, pp. 1354-1357.

13. Altman, D., and Grant, A.F., Jr., "Thermal Theory of Solid-propellant Ignition by Hot Wires," Fourth Symposium (International) on Combustion (Williams, and Wilkins Co., Baltimore, Md., 1953), pp. 158-161.

14. Bastress, E.D., Allan, D.S., and Richardson, D.L., "Solid Propellant Ignition Studies," Arthur D. Little, Inc., Air Force Rocket Research Laboratories, Edwards AFB Calif., Technical Documentary Report No. RPL-TDR-64-65, Final Report (October 1964), CONFIDENTIAL.

15. Keller, J.A., "Ignition of Ammonium Perchlorate-Based Propellants by Convective Heating," University of Utah, Technical Report, August 1, 1966.

16. Wightower, J.D., "An Investigation of the Effect of Environmental Gases and Pressure on the Ignition of Solid Rocket Propellants," Naval Weapons Center, China Lake, Calif., NWC TP 4431, Oct.1967.

17. Evans, M.W., and Moore, D.B., "Ignition of Solid Rocket Propellant Surfaces," Stanford Research Institute, Menlo Park, Calif., SRI Project No. GHU-5277, January 1966. (AD477884).

18. Miller, C.L., "Fundamental Investigation of Hypergolic Ignition of Solid Propellants," United Technology Center, Sunnyvale, Calif., UTC 2074-FR, 15 April 1966. 2 volumes, (CONFIDENTIAL).

19. Allen, H., Jr., and Finns, M.L., "Relative Ignitiblity of Typical Solid Propellants with Chlorine Trifluoride." Washington, D.C., National Aeronautics and Space Administration, January 1963. (NASA Technical Note D-1533).

20. Bircumshaw, L.L. and Newman, B.H., "The Thermal Decomposition of Ammonium Perchlorate: I. Introduction, Experimental Analysis of Gaseous Products, and Thermal Decomposition Experiments," Proc. Roy. Soc. (London) Ser. A 227, pp. 115-132 (1954).

21. Bircumshaw. L.L., and Newman, B.H., "The Thermal Decomposition of Ammonium Perchlorate: II. The Kinetics of Decomposition, The Effect of Particle Size, and Discussion of Results," Proc. Roy. Soc. (London) Ser. A. 227, pp. 228-241 (1954).

22. Galway, A.K., and Jacobs, P.W.M., "The Thermal Decomposition of Ammonium Perchlorate at Low Temperatures," Pro. Roy. Soc. (London) Ser. A 254, pp. 455-469 (1960).

23. Kuratani, K., "Some Studies on Solid Propellants, Part I. Kinetics of the Thermal Decomposition of Ammonium Perchlorate," Report No. 372, Aeronautical Research Institute, University of Tokyo (In English) (July 1962).

24. Goshgarian, B.B., and Walton, J.A., "Mass Spectrometric Study of Ammonium Perchlorate Decomposition," Air Force Rocket Propulsion Laboratory, Edwards, Calif., AFRPL-TR-65-87, April 1965.

25. Levy, J.B., and Friedman, R., "Further Studies of Pure Ammonium Perchlorate Deflagration." 8th Symposium on Combustion, pp. 663-672, Williams and Wilkins, Baltimore, 1961.

26. Bircumchaw, L.L. and Phillips, T.R., Journal Chem. Society, London, (1957) pp. 4741-7.

27. Shannon, L.J., "Composite Solid Propellant Ignition Machanisms" United Technology Center, Sunnyvale, Calif., UTC 2138-ASR1, Nov. 1966. (AD 484048).

28. Madorsky, S.L., Thermal Degradation of Organic Polymers, Interscience, N.Y., 1964.

29. McAlevy, R.F. III, and Hansel, J.G., "Energetics and Chemical Kinetics of Polystyrene Surface Degradation in Inert and Chemically Reactive Environments," Stevens Institute of Technology, Hoboken, N. Jersey, Tech Report ME-TR-65006, July 1965.

30. McAlevy, R.F. III, Lee, S.Y., and Smith, W.H., "The Linear Pyrolysis of Polymethylmethacrylate," Stevens Institute of Technology, Hoboken, N. Jersey, Tech Report ME-TR-66006, July 1966.

31. Ryan, N.W. et al, "Ignition and Combustion of Solid Propellant," University of Utah, Salt Lake City, Utah, AFOSR Grant 40-65, Sept. 1965.

32. French, D.M., and Rosborough, L., "Oxidation and Heat Aging of Carboxyl-Terminated Polybutadiene," Journal of Applied Polymer Science, Vol. 10, pp. 273-289 (1966).

33. Pearson, G.S., and Sutton, D., "Composite Solid Propellant Ignition: Ignition of Ammonia and other fuels by Perchloric Acid Vapour," Rocket Propulsion Establishment, Wescott, Great Britain. RPE Report No. 66/8, June 1966. (AD 640809).

34. Anderson, R., Brown, R.B., Ebeling, R., and Hawk, R.W., "Fundamental Investigation of Hypergolic Ignition for Solid Propellants," United Technology Center, Sunnyvale, Calif., UTC 2018 FR, Dec. 1963 (CONFIDENTIAL).

35. McAlevy, R.F. III, Lee, S.Y., and Magee, R.S., "The Solid Propellant Ignition Mechanism: A Simple Diagnostic Experiment," Astronautica Acta, Vol. 11, No. 2 (1965), pp. 144-45.

36. Bastress, E.K., Allan, D.S., and Richardson, D.L., "Solid Propellant Ignition Studies," Arthur D. Little, Inc., Cambridge, Mass., RPL-TDR-64-65, Oct. 1964. (AD 355441).

37. Glaser, P.E., "Imaging Furnace Developments for High Temperature Research," Journal of the Electrochemical Society, Vol. 107, March 1960, pp. 226-231.

38. Summerfield, M., and Ohlemiller, T.J., "A Critical Analysis of Arc Image Ignition of Solid Propellants," Princeton University, Aerospace and Mechanical Sciences Report No. 789, July 1967 (also AFOSR Scientific Report No. 67-1534).

39. Levenspiel, O., Chemical Reaction Engineering; An Introduction to the Design of Chemical Reactors, N. Y., Wiley (1962).

40. Kiser, R.W., Introduction to Mass Spectrometry and Its Applications, Prentice-Hall, Inc., Englewood Cliffs, N. J., 1965.

41. Uncertified Mass Spectra of Benzyl Chloride, B.F. Goodrich Chemical Co., Calvert City, Ky. From Mass Spectra Data Table, Chemistry Library, Purdue University.

42. Mellor, A.M., "Heterogeneous Ignition of Metals: Model and Experiment," Ph. D. Dissertation, Princeton University, 1967.

43. Frank-Kamenetskii, D.A., Diffusion and Heat Exchange in Chemical Kinetics, Princeton University Press (Translation) 1955.

44. Bird, R.B., Stewart, W.E., and Lightfoot, E.N., Transport Phenomena, John Wiley & Sons, New York, 1960.

45. Laidler, K.J., Chemical Kinetics, McGraw Hill, Inc., New York, 1965.

46. Gaydon, A.G., and Wolfhard, H.G., Flames, Their Structure Radiation and Temperature, 2nd Ed., Chapman and Hall, London, 1960.

47. Pearse, R.W.B., and Gaydon, A.G., The Identification of Molecular Spectra, 3rd Ed., Chapman and Hall, London, 1963.

48. Stephens, W.D., Thiokol Chemical Corporation, Personal correspondence, April 18, 1968.

49. Keenan, J.H., and Kaye, J., Gas Tables, John Wiley, Inc., New York, 1948.

50. Selected Values of the Properties of Hydrocarbons, NBS Circular C461, U.S. Department of Commerce, 1947.

APPENDIX A

NOMENCLATURE

Throughout this report, symbols are defined as they are used. The following symbols which occur more frequently are presented here in addition.

Symbol

C	concentration, appropriate units
D	mass diffusivity, cm^2/sec
E	activation energy, kcal/mole
Le	Lewis number, dimensionless
$\dot{q}$	heat flux, cal/cm^2-sec
T	Temperature, ^oK or ^oC
t	time, sec or millisec

Greek Symbols

α	thermal diffusivity, cm^2/sec
λ	thermal conductivity, cal/cm-sec-^oK

Superscripts

*	ignition condition

Abbreviations

AP	ammonium perchlorate
CTPB	carboxy terminated polybutadiene

ITA	ignition test apparatus
m/e	mass to charge ratio
PBAA	polybutadiene acrylic acid
PS	polystyrene.
TOFMS	time-of-flight mass spectrometer

APPENDIX B

DESCRIPTION OF IGNITION TEST APPARATUS

General

As mentioned earlier the five subsystems of the ignition test apparatus, (ITA) will be described here. A sketch of the ignition test chamber assembly is depicted in Figure 22. The chamber assembly may be considered as the heart of the ITA, since sample conditioning and exposure to the oxidizer occur there.

In the original design, provision was made for a cam-operated cutter to slice a thin wafer from the sample surface just after the sample entered the oxidizer chamber. However, since such high temperatures were required for ignition and the physical properties of the polymers made them unsuitable for cutting, this feature was abandoned when problems with operation of the cutter occurred. Another original feature of the ITA was a gas sampling system which would permit gas samples to be withdrawn from the small enclosed volume near the viewing window. The objective here was to remove the gas sample at some predetermined fraction of the ignition time and analyze the reactant gases for the mole fraction of fuel present. This feature was not utilized due to the large experimental variation in the ignition times.

Pressure Vessel Assembly

The components of the pressure vessel assembly include the inert and oxidizer cylinders, the mating V-flanges together with the V-clamp,

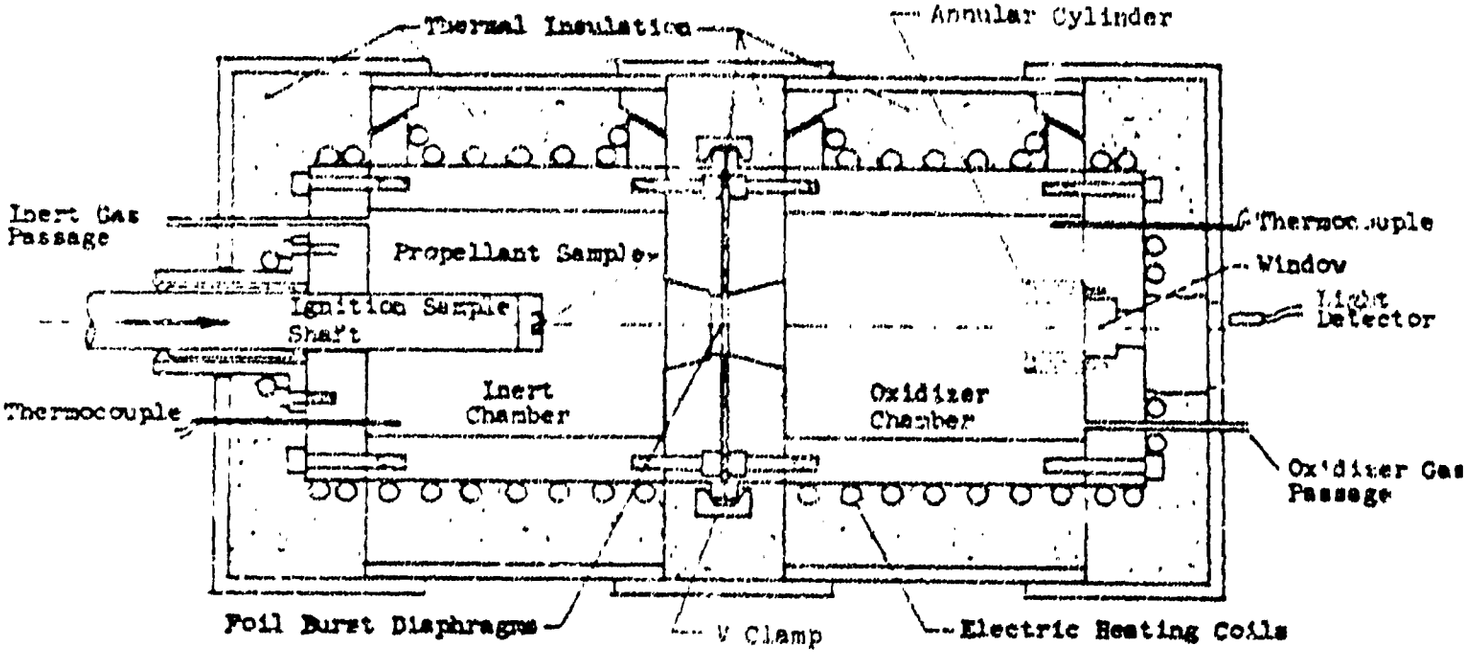

Figure 22 Sketch of Ignition Test Chamber Assembly

and the two end flanges. The two cylinders were fabricated from Type 317 stainless steel and the other components were fabricated from alloy steel. The alloy steel parts were heat treated and then plated with either chromium or nickel for corrosion resistance. During the tests with chlorine gas the plated parts were pitted slightly by the extremely corrosive chlorine and hydrogen chloride gas.

O-rings were employed throughout the test chamber assembly for sealing. O-rings made of a high temperature elastomeric compound (Viton A) were utilized, but still the o-ring properties were the limiting factor for high temperature operation. Even though the maximum sustained operating temperature was limited to about 260°C, several experiments were conducted at temperatures up to 320°C. It was experimentally determined that the ITA could be operated with oxygen at these temperatures for times up to about one hour without o-ring failure. However, at these conditions, the o-rings were severely degraded and o-ring replacement was required after each test. Since complete replacement of the o-rings in the ignition chamber assembly was rather difficult and time consuming (requiring realignment and adjustment of the kinematic system), only a few tests were conducted at temperatures in excess of 300°C.

Thermal Control System

The thermal control system is composed of the electrical heating coils, thermal insulation, sensing thermocouples and two

temperature controllers. Independent temperature control is provided for both the inert chamber and the oxidizer chamber. Electrically insulated nichrome wire heating elements are wrapped on the outside surface of the inert and oxidizer cylinders and the outer surface of the end flanges. The heating coils are covered with thermal insulation and a structural shell is fitted outside this insulation. Separate thermocouples monitor the oxidizer and inert chamber temperatures. Two proportional temperature controllers (Alnor Type N-19 and West Model JP-53) compare signals from the thermocouples with the set point temperature, and control power relays which are connected to the heating coils. A single temperature controller regulates power to the flange heating coil and the cylinder heating coil for each chamber. A thermal insulator of glass bonded mica is located between the V-flanges so that experiments may be conducted at a fixed temperature difference.

Pressure Control System

A schematic diagram of the pressure control system is presented in Figure 23. This system provides for pressurization and evacuation of the test chamber assembly. It is composed of helium, oxygen and chlorine supplies; a vacuum pump, and the required tubing, valves and pressure gauges for controlling gas species and pressure. The chlorine supply includes a heated water container to raise the vapor pressure of the chlorine for high pressure tests.

Operations with chlorine gas required several additional safety

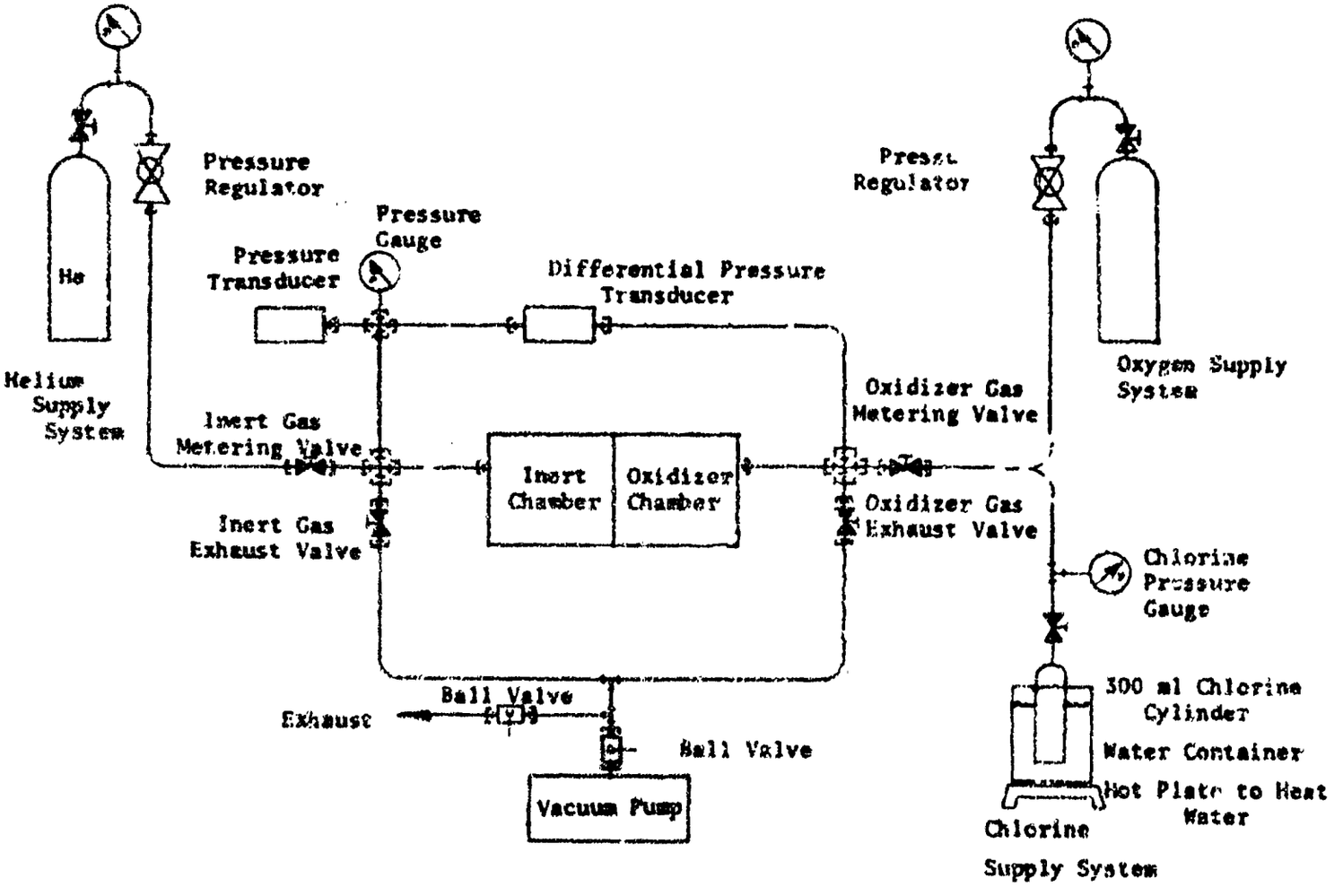

Figure 23 Schematic Diagram of Pressure Control System

precautions. An exhaust hood was constructed over the TTA and a gas mask was available during all chlorine tests. The waste chlorine gas was exhausted into a tank containing an aqueous sodium hydroxide solution.

Kinematic System

The kinematic system provides for the movement of the sample shaft into the oxidizer chamber. This system consists of a pneumatic cylinder, trigger mechanism, shock absorber, load transferring device, and the sample shaft. The pneumatic cylinder (Miller Fluid Power, Model J74, 5¼ in. bore by 23 in. stroke) was specially modified for only a 7 in. working stroke. The piston rod of the pneumatic cylinder is connected to the sample shaft with a clevis pin adapter.

The solenoid operated trigger mechanism is mounted on the rod end of the pneumatic cylinder and restrains the movable mass by engagement with the clevis adapter when the piston is fully retracted. The shock absorber is offset to the side of the ignition chamber assembly (see Figure 9) and the decelerating force is transferred from the shock absorber to the sample shaft by a swinging arm which is struck by the clevis adapter after the sample shaft has traveled a distance of five inches. The entire moving mass is decelerated to zero velocity in a distance of two inches. The shock absorber is a variable energy, constant force type (Efdyn Corporation, Model ASA-2-2-PS).

A brief description the operation of the kinematic system follows. The movable mass (piston, piston rod, clevis adapter and sample shaft) is fully retracted so that the free end of the sample shaft is located in the inert chamber. The trigger mechanism is cocked and the piston end of the pneumatic cylinder is pressurized with nitrogen (usually to about 148 psig). Upon energization of the trigger solenoid, the movable mass is accelerated by the compressed nitrogen behind the piston. After the movable mass has traveled five inches the clevis adapter impacts with the swinging arm assembly and the moving mass is decelerated by the shock absorber in the last two inches of the seven inch stroke.

The sample travels from its initial position in the inert chamber to the burst diaphragm in about 0.014 to 0.030 seconds depending on the pressure in the chambers. Exposure to the oxidizer gas is essentially "instantaneous" (the time taken to shear the diaphragm) and the entire stroke is completed in about 0.12 to 0.15 seconds.

The Instrumentation System

The following parameters were recorded by the instrumentation system: inert chamber temperature, oxidizer chamber temperature, inert chamber pressure, differential pressure between the inert and oxidizer chambers, and ignition time. Temperatures were measured by thermocouples projecting into each test chamber and were recorded by Brown temperature compensated millivolt recorders. Both the inert chamber pressure and the differential pressure were measured by

Wiancko variable reluctance transducers and were recorded by Brown millivolt recorders. The differential pressure transducer output was also recorded by a direct writing oscillograph (CEC Model 5-124). The pressure transducers were calibrated electrically prior to each run, and periodically against a precision pressure gauge which had been dead weight calibrated. The accuracy of the inert and differential pressure transducers is estimated to be ± 2psi and ± 0.5psi respectively.

The ignition of the sample was monitored by either, or both, of two photodetectors. A photodiode (Texas Instruments Type 1N2175) which was connected to a small transistor amplifier circuit was utilized as the principal sensor for all of the ignition experiments. Its amplified output was recorded on the oscillograph. The spectral response of this photodiode is presented in Figure 24. The other photodetector, sensitive in the ultraviolet (UV) spectrum, was a prototype of a device which is currently under development by Honeywell, Inc. for use in fire detection applications. This UV detector is an ionization type detector and is much more sensitive than the photodiode. The spectral response of the UV detector is depicted in Figure 25, and the electrical schematic employed with the UV detector is presented in Figure 26. Fused quartz windows were employed in the ITA when the UV detector was utilized. Ignition was detected by both devices within one millisecond of the same time for all tests in which both detectors were utilized.

The beginning of the ignition time interval was indicated on

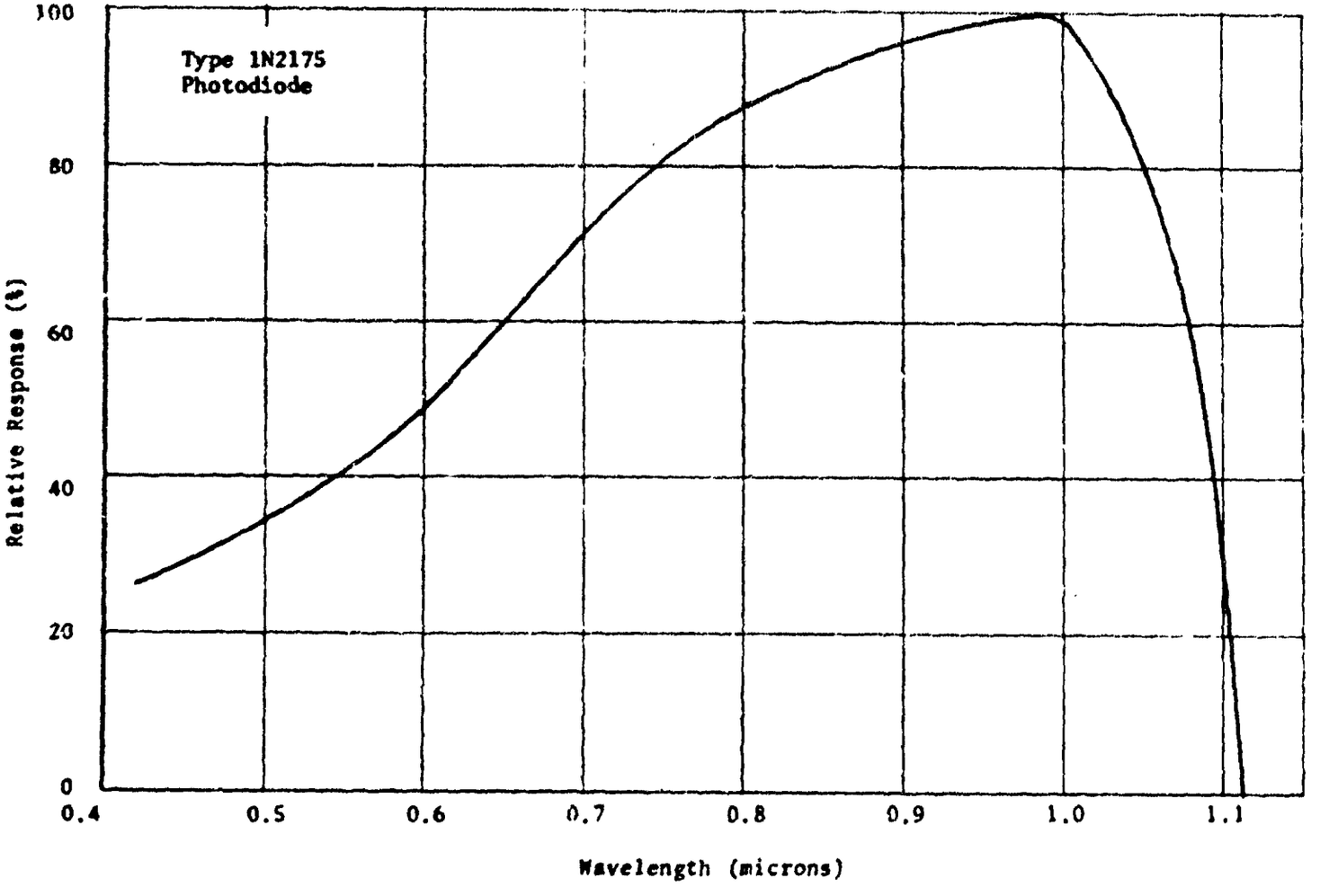

Figure 24 Relative Spectral Response of Photodiode Detector

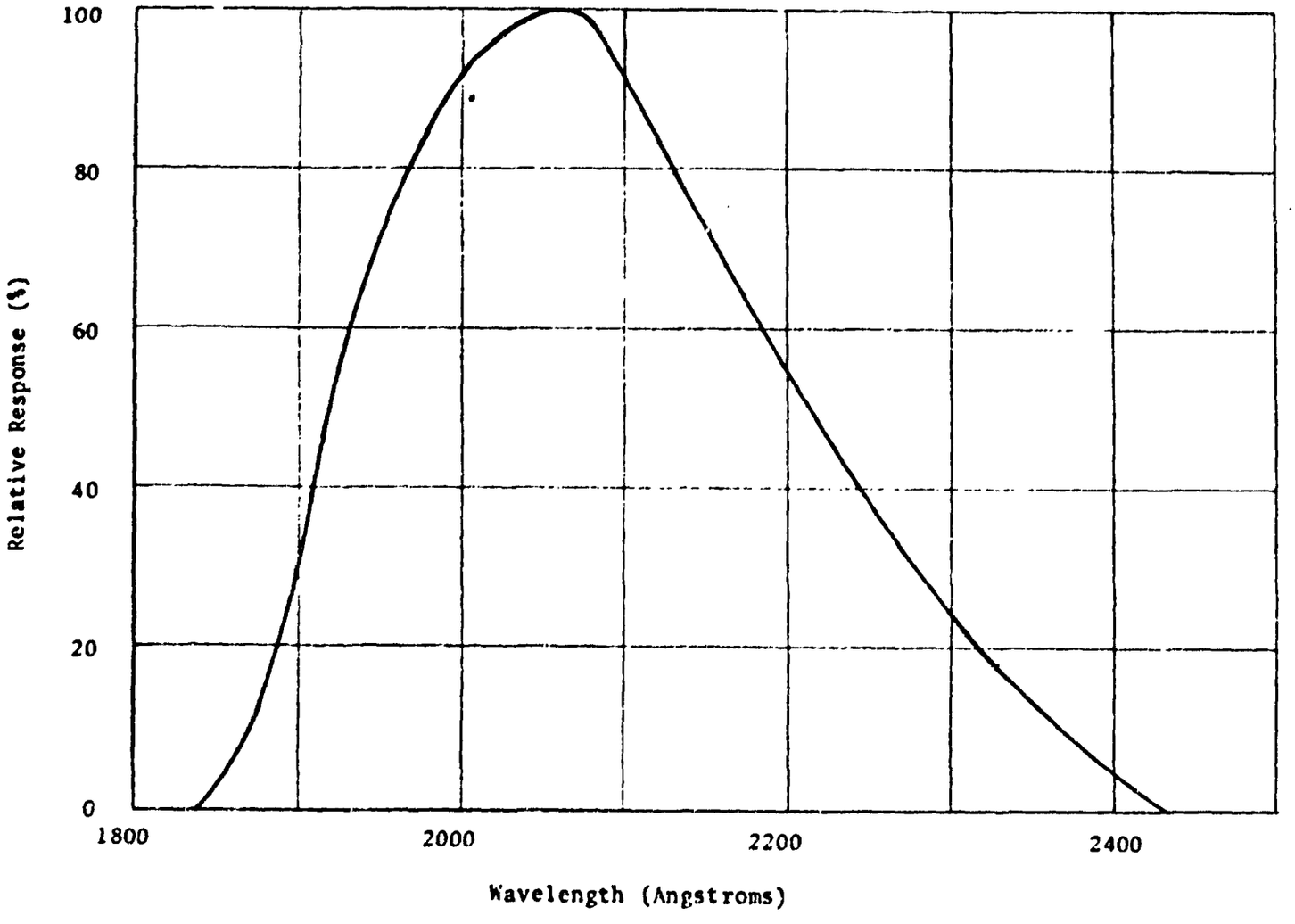

Figure 25 Relative Spectral Response of Ultraviolet Detector

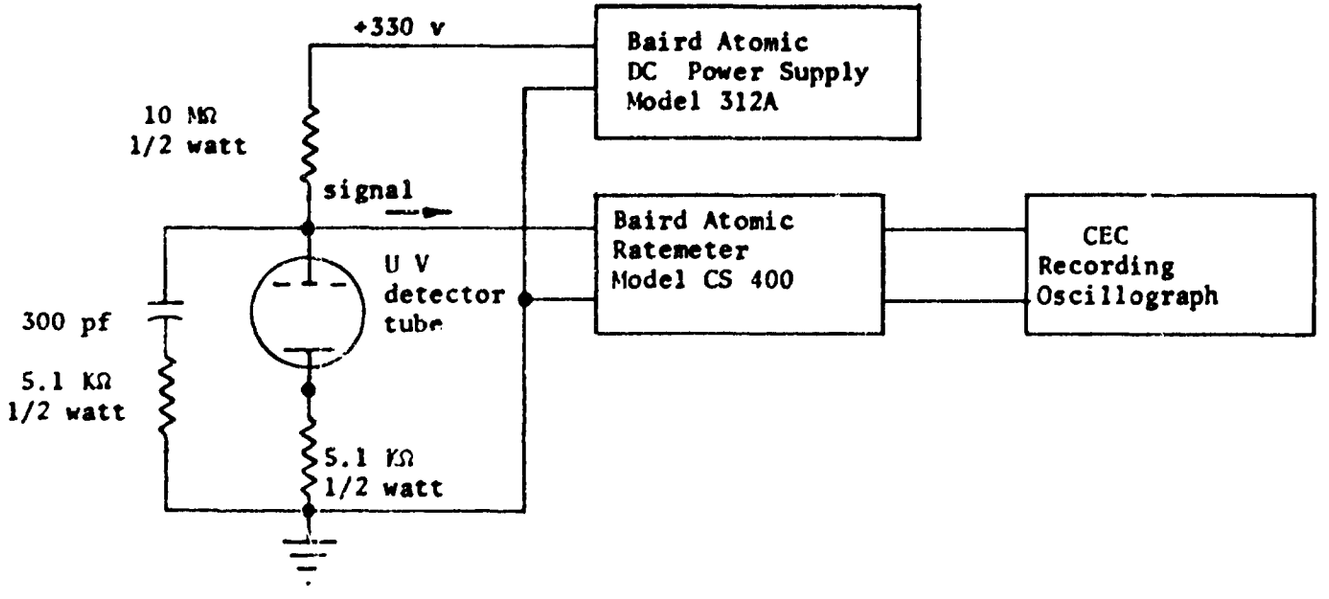

Figure 26 Electrical Schematic for Ultraviolet Detector

the oscillograph by the actuation of a microswitch. The microswitch was located so that actuation would occur as the sample entered the oxidizer chamber. The time interval between the actuation of the microswitch and the first indication of a sustained photodectector signal was taken as the ignition time. A typical oscillogram of an ignition test showing the detector signals and the measurement of ignition time is presented in Figure 37.

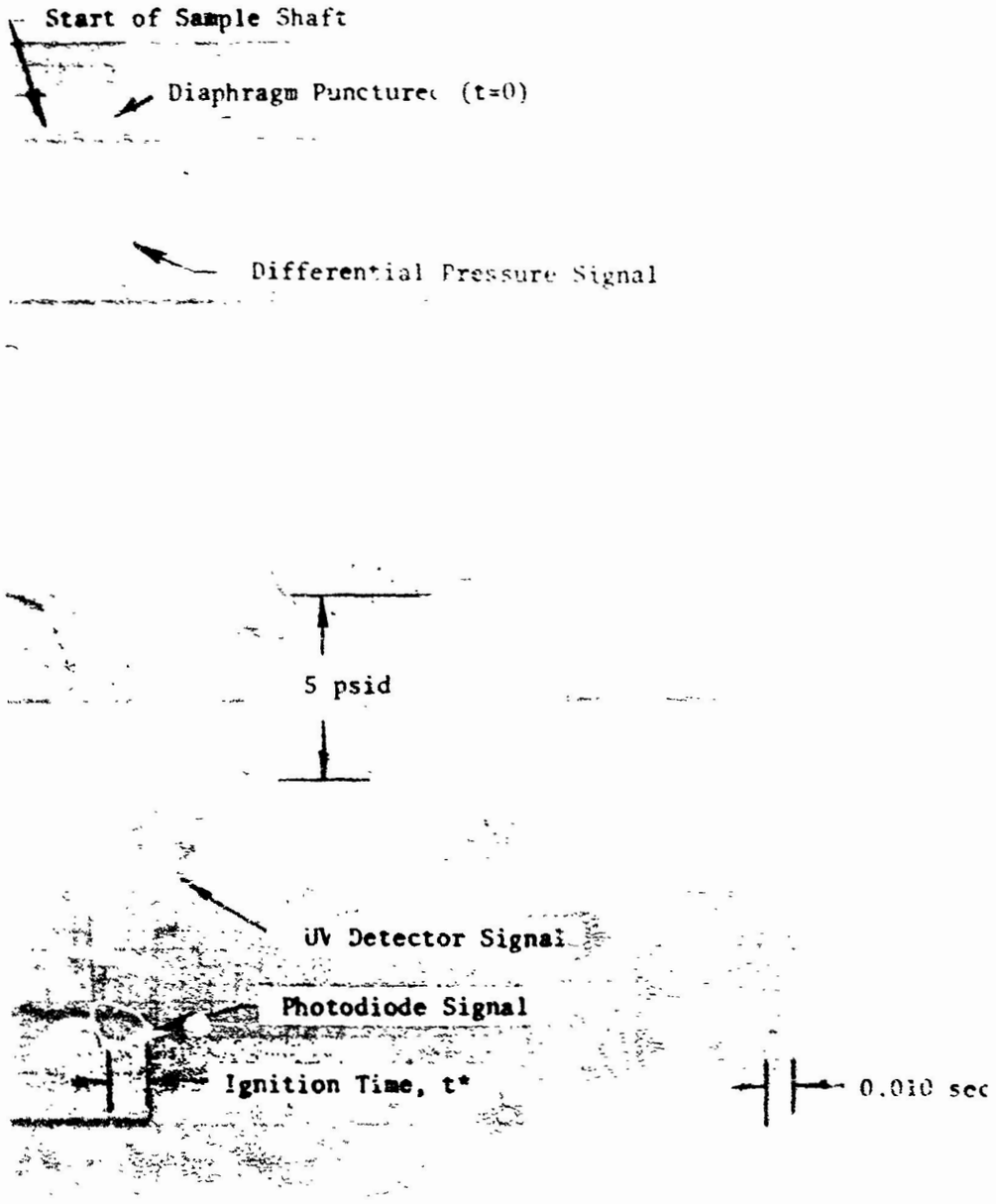

Figure 27 Typical Oscillogram from an Ignition Test

APPENDIX C

IGNITION TEST PROCEDURE

The procedures described below for conducting the ignition tests are similar for the experiments employing each of the oxidizing gases and gas mixtures.

The appropriate polymer sample was first prepared and installed in the sample holder as described earlier, and the ITA was checked for cleanliness of the interior surfaces and of the observation window in the oxidizer end flange. The sample holder was installed on the sample shaft, and the projecting surface of the sample was trimmed with a razor blade. The sample shaft was then retracted into the inert chamber by momentarily pressurizing the rod end of the pneumatic cylinder. The V-flange was assembled by installing the burst diaphragm(s), o-rings and the thermal insulation spacer. The oxidizer end cap was next attached to the oxidizer cylinder with eight socket head cap screws. After connecting the environmental gas supply lines to each chamber, the chamber assembly was pressurized for leak check purposes with inert gas. Any observable leaks were repaired, and the chamber assembly was vented to one atmosphere pressure. While the chambers remained at atmospheric pressure the pressure instrumentation was calibrated

electrically and the temperature recorders were checked to insure that they were indicating the correct room temperature. The inert and oxidizing chambers and the gas supply feed lines were evacuated to a pressure of one torr or less. The vaccuum pump was isolated from the chamber assembly by closing the ball valve (see Figure 23) and the two chambers were individually and simultaneously filled with inert and oxidizing gas to one atmosphere pressure. This (and subsequent) simultaneous filling operations were performed by manually controlling the metering valves to the chambers in a manner to minimize the differential pressure. A meter indicating the signal from the differential pressure transducer was mounted on the valve control panel to permit monitoring of the differential pressure. Once the chambers had been filled to one atmosphere, the heaters were energized and allowed to heat to the predetermined test temperature. During heating, the trigger mechanism was cocked and the photodetectors were installed and checked out. After the prescribed temperature had been attained in both chambers, the chambers were either promptly filled to the predetermined test pressure (normal heating) or there was an additional eight minute waiting period before filling (slow heating). The chambers were slowly and simultaneously filled to the test pressure in the aforementioned manner minimizing the pressure differential between chambers. This filling process usually required about two minutes. The signal from the differential pressure transducer was recorded during the filling process to ensure that no large pressure

differentials occurred which would cause diaphragm damage and leakage between the chambers.

For the experiments with mixed gases in the oxidizer chamber, both chambers were filled with inert gas to the predetermined partial pressure. Then the chambers were individually pressurized to the prescribed total pressure with the oxidizing and inert gases. Mixing of the gases was accomplished by diffusion.

Once the proper pressures had been attained in the chambers, the pneumatic cylinder was charged with nitrogen to about 148 psig, and a final check was made of all instrumentation and test conditions. The fire switch was then acturated, starting the oscillograph and next energizing the trigger release solenoid a fraction of a second later. After a duration of about twenty seconds the oscillograph was automatically stopped by a time delay relay.

After the ignition test, the chambers were vented to atmospheric pressure and cooled. The recorded data was reduced, the sample examined, and the ITA was cleaned in preparation for the next test.

APPENDIX D

POLYMER CONSTITUENTS

The CTPB and PBAA polymers were furnished by the Huntsville Division of Thiokol Chemical Corporation. The constituents of both polymers and for the CTPB-AP propellant are presented below (48). The CTPB Polymer (Mix No. 004500) contains the following ingredients: ZL-434, carboxy terminated polybutadiene; MAPO, tris-(2 methylaziridinyl) phosphine oxide; ERLA-0510, epoxy curing agent; DOS, dioctyl sebacte; and iron linoleate. The CTPB-AP propellant (Mix No. JA860) contains the following ingredients in addition to the above polymer constituents: ground and unground ammonium perchlorate; Fe_2O_3, burning rate catalyst; and small percentage of aluminum powder. The PBAA polymer (Mix. No. 004501) contains the two ingredients: PBAA; and BPABGE, Bis-phenolacetone-bis-glycidyl ether.

Because of both the classified and proprietary nature of propellant formulations, the percentages of each ingredient are not known. However, the manufacturer of the polymers is able to provide such information to qualified requestors.

The polystyrene samples were cut from commercial polystyrene rod which is marketed by Westlakes Plastic Co., Lenni Mills, Pennsylvania under the trade name of "Stryolux."

APPENDIX E

CALCULATION OF IGNITION TIME BY WILLIAMS' METHOD

Williams (12) has analyzed the problem of propellant ignition by heterogeneous reaction and presented a graphical solution in terms of dimensionless variables for the case of zero heat flux to the surface (i.e. the hypergolic case). The dimensionless time, τ, is defined by

$$\tau \equiv \frac{\pi \{(QBY_o^n/T_o) \exp(-\beta)\}^2 t}{\{(\lambda_s\rho_s c_s)^{1/2} + (\lambda_g\rho_g c_g)^{1/2}\}^2} \qquad \text{(E-1)}$$

and the dimensionless parameter α by

$$\alpha \equiv \{(\lambda_s\rho_s c_s)^{1/2} + (\lambda_g\rho_g c_g)^{1/2}\}T_o/(\rho_g Y_o Q D_g^{1/2}) \qquad \text{(E-2)}$$

where

Q = energy of reaction, cal/g of oxygen

B = pre-exponential factor, g/cm^2-sec

Y_o = initial mass fraction of oxygen in the gas phase, dimensionless

n = overall order of the reaction, dimensionless

β = dimensionless activation energy, E/RT_o

t = time, sec

E = activation energy, cal/mole

R = universal gas constant, cal/mole$^\circ$K

T_o = initial temperature, $^\circ$K

λ = thermal conductivity, cal/cm-sec-^{o}K

ρ = density, g/cm^{3}

c = specific heat, cal/g-^{o}K

D_g = diffusion coefficient in gas phase, (cm^{2}/sec)

and the subscripts s and g indicate the solid and gas phases respectively.

The results of the numerical calculations are presented in the graphical form of τ as a function of dimensionless surface temperature rise $(T-T_o)/T_c$ with α and β as parameters for a first order reaction. In order to compute the ignition time, α and β must first be calculated and employed to determine τ^* from the graphical solutions. Then t^* is computed directly by Equation E-1.

The calculation of the ignition time is presented below for the following given conditions.

PMMA polymer and pure oxygen gas at 20 atmospheres and 533^{o}K.

Assume E = 16 kcal/mole.

The oxygen density (concentration) computed at the above conditions is $\rho_g = 14.6 \times 10^{-3}$ g/cm^{3}.

Computation of α:

The thermal properties of PMMA are taken from Reference (15) p. 361.

$(\lambda_g \rho_s c_s)^{\frac{1}{2}} = 1.39 \times 10^{-2}$ cal/(cm)^{2}(sec)$^{\frac{1}{2}}$(^{o}K)

The thermal properties of O_2 at 533^{o}K and 20 atmospheres are obtained as follows:

λ_g = 9.8 x 10^{-5} cal/cm-sec-^oK. This value is estimated from λ_g = 6.35x10^{-5} cal/cm-sec-^oK at 300^oK and 1 atm by the procedure given in Reference 44 pp. 250-251.

c_g = 6.988 cal/mole-^oK. This value was obtained directly from Table 14, Reference (49).

Q is calculated from a stoichiometric reaction of O_2 and butadiene

$$2C_4H_6 + 11O_2 \rightarrow 6H_2O(g) + 8CO_2 - 2(\Delta H_c)$$

where the ΔH_c is the heat of combustion for butadiene

ΔH_c = -10.8 kcal/g fuel (Reference 50)

and

$$Q = (10.8 \text{ kcal/g fuel})\left(\frac{108 \text{ g fuel}}{352 \text{ g oxygen}}\right)$$

Q = 3380cal/g-oxygen

The diffusion coefficient, D_g, is computed for the self diffusion of oxygen since there is no diluent in the gas phase.

D = 2.84x10^{-2}cm^2/sec computed from Equation 16.4-13 of Reference 44.

Using the above values, α was calculated by Equation E-2.

α = 6.4

Computation of β:

$$\beta = \frac{P}{\tau} = \frac{(16,000)}{(1.986)(533)} = 15.1$$

From α = 6.4 and β = 15.1, τ^* is estimated from Figure 2 of Reference (12).

τ^* = 6x10^{-3}

The ignition time may now be computed from Equation E-1 if a value of B is chosen. From Reference (15), p. 391, the experimentally determined pre-exponential factor, QB for a PBAA-AP propellant is recorded as 6.7×10^{9} cal/cm^2-sec. Employing the aforementioned value of QB, t* is calculated to be

$$t^* = 0.45 \times 10^{-7} \ .$$

or roughly seven orders of magnitude from the measured value of about 0.150 sec. Of course, the agreement may be improved by merely changing the value of the pre-exponential factor, B.

APPENDIX F

METHOD OF ESTIMATING MASS FLUXES FROM BULK THERMAL DEGRADATION DATA

The bulk thermal degradation of polymers is expressed as mass per cent of sample vaporized per unit time. Because the shape and condensed phase of the sample is unknown it is necessary to assume a sample shape. In order to make a conservative analysis, (i.e. predict a high value of mass flux for a given bulk thermal degradation rate) a spherical shape is assumed. In addition, the surface to volume ratio of a sphere will be further reduced by a order of magnitude to account for almost any conceivable shape of the sample and thus give a highly conservative estimate of the mass flux.

The following sample calculation will illustrate the calculation procedure.

Assume a mass thermal degradation rate, k

$$k = 1.25 \times 10^{-6} \%/\text{sec.}$$

Now, compute the radius of sphere of polymer having a mass of one gram.

$$M_s = \rho V_s = \rho \frac{4}{3} \pi r^3$$

where M_s = mass of sphere = 1 g

ρ = density of sample, say 1.05 g/cm^3

V_s=volume of sphere, cm^3, and

r=radius of sphere, cm.

Solving this equation for, r

$$r = \left[\frac{M_s\ 3}{\rho\ 4\pi}\right]^{1/3} = (0.227)^{1/3} cm.$$

Now the equation for the surface of a sphere, S_s is

$$S_s = 4\pi r^2 = 4\pi\ (0.227)^{2/3} = 4.66 cm^2,$$

and one tenth of this area is

$$(0.1)\ S_s = 0.466 cm^2.$$

Write the mass flux, $\dot{m}$, (g/cm^2-sec) as

$$\dot{m} = \frac{(\text{mass of sample})}{(0.1)\ (S_s)}\ \left(\frac{k}{100}\right)\ g/cm^2\text{-sec}.$$

Thus,

$$\dot{m} = \frac{(1.0)\ (1.25 \times 10^{-6})}{(0.466)\ (100)} = 2.69 \times 10^{-8}\ g/cm^2\text{-sec},$$

or

$$\dot{m} = 0.0215\ k\ .$$

APPENDIX G

TABULATED IGNITION DATA

Table 1 presents the experimental data and calculated concentrations for the ignition tests.

Table 1 Ignition Test Data

Ignition Time (sec)	Pressure (atm)	Temperature Oxidizer Chamber (°C)	Temperature Inert Chamber (°C)	Oxidizer[c] Concentration ($g/cc \times 10^3$)	Oxidizer Gas Species	Inert Gas Species	Sample Type	Heating[d] Rate
Part a. CTPB Data for Figure 12								
0.811	10.2	258	258	7.5	O_2	He	CTPB	H
0.172	12.4	261	261	9.1	O_2	He	CTPB	H
0.364	15.0	261	260	11.0	O_2	He	CTPB	M
0.767	14.8	264	266	10.7	O_2	He	CTPB	M
0.185	14.9	269	269	10.8	O_2	He	CTPB	H
0.385	17.4	263	263	12.7	O_2	He	CTPB	M
0.450	20.2	262	261	14.8	O_2	He	CTPB	H
0.170	20.2	263	263	14.7	O_2	He	CTPB	H
1.170	20.2	265	262	7.5	O_2-He	He	CTPB	M
0.571	20.2	270	272	7.4	O_2-He	He	CTPB	H
0.795	12.6	266	266	9.1	O_2	He	CTPB	H
0.089	12.5	260	260	9.1	O_2	He	CTPB	H
0.386	8.3	255	260	6.5	O_2	He	CTPB	S
0.313	20.6	260	260	15.1	O_2	He	CTPB	S
0.405	14.9	260	261	10.9	O_2	He	CTPB	S
0.314	20.0	260	261	14.6	O_2	He	CTPB	S
0.249	14.9	260	260	10.9	O_2	He	CTPB	S
Part b. PBAA Data for Figure 15								
0.295	14.8	259	260	10.9	0	He	PBAA	S
0.305	10.7	260	260	7.8	O_2	He	PBAA	S

Table 1 (cont'd.)

Ignition Time (sec)	Pressure (atm)	Temperature Oxidizer Chamber (°C)	Temperature Inert Chamber (°C)	Oxidizer[c] Concentration (g/cm³ x10³)	Oxidizer Gas Species	Inert Gas Species	Sample Type	Heating[d] Rate
0.205	20.0	260	257	14.7	O_2	He	PBAA	S
0.155	20.4	261	260	14.9	O_2	He	PBAA	S
0.107	15.0	260	260	10.9	O_2	He	PBAA	S
0.159	10.1	260	261	7.4	O_2	He	PBAA	S
0.014	20.6	321	318	13.3	O_2	He	PBAA	S
			Part c. Other CTPB Data					
a	4.8	204	202	--	O_2	H_2	CTPB	H
a	4.9	260	260	--	O_2	H_2	CTPB	H
1.237	10.2	312	256	6.8	O_2	He	CTPB	H
0.134	10.2	324	253	6.7	O_2	He	CTPB	H
2.376	10.2	312	249	6.8	O_2	He	CTPB	H
b	10.2	316	257	--	O_2	He	CTPB	H
a	10.2	202	203	--	O_2	He	CTPB	H
a	10.2	205	207	--	O_2	He	CTPB	H
a	10.2	316	204	--	O_2	He	CTPB	H
0.001	10.0	327	204	6.5	O_2	He	CTPB	H
a	10.1	317	202	--	O_2	He	CTPB	H
a	10.1	326	206	--	O_2	He	CTPB	H
0.059	10.0	327	207	6.5	O_2	He	CTPB	H
a	10.1	327	157	--	O_2	He	CTPB	H
0.165	12.4	272	265	8.9	O_2	He	CTPB	H
b	15.0	261	262	--	O_2	He	CTPB	H
b	20.2	260	252	7.3	O_2-He	He	CTPB	H

Table 1 (cont'd.)

Ignition Time (sec)	Pressure (atm)	Temperature Oxidizer Chamber (°C)	Temperature Inert Chamber (°C)	Oxidizer[c] Concentration ($g/cm^3 \times 10^{-6}$)	Oxidizer Gas Species	Inert Gas Species	Sample Type	Heating[d] Rate
b	20.0	264	263	7.5	O_2-He	He	CTPB	N
a	7.6	262	260	--	O_2	He	CTPB	N
a	7.4	264	263	--	O_2	He	CTPB	N
b	7.5	266	267	--	O_2	He	CTPB	S
b	10.0	262	260	--	O_2	He	CTPB	S
b	10.0	262	263	--	O_2	He	CTPB	S
b	10.0	261	261	--	O_2	He	CTPB	S
b	10.0	258	261	--	O_2	He	CTPB	S
b	15.2	262	262	--	O_2	He	CTPB	S
b	20.3	260	260	7.4	O_2-He	He	CTPB	S
b	20.2	260	262	7.4	O_2-He	He	CTPB	S
b	12.6	260	260	--	O_2	He	CTPB	S
a	4.9	21	21	--	Cl_2	N_2	CTPB	N
a	5.1	128	119	--	Cl_2	N_2	CTPB	N
a	4.9	124	116	--	Cl_2	N_2	CTPB	N
a	2.0	124	124	--	Cl_2	N_2	CTPB-AP	N
a	5.1	180	191	--	Cl_2	N_2	CTPB-AP	N
a	5.1	174	171	--	Cl_2	N_2	CTPB-AP	N
a	5.1	244	233	--	Cl_2	He	CTPB-AP	N
a	10.2	316	260	--	Cl_2	He	CTPB	N
a	4.4	316	260	--	Cl_2	He	CTPB	N
			Part d. Other PBAA Data					
a	7.5	259	264	--	Cl_2	He	PBAA	S
a	9.8	263	260	--	Cl_2	He	PBAA	S

Table 1 (cont'd.)

Ignition Time (sec)	Pressure (atm)	Temperature Oxidizer Chamber (°C)	Temperature Inert Chamber (°C)	Oxidizer[c] Concentration ($g/cm^3 \times 10^3$)	Oxidizer Gas Species	Inert Gas Species	Sample Type	Heating[d] Rate
a	10.0	254	259	--	Cl_2	He	PBAA	S
a	10.0	263	259	--	Cl_2	He	PBAA	S
a	20.3	260	263	7.3	O_2-He	He	PBAA	S
a	20.3	260	261	7.7	O_2-He	He	PBAA	S
a	20.3	260	260	7.6	O_2-He	He	PBAA	S
a	7.4	259	260	--	O_2	He	PBAA	S
e	20.6	259	260	11.3	O_2-He	He	PBAA	S
			Part e. PS Data					
a	14.9	226	212	12.0	O_2	N_2	PS	S
b	20.2	260	260	14.7	O_2	He	PS	S
>18.1	20.0	259	260	14.7	O_2	He	PS	S

[a] No ignition

[b] No ignition and no fresh sample surface exposed

[c] Oxidizer concentration not computed for tests in which ignition failed to occur, unless oxidizer chamber environment was mixture of helium and oxidizer

[d] N=Normal; S=Slow, i.e., eight minute wait at test temperature

APPENDIX H

MASS SPECTRAL DATA

The Model 12-107 Bendix Time-of-Flight Mass Spectrometer was operated at the following conditions for all of the polymer spectra experiments.

Filament Current: 3.1 amps

Trap Current: 0.125 μamps

Pressure: $< 10^{-6}$ torr

Ion Lens: Off

Ion Focus: Maximum gain

Electron Energy: 70 volts

Helium flow rates in the sample inlet system were between 8.5 and 13.1 milliliters per minute for all samples. The following tabulated mass spectral data for each polymer are preceded by a graph of the temperature history of the polymer sample.

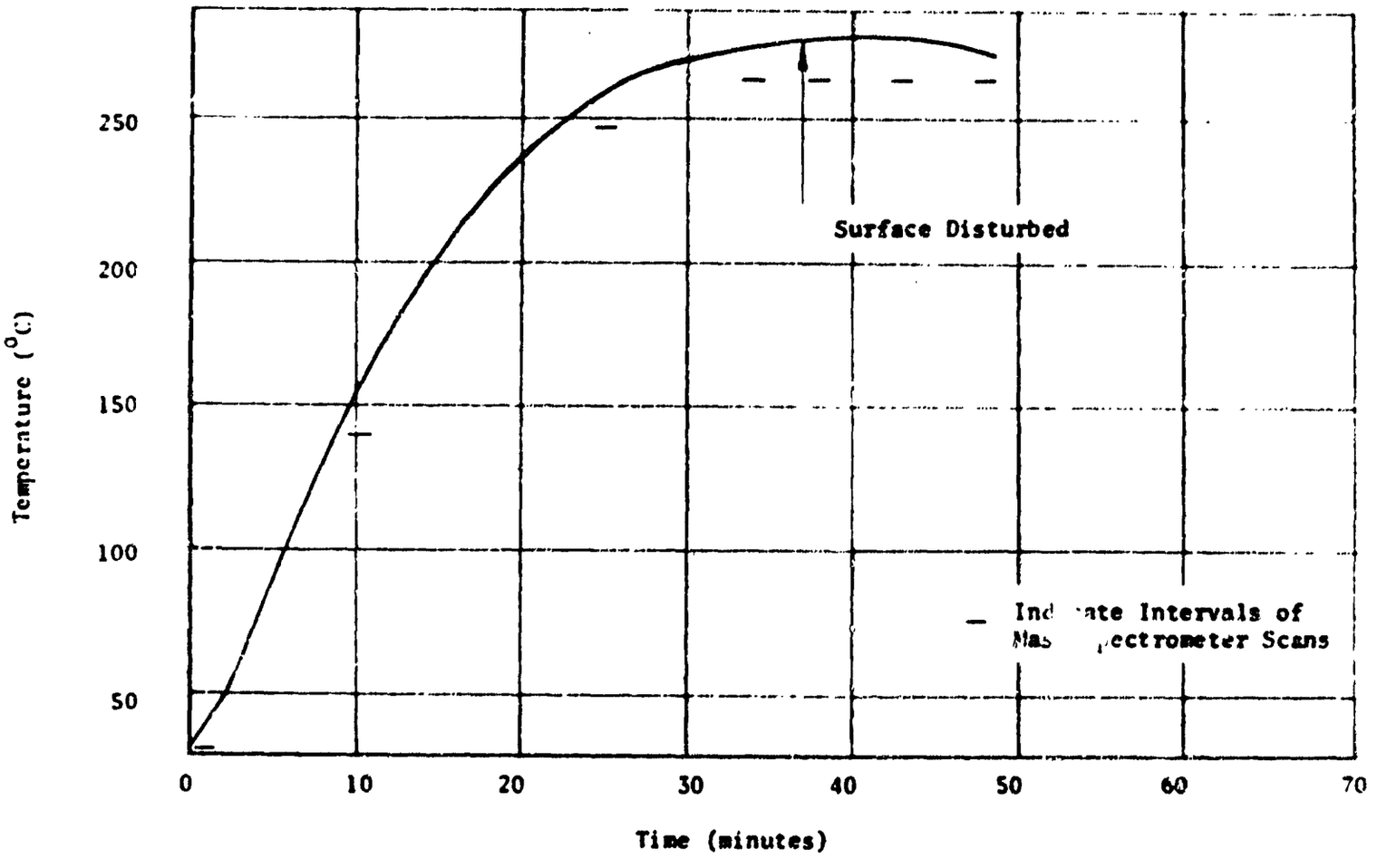

Figure 28 Heating Curve for CTPB Sample

Table 2 Mass Spectra of CTPB Polymer

m/e	Relative Abundance
Scans 1 and 2	
4	100
14	2.20
15	0.50
16	1.05
17	1.50
18	5.20
26	0.30
27	0.40
28	38.0
29	0.70
32	10.5
39	0.25
40	0.60
41	0.60
42	0.40
43	3.03
44	0.50
58	0.90
Scans 3 and 4	
4	100
12	0.75
13	0.75
14	4.40
15	7.45
16	1.90
17	5.20
18	13.3
19	0.30
20	0.25
24	0.25
25	0.90
26	1.80
27	2.80
28	38.0
29	2.30
30	0.20
32	4.95
35	0.20
Scans 3 and 4 (Cont'd.)	
36	0.50
37	0.60
38	0.80
39	1.80
40	1.20
41	2.00
42	2.60
43	16.8
44	6.60
45	0.25
46	0.25
50	0.65
52	0.20
53	0.30
54	0.35
55	0.80
56	0.60
57	0.70
58	8.10
59	0.40
60	0.65
62	0.20
67	0.40
69	0.35
81	0.50
91	0.60
92	0.35
97	0.50
98	0.30
100	0.25
Scans 5 and 6	
4	100
12	0.25
14	1.00
15	1.65
16	0.40
17	2.30
18	9.78
Scans 5 and 6 (Cont'd.)	
26	0.30
27	0.70
28	16.0
29	0.60
32	3.0
36	0.20
39	0.80
40	0.25
41	0.60
42	0.60
43	5.45
44	0.40
57	0.30
58	1.45
59	0.25
96	0.20
Scans 7 and 8	
4	100
14	1.00
15	1.00
16	0.70
17	2.10
18	6.73
25	0.35
26	0.40
27	0.80
28	14.0
29	0.70
31	0.20
32	3.22
37	0.20
38	0.25
39	0.40
40	0.60
41	0.50
42	0.50
43	5.90
44	0.70

Table 2 (Cont'd.)

m/e	Relative Abundance
Scans 7 and 8 (Cont'd.)	
55	0.30
56	0.40
57	0.40
58	2.00
93	0.30
Scans 9 and 10	
4	100
13	0.25
14	1.00
15	1.10
16	0.60
17	1.95
18	6.30
26	0.60
27	1.10
28	15.0
29	1.30
31	0.20
32	2.35
37	0.20
39	0.70
40	0.60
41	0.85
42	0.90
43	4.20
44	0.85
53	0.25
54	0.25
55	0.40
56	0.25
57	0.50
58	1.75
67	0.20
68	0.30
69	0.30
79	0.40
80	0.20
81	0.35

m/e	Relative Abundance
Scans 9 and 10 (Cont'd.)	
91	0.25
131	0.20
Scans 11 and 12	
4	100
14	1.70
15	1.60
16	0.80
17	3.00
18	11.0
25	0.20
26	0.30
27	1.00
28	22.0
29	1.25
30	0.20
31	0.20
32	4.00
38	0.45
39	0.75
40	0.30
41	1.15
42	0.90
43	6.25
44	1.00
53	0.50
54	0.30
55	0.70
56	0.70
57	0.90
58	3.70
59	0.20
67	0.70
68	0.35
69	0.30
70	0.30
71	0.30
77	0.40
78	0.20

m/e	Relative Abundance
Scans 11 and 12 (Cont'd.)	
79	0.40
80	0.40
81	0.30
82	0.20
83	0.30
84	0.20
85	0.20
91	0.50
92	0.60
93	0.40
99	0.30
105	0.30
107	0.20
109	0.30
Scans 13 and 14	
4	100
14	1.60
15	1.65
16	0.60
17	2.40
18	8.55
26	0.40
27	1.00
28	18.6
29	1.30
31	0.20
32	2.80
37	0.20
38	0.30
39	0.80
40	0.40
41	1.50
42	0.55
43	5.75
44	1.30
45	0.20
46	0.20
51	0.20

Table 2 (Cont'd.)

m/e	Relative Abundance
Scans 13 and 14 (Cont'd.)	
54	0.30
55	0.60
56	0.60
57	0.60
58	3.50
59	0.30
65	0.20
67	0.70
69	0.40
70	0.30
71	0.30
77	0.40
79	0.50
81	0.40
85	0.30
91	0.30
93	0.20
97	0.25
105	0.30
107	0.20
108	0.20
115	0.25
118	0.25
131	0.30
146	0.25

m/e	Relative Abundance
Scans 15 and 16 (Cont'd.)	
39	0.85
40	0.30
41	1.00
42	0.80
43	5.90
44	0.85
46	0.20
53	0.40
55	0.60
56	0.40
57	0.70
58	3.50
59	0.30
67	0.40
69	0.35
77	0.30
79	0.30
80	0.30
83	0.30
85	0.20
91	0.50
93	0.20
95	0.20
105	0.20

m/e	Relative Abundance
Scans 17 and 18 (Cont'd.)	
39	0.60
40	0.30
41	1.20
42	0.70
43	5.30
44	0.90
45	0.25
53	0.20
54	0.30
55	0.70
56	0.60
57	0.50
58	3.90
59	0.20
67	0.40
69	0.40
71	0.25
72	0.20
74	0.20
79	0.30
81	0.40
91	0.20
92	0.20
95	0.20
105	0.30

m/e	Relative Abundance
Scans 15 and 16	
4	100
14	0.80
15	1.50
16	0.50
17	2.25
18	8.70
26	0.40
27	0.80
28	15.6
29	1.30
32	2.80

m/e	Relative Abundance
Scans 17 and 18	
4	100
14	0.80
15	1.15
16	0.60
17	1.95
18	8.48
26	0.40
27	0.50
28	16.9
29	1.20
32	2.88
38	0.30

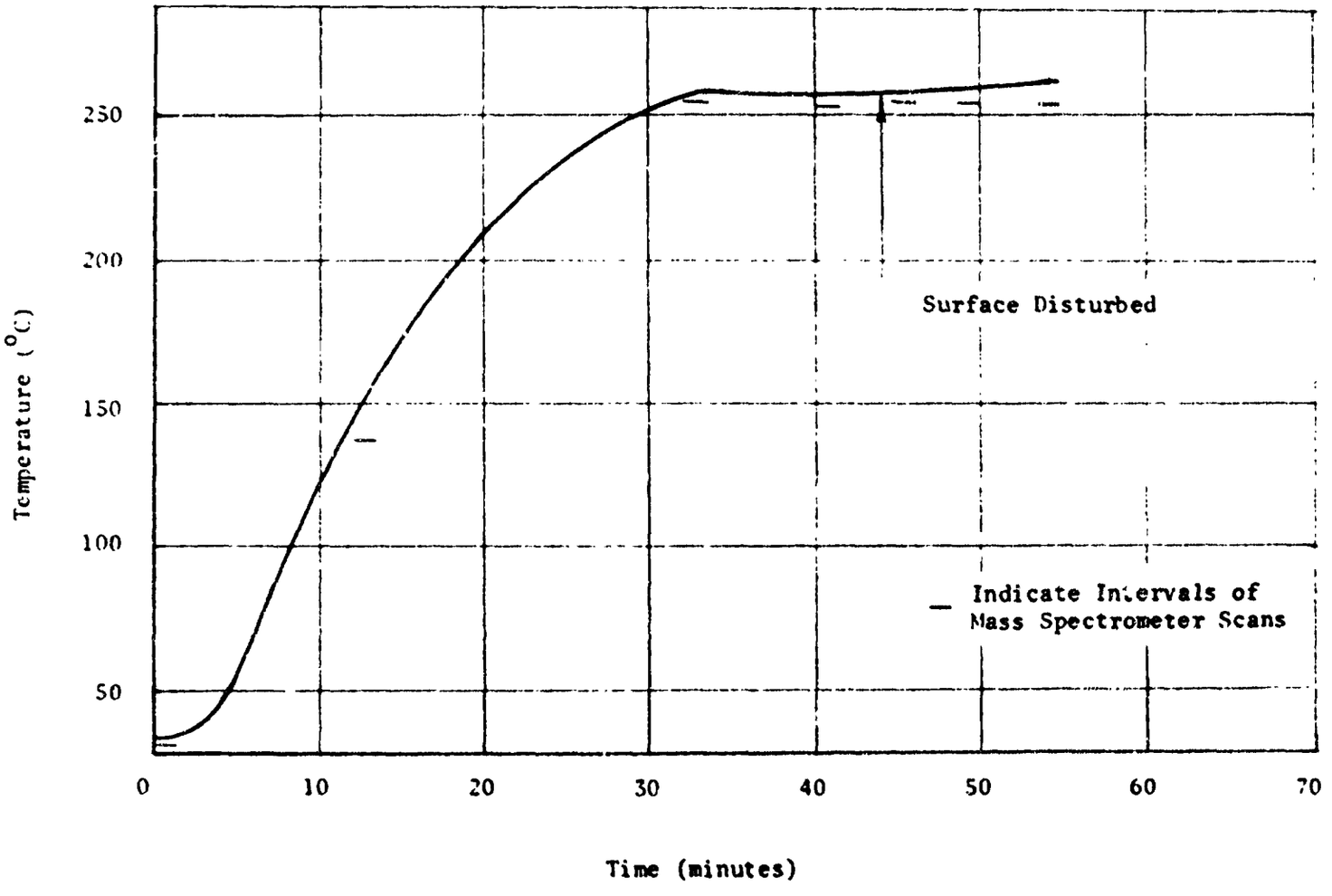

Figure 29 Heating Curve for PBAA Sample

Table 3 Mass Spectra of PBAA Polymer

m/e	Relative Abundance
Scans 1 and 2	
4	100
14	0.60
15	0.40
16	0.25
17	1.40
18	6.35
27	0.15
28	8.25
29	0.40
32	1.65
39	0.20
41	0.25
42	0.25
43	2.20
44	0.40
56	0.10
58	0.60
Scans 3 and 4	
4	100
12	0.30
14	1.80
15	1.45
16	~1.00
17	4.60
18	26.0
26	0.60
27	1.00
28	32.0
29	1.15
31	0.40
32	3.50
39	0.50
41	1.00
42	0.90
43	6.10
44	2.50
53	0.20
55	0.50
56	0.30
57	0.50
58	1.45
69	0.40
Scans 5 and 6	
4	100
14	2.90
15	1.70
16	1.40
17	3.60
18	12.0
20	0.20
26	0.35
27	0.60
28	43.0
29	0.85
32	9.05
36	0.30
38	0.30
39	0.50
40	0.70
41	0.40
42	0.60
43	6.10
44	0.90
45	0.30
51	0.20
55	0.40
56	0.40
57	0.40
58	1.30
59	0.30
71	0.25
81	0.20
Scans 7 and 8	
4	100
14	2.16
15	2.52
17	2.88
18	10.4
26	0.72
27	2.06
28	36.0
29	2.34
32	6.85
37	0.72
38	1.44
39	4.30
40	1.08
41	2.50
42	0.72
44	1.44
45	1.08
50	2.52
51	1.80
52	1.44
55	1.44
56	0.72
57	2.06
58	1.80
62	1.08
63	2.88
65	2.52
89	1.44
90	1.26
91	21.2
92	2.52
126	3.96
128	1.08
Scans 9 and 10	
4	100
12	0.30
13	0.40

Table 3 (Cont'd.)

m/e	Relative Abundance
Scans 9 and 10 (Cont'd.)	
14	2.70
15	3.10
16	1.20
17	5.70
18	24.0
26	1.00
27	4.90
28	35.0
29	5.40
30	0.60
31	0.40
32	3.30
37	0.35
38	0.40
39	3.40
40	1.60
41	6.40
42	2.50
43	12.2
44	4.90
45	0.95
46	0.25
48	0.35
49	0.20
50	0.60
51	0.70
52	0.75
53	1.50
54	2.20
55	3.80
56	2.60
57	4.50
58	7.80
59	0.70
63	0.30
65	0.40
66	0.80
67	1.80
68	1.20
69	1.30
70	1.40
71	1.35

m/e	Relative Abundance
Scans 9 and 10 (Cont'd.)	
72	0.60
73	0.20
77	1.30
78	0.40
79	1.70
80	1.50
81	0.30
82	0.60
83	1.00
84	0.70
85	0.90
86	0.50
87	0.20
91	1.50
92	0.30
93	1.10
94	0.40
95	0.40
96	0.30
97	0.70
98	0.60
99	0.30
103	0.20
105	0.50
106	0.40
107	0.30
108	0.60
109	0.40
110	0.40
111	0.50
119	0.30
Scans 11 and 12	
4	100
12	0.25
14	2.80
15	2.60
16	1.25
17	5.90
18	19.7

m/e	Relative Abundance
Scans 11 and 12 (Cont'd.)	
25	0.30
26	0.90
27	3.65
28	34.6
29	5.20
30	0.60
31	0.70
32	3.74
37	0.35
38	0.40
39	3.25
40	0.80
41	6.00
42	2.95
43	11.5
44	4.30
45	0.60
50	0.30
51	0.70
52	0.40
53	1.40
54	1.50
55	4.90
56	2.70
57	4.40
58	7.78
59	1.90
62	0.40
63	0.30
64	0.30
65	0.50
66	0.55
67	2.50
68	0.70
69	1.50
70	1.20
71	1.30
72	0.30
77	1.20
78	0.40
79	1.60
80	1.20

Table 3 (Cont'd.)

m/e	Relative Abundance
Scans 11 and 12 (Cont'd.)	
81	1.25
82	0.80
83	1.30
84	1.10
85	0.70
91	1.70
92	0.80
93	0.95
94	0.40
95	1.00
96	0.40
97	0.70
98	0.50
99	0.40
105	0.40
107	0.40
108	0.60
121	0.40
Scans 13 and 14	
4	100
12	0.25
13	0.20
14	2.50
15	2.30
16	0.85
17	4.30
18	16.8
25	0.30
26	0.90
27	3.20
28	29.0
29	4.35
30	0.45
31	0.45
32	3.02
37	0.20
38	0.30
39	2.80

m/e	Relative Abundance
Scans 13 and 14 (Cont'd.)	
40	1.20
41	4.50
42	1.70
43	8.28
44	2.80
45	0.50
47	0.25
50	0.50
51	0.40
52	0.30
53	0.70
54	1.00
55	3.30
56	1.60
57	3.15
58	7.35
59	0.55
63	0.25
65	0.60
66	0.40
67	1.10
68	0.60
69	1.45
70	0.60
71	0.75
73	0.30
77	0.50
78	0.40
79	1.20
80	0.70
81	0.80
82	0.85
83	1.00
84	0.40
85	0.55
87	0.25
91	1.00
92	0.40
93	0.55
94	0.30
95	0.40

m/e	Relative Abundance
Scans 13 and 14 (Cont'd.)	
96	0.30
97	0.55
98	0.50
106	0.30
108	0.30
109	0.30
132	0.25
140	0.25
Scans 15 and 16	
4	100
12	0.40
14	3.30
15	2.80
16	1.10
17	7.70
18	21.8
20	0.30
26	0.95
27	3.40
28	37.0
29	3.75
32	4.59
36	0.20
38	0.40
39	2.40
40	1.20
41	5.10
42	1.90
43	10.9
44	4.50
45	0.40
46	0.25
49	0.40
51	0.60
52	0.50
53	0.80
54	1.30
55	4.10

Table 3 (Cont'd.)

m/e	Relative Abundance
Scans 15 and 16 (Cont'd.)	
56	2.10
57	2.60
58	10.0
59	0.50
61	0.30
65	0.50
66	0.30
67	1.70
68	0.50
69	1.20
70	1.20
71	1.30
73	0.40
77	0.80
78	0.50
79	1.40
80	1.00
81	1.00
82	0.30
83	0.80
84	0.80
85	0.90
86	0.30
91	1.50
92	0.70
93	0.90
94	0.40
95	0.50
96	0.45
97	0.50
104	0.30
105	0.40
108	0.50
112	0.50
113	0.40
121	0.60
133	0.30
135	0.45
169	0.30

m/e	Relative Abundance
Scans 17 and 18	
4	100
12	0.20
14	2.10
15	2.20
16	8.80
17	4.70
18	16.8
26	0.60
27	2.25
28	30.5
29	3.20
30	0.50
31	0.40
32	4.62
37	0.20
38	0.40
39	1.75
40	1.10
41	4.10
42	1.50
43	9.70
44	3.95
45	0.50
50	0.20
51	0.45
52	0.30
53	0.50
54	0.90
55	2.60
56	1.60
57	2.60
58	8.30
59	0.60
61	0.40
63	0.30
65	0.40
67	0.60
69	0.90
70	0.80

m/e	Relative Abundance
Scans 17 and 18 (Cont'd.)	
71	0.80
72	0.30
76	0.40
78	0.20
79	0.70
80	0.40
81	0.90
82	0.40
83	0.70
84	0.70
85	0.50
91	1.10
92	0.40
93	0.50
95	0.40
107	0.50
112	0.40
120	0.30
121	0.30
125	0.30
126	0.20
169	0.20

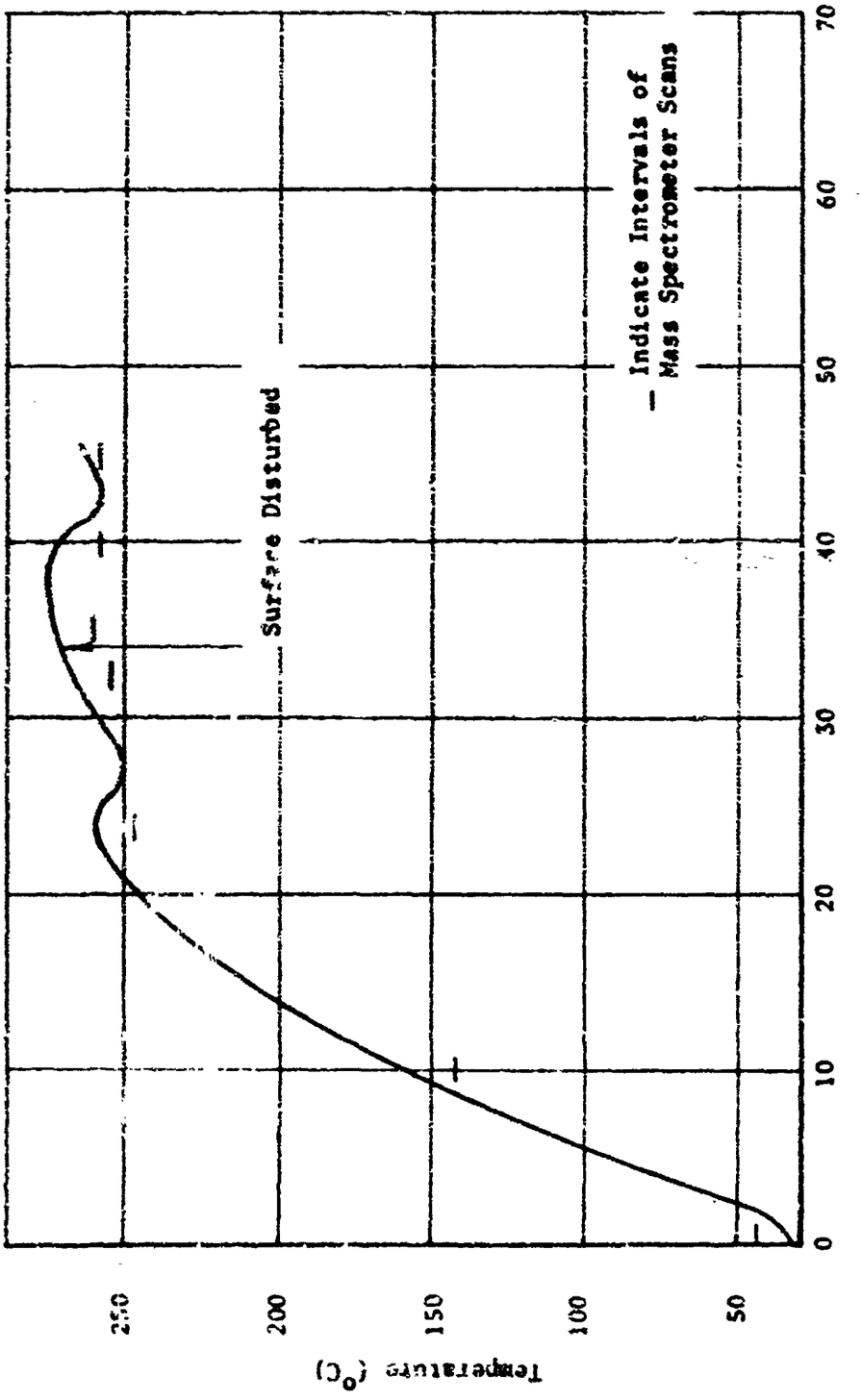

Figure 30 Heating Curve for PS Sample

Table 4 Mass Spectra of PS Polymer

m/e	Relative Abundance
Scans 1 and 2	
4	100
14	0.90
15	0.65
16	0.40
17	0.80
18	3.10
28	12.3
32	2.70
39	0.30
40	0.30
41	0.20
42	0.20
43	2.60
44	0.40
58	0.70
Scans 3 and 4	
4	100
14	3.00
15	1.60
16	1.50
17	4.10
18	15.9
20	0.50
25	0.40
26	0.70
27	1.00
28	55.0
29	1.30
32	8.25
37	0.40
39	0.40
40	0.70
41	0.85
42	0.90
43	6.80
44	2.80
45	0.70
55	0.40
Scans 3 and 4 (Cont'd.)	
56	0.30
57	0.55
58	1.85
69	0.65
73	0.25
82	0.30
84	0.30
92	0.35
134	0.25
151	0.25
Scans 5 and 6	
4	100
14	0.80
15	0.90
16	0.45
17	1.20
18	5.78
27	0.25
28	17.0
29	0.30
32	3.74
38	0.20
39	0.20
40	0.50
41	0.25
42	0.40
43	3.35
44	0.35
58	0.85
Scans 7 and 8	
4	100
14	1.95
15	0.73
16	0.84
17	0.90
Scans 7 and 8 (Cont'd.)	
18	5.25
20	0.11
25	0.19
26	0.24
27	0.47
28	39.0
29	0.54
32	7.50
37	0.13
38	0.52
39	0.82
40	0.88
41	0.49
42	0.35
43	2.73
44	0.63
50	0.82
51	1.20
52	0.46
55	0.27
57	0.22
58	0.82
62	0.22
63	0.30
74	0.27
75	0.33
77	0.95
78	0.95
79	0.27
91	1.06
102	0.27
103	1.10
104	2.70
105	1.00
106	0.46
107	0.19
117	0.19
120	0.19

Table 4 (Cont'd.)

m/e	Relative Abundance
Scans 9 and 10	
4	100
14	3.10
15	1.00
16	0.95
17	2.40
18	9.00
26	0.50
27	2.65
28	49.0
29	1.40
32	7.30
37	0.40
38	0.60
39	2.20
40	0.55
41	0.70
42	0.30
43	3.90
44	2.35
49	0.40
50	2.05
51	3.70
52	1.25
53	0.40
55	0.30
57	0.20
58	1.30
61	0.20
62	0.45
63	0.75
64	0.40
65	0.80
66	0.20
73	0.30
74	0.80
75	0.50
76	0.40
77	2.35
78	3.20
79	0.50
89	0.60
91	1.60
92	0.60
102	0.80
103	3.00
104	8.10
105	2.50
106	0.90
109	0.20
120	0.40
135	0.20
165	0.20
Scans 11 and 12	
4	100
14	3.25
15	1.20
16	1.00
17	2.70
18	8.90
26	0.65
27	1.55
28	48.0
29	0.94
32	8.00
37	0.70
38	1.00
39	2.20
40	1.15
41	0.85
42	0.85
43	5.10
44	1.95
50	2.60
51	4.80
52	2.00
53	0.30
55	0.40
56	0.40
57	0.45
58	2.05
59	0.30
61	0.30
62	1.05
63	1.35
64	0.35
65	0.50
67	0.25
69	0.30
73	0.30
74	1.00
75	0.60
76	1.05
77	2.20
78	4.40
79	0.60
80	0.30
82	0.25
86	0.30
89	0.50
90	0.30
91	1.95
92	0.70
93	0.30
98	0.30
102	0.70
103	4.75
104	12.0
105	3.50
106	0.75
109	0.30
110	0.30
117	0.30
118	0.25
119	0.30
120	0.40

Table 4 (Cont'd.)

m/e	Relative Abundance
Scans 13 and 14	
4	100
12	0.15
13	0.15
14	2.78
15	1.05
16	1.20
17	2.75
18	9.00
26	0.90
27	1.45
28	49.0
29	1.10
32	8.00
37	0.40
38	0.80
39	2.50
40	0.80
41	0.70
42	0.42
43	5.30
44	2.00
49	0.45
50	2.85
51	4.36
52	1.70
53	0.40
55	0.60
56	0.35
58	1.60
59	0.20
61	0.40
62	1.05
63	1.35
64	0.40
65	0.30
73	0.35
74	1.30
75	0.95
76	0.50
77	2.45
78	4.30

m/e	Relative Abundance
Scans 13 and 14 (Cont'd.)	
79	0.72
86	0.20
87	0.20
89	0.25
91	1.45
92	0.75
97	0.20
101	0.20
102	0.95
103	4.60
104	11.8
105	2.70
115	0.20
Scans 15 and 16	
4	100
14	3.30
15	1.60
16	1.20
17	3.30
18	10.0
20	0.20
25	0.40
26	1.00
27	2.65
28	49.0
29	0.95
32	8.00
37	0.70
38	1.10
39	3.10
40	0.95
41	0.95
42	0.70
43	5.50
44	2.20
45	0.20
49	0.35
50	3.50

m/e	Relative Abundance
Scans 15 and 16 (Cont'd.)	
51	6.50
52	2.70
53	0.45
55	0.50
57	0.65
58	1.90
60	0.20
61	0.60
62	0.60
63	2.00
64	0.20
65	0.80
70	0.30
73	0.40
74	1.20
75	1.20
76	1.00
77	3.70
78	4.65
89	0.45
91	1.00
92	0.65
93	0.30
98	0.30
102	1.20
103	6.80
104	15.0
105	2.80
107	0.30
110	0.20
116	0.30
Scans 17 and 18	
4	100
14	2.57
15	0.90
16	1.32
17	2.35
18	7.80

Table 4 (Cont'd.)

m/e	Relative Abundance	m/e	Relative Abundance
Scans 17 and 18 (Cont'd.)		Scans 17 and 18 (Cont'd.)	
20	0.20	104	7.30
26	0.50	105	1.05
27	1.03	106	0.55
28	51.0	107	0.20
29	0.92		
32	7.70		
37	0.55		
38	0.62		
39	1.52		
40	0.74		
41	0.63		
42	0.60		
43	4.80		
44	1.50		
50	1.74		
51	3.05		
52	1.38		
53	0.27		
55	0.40		
56	0.50		
57	0.52		
58	1.60		
61	0.35		
62	0.28		
63	0.70		
64	0.20		
65	0.37		
67	0.20		
68	0.20		
69	0.20		
74	0.85		
75	0.62		
76	0.30		
77	2.15		
78	2.10		
79	0.60		
87	0.30		
91	0.65		
92	0.30		
102	0.65		
103	2.74		